Development and Validation of a Subject-Specific Finite Element Model of the Human Craniofacial Skeleton

by

Tomasz Daniel Szwedowski

A thesis submitted in conformity with the requirements
for the degree of Master of Applied Science - Biomedical Engineering
Graduate Department of the Institute of Biomaterials and Biomedical Engineering
University of Toronto

Library and
Archives Canada

Published Heritage
Branch

395 Wellington Street
Ottawa ON K1A 0N4
Canada

Bibliothèque et
Archives Canada

Direction du
Patrimoine de l'édition

395, rue Wellington
Ottawa ON K1A 0N4
Canada

Your file Votre référence
ISBN: 978-0-494-40053-1
Our file Notre référence
ISBN: 978-0-494-40053-1

NOTICE:
The author has granted a non-exclusive license allowing Library and Archives Canada to reproduce, publish, archive, preserve, conserve, communicate to the public by telecommunication or on the Internet, loan, distribute and sell theses worldwide, for commercial or non-commercial purposes, in microform, paper, electronic and/or any other formats.

The author retains copyright ownership and moral rights in this thesis. Neither the thesis nor substantial extracts from it may be printed or otherwise reproduced without the author's permission.

AVIS:
L'auteur a accordé une licence non exclusive permettant à la Bibliothèque et Archives Canada de reproduire, publier, archiver, sauvegarder, conserver, transmettre au public par télécommunication ou par l'Internet, prêter, distribuer et vendre des thèses partout dans le monde, à des fins commerciales ou autres, sur support microforme, papier, électronique et/ou autres formats.

L'auteur conserve la propriété du droit d'auteur et des droits moraux qui protège cette thèse. Ni la thèse ni des extraits substantiels de celle-ci ne doivent être imprimés ou autrement reproduits sans son autorisation.

In compliance with the Canadian Privacy Act some supporting forms may have been removed from this thesis.

While these forms may be included in the document page count, their removal does not represent any loss of content from the thesis.

Conformément à la loi canadienne sur la protection de la vie privée, quelques formulaires secondaires ont été enlevés de cette thèse.

Bien que ces formulaires aient inclus dans la pagination, il n'y aura aucun contenu manquant.

Canada

Thesis Title: Development and Validation of a Subject-Specific Finite Element Model of the Human Craniofacial Skeleton

Degree and Year: Master of Applied Science, 2007

Name: Tomasz Daniel Szwedowski

Department: Institute of Biomaterials and Biomedical Engineering

University: University of Toronto

ABSTRACT

In spite of the development of new technologies and treatments in the field of craniofacial surgery, the reconstruction of post-traumatic, post-ablative and congenital deformities of the facial skeleton remains a challenge. Complications, which in part can be attributed to an incomplete understanding of the biomechanical environment of the craniofacial skeleton, continue to result in significant rates of morbidity and re-operation. A subject-specific finite element model of a fresh frozen human craniofacial skeleton was developed and validated against strain measurement from *in vitro* mechanical testing. The most accurate model was found to have a correlation of 0.73 against *in vitro* data. The most accurate model assigned local cortical thickness measurements from CT imaging data. The developed model was sensitive to assumptions regarding the elastic modulus of cortical bone, but not the Poisson's ratio. Validated computational models have tremendous potential for providing valuable insights into the biomechanics of the human craniofacial skeleton.

ACKNOWLEDGEMENTS

Completing this master's degree has been the most challenging and enlightening experience in my life yet. The past two years of my life have seen me grow tremendously, giving me the opportunity to explore may different satisfying experiences and learning a great deal about the role engineering can play in medicine. It is very satisfying to finally bring this work to a conclusion. However, this success could not have been possible without the many people that have helped me along the way.

First, I would like to thank Cari for her support, advice and enduring belief that I would succeed especially in the particularly trying time of the last few weeks of the project. Thank you Cari, I appreciate your guidance and your passion for research has been inspiring. I am confident that your enthusiasm will attract excellent students for the many great challenges in musculoskeletal medicine.

Secondly, I would like to thank Dr. Jeffrey Fialkov for bringing this project to light and starting a piece of research that will surely address many important questions about craniofacial surgery. Going to the 2006 Plastic Surgery Research Council Meeting was an exciting experience despite our friend and Dana Point will be tough to beat.

I would also like to thank all my fellow lab mates that have made working at the Orthopaedic Biomechanics Laboratory that much better. I would like to thank Michael Hardisty who demonstrated considerable restraint in mentoring a C++ rookie and whose excellent knowledge of all things related to programming and image processing was of paramount help. The coffee was always provided with a side of social justice. I would

also like to thank Cory Goldberg who started the experimental side of this project and Sandie Roth for her initial modeling work that got me going those first few months. Tomas Skrinskas was an excellent resource and his expertise in mechanical testing was greatly valued. I would like to thank Allan Morris for his interest and input in many different areas.

I would also like to thank all the many co-op and summer students that have come and gone during my time at the lab. In particular, Lyle Gordon, Charlotte Curtis, Shawn Klein, Raphael Rush, Annie Leung, Meaghan O'Reilly and Sohaib Qureshi.

Finally I want to dedicate this thesis to my parents Wieslawa and Leszek Szwedowski, whose support was above anything that I could have ever expected. Dziekujie Mama I Tata, to zrobilem dla was

TABLE OF CONTENTS

Chapter 5: Finite Element Model Development and Validation

List of Figures

List of Tables

Chapter 1: Introduction

1.1 Motivation

In spite of the development of new technologies and treatments in the field of craniofacial (CF) surgery, specifically methods of osteosynthesis, bone substitution and bone regenerative technologies, very little is known about the biomechanical environment of the facial skeleton in which these technologies are expected to perform. As a consequence many of these new technologies and techniques have inherent weaknesses and continue to result in clinical failure. In order to develop materials and techniques that truly address the clinical problems seen in this field, an accurate and complete understanding of the biomechanical environment of the facial skeleton is essential.

The craniofacial skeleton is unique when compared to the axial skeleton, exhibiting intricate and delicate architecture that is unparalleled in any other human skeletal anatomy. The craniofacial skeleton serves a myriad of roles absolutely crucial to the survival of the human. It protects sensitive neural tissue, it is the sole location for entry of life sustaining nourishment and houses many of sensory organs like vision, smell, taste and hearing that allow people to function and derive enjoyment in everyday life. The craniofacial skeleton has significant cultural and social implications and is the single most defining feature of a person; a simple image of a person's face is most often used to officially determine identity. As such restoring and reconstructing the craniofacial skeleton can significantly impact the quality of life of a patient suffering from deformity both cosmetically and functionally. Simple mechanical assumptions, upon which all clinical expertise is based, have not been successful in modeling these structures and such assumptions have resulted in a lack of success in many reconstructive designs with significant clinical consequences.

Complications of craniofacial surgery can often require re-operation that places additional strain on medical systems through added costs for surgery, care and rehabilitation, not to mention the emotional toll that such experiences take on patients and their families. As such there is tremendous incentive to pursue further improvements in existing methods for reconstruction of the craniofacial skeleton.

1.2 Objectives

The purpose of this study was to demonstrate the effectiveness of the finite element method in accurately modeling craniofacial biomechanics through the development and validation of a subject-specific model of a human craniofacial skeleton. The accuracy of the models at predicting strains in the skeleton due to applied loads will be assessed by comparing numerically computed strains against directly measured strains from *in vitro* mechanical testing of fresh frozen cadaveric human tissue. The finite element method is a ground up approach that requires a fundamental understanding of underlying principles behind the deformation behaviour of craniofacial skeletal tissues and generation of the model involved developing an understanding of the sensitivities of the underlying factors that affect the biomechanics.

The ultimate purpose of developing accurate finite element modeling capabilities for the craniofacial skeleton is to leverage the predictive ability of a model to investigate not only craniofacial biomechanics in undamaged tissues, but also how changes in morphology due to deformities impact craniofacial mechanics and to test the effectiveness of proposed treatments prior to clinical application. This is a typical engineering approach where modeling presents an excellent economic alterative to conducting numerous and costly empirical tests.

The thesis seeks specifically to:

1. Develop a subject-specific finite element model of a human craniofacial skeleton incorporating subject-specific bone material properties.
2. To validate the developed models against *in vitro* strain measurement in simulated occlusion with loading through masticatory musculature.

1.3 Thesis Organization

The first chapter introduced the motivation of this thesis. The second chapter presents a review of background information and theoretical basis for the methods employed in this study. Chapter 3 details the *in vitro* mechanical testing protocol and the resulting measured strains for different loading conditions. Chapter 4 examines the semi-automated segmentation methods employed in reconstructing the three-dimensional geometry and internal morphology of the cadaveric specimen. Chapter 5 outlines the development of the subject-specific finite element model and provides comparison with experimental data as well as reviewing the limitations of the experimental and finite element models while presenting the sensitivity of the developed model to input parameters. Chapter 6 summarizes the major outcomes of the study and discusses the future application of the developed methods to additional specimens and an approach to the simulation of physiological loading for characterization of the craniofacial biomechanical environment as well as possible improvements to the developed methods.

Chapter 2: Background

2.1 Craniofacial Reconstruction

2.1.1 Objectives

Restoration of an asymmetric or deformed facial skeleton to its normal form and therefore function is the primary goal of the craniofacial surgeon. Much of current practice in the treatment of facial fractures is focused on the stabilization of the anatomy of the facial skeleton against functional loads from musculature and overlying soft tissues. This is built on the original observation by Danis of promoted bone healing subsequent to stabilization [1]. This stabilization promotes fracture healing by preventing excessive motion of bone fragments that would otherwise disrupt the callus delaying or preventing fusion. Stabilization is important to many aspects of fracture healing such as development of vasculature, which numerous studies have demonstrated is related to the rate of formation and mechanical properties of bone [1]. Vasculature is necessary for the migration of immune and undifferentiated progenitor cells towards the site of injury to facilitate healing and combat foreign pathogens introduced in traumatic injuries involving breaching of the cutaneous boundaries and mucous membranes.

2.1.2 Pathologies

Deformities of the craniofacial skeleton can be the result of traumatic injury, birth defects, infection and tumor ablation. Such deformities can have significant functional and cosmetic implications that can severely impact the quality of life of the patient. The functional consequences of deformities include facial asymmetry, double vision due to changes in orbital volume or position, collapse of the nasal and sinus structures that obstruct airflow, as well as problems with mastication due to malocclusion. Alterations in the relative positions of the occluding structures (mandible, maxilla) impact the occlusal pattern and can change the biomechanics of the temporomadibular joint (TMJ) leading to dislocation and increased incidence of pain. Pathologies that require restoration and management through surgical intervention are widely varied. Typical traumatic injuries include fractures to the mandible body, angle and condylar process, Le Fort, orbital and zygomatic fractures.

2.1.1 Treatment

The emergence of open reduction internal fixation (ORIF) has effectively made obsolete all previous methods for stabilizing the craniofacial skeleton against functional loads. Before the emergence of plate and screw fixation, CF reconstruction often involved fixation through the wiring of bone fragments, staples, screws and pins [1]. The use of plate and screw systems is further subdivided between compression plating and locked plates and screws. Conventional compression plate techniques provide absolute stability by compressing the two bone fragments together as the screws are tightened. This torque then determines the friction force between the plate and the bone surface to resist axial loads, transmitted as shear through the screws to the plate [2]. However, this method requires excellent bone quality necessary to provide the resistance torque that determines the normal force and therefore the friction. However, as friction is overcome by functional loading the fixation strength becomes equal to the stiffness of the screw farthest from the fracture concentrating the load. If bone quality is poor this increases the likelihood bone failure and fixation loosening. Locked plates and screws on the other hand are like external fixators in that the orientation of the screw to the plate is fixed. This method does not depend on a friction force and is less disruptive to the periosteal blood supply and does not induce stress shielding [2].

Treatment of mandibular deformities seeks to take advantage of stress distributions to strategically place plates for a mechanical advantage so that force vectors in the bone are used to aid fracture stabilization and promote healing [3]. However, Rudderman and Mullen state that this approach is not employed in the stabilization of midfacial fractures, because the force vectors are intuitively considered and have yet to be quantitatively confirmed and characterized for application in clinical practice. Even though open reduction internal fixation (ORIF) procedures are the standard in reconstruction of craniofacial fractures, disparity exists as to the fixation procedures most beneficial to ensuring sufficient bone healing and long-term stability. This controversy is accredited to an insufficient understanding of craniofacial biomechanics [4].

2.1.2 Complications

In spite of the development of new technologies and treatments in the field of craniofacial surgery, the reconstruction of post-traumatic, post-ablative and congenital deformities of the facial skeleton remains a challenge for the craniofacial surgeon. Complications, which in part can be attributed to an incomplete understanding of the biomechanical environment of the craniofacial skeleton, continue to result in significant rates of morbidity and re-operation [5,6,7]. Complications from craniofacial surgery involve many different aspects of the physiology and often require reoperation for correction. These complications are far ranging and often have significant negative impacts on patient quality of life.

Failure of the osteosynthesis in which there is non-union or malunion of the bone can cause a relapse to pre-surgical pathology. Osteosynthesis failure can be the result of several events that prevent adequate stabilization of the bone fragments. Excessive motion can cause tissue rupture of the forming bone in the callus that can cause tissue necrosis. Inadequate reduction can also precipitate failure of the hardware [8],[9] , manifesting either in pullout of the screws from the bone, fatique failure of the screw head due to excessive cyclic shear loads or the plate itself may yield. Such reduction failure can cause numerous problems such as malocclusion, diplopia, anosmia and are a consequence of inadequate osteosynthesis, or stabilization [6,10,5,11,12,13,14]. Gross relative fragment motion can lead to nonunion or fibrocartilage tissue formation possibly resulting in malunion. Healing is dependent on the level of blood supply, necessary for delivering inflammatory elements such as immune cells and polymorphonulcear progenitor cells required for reconstruction of the lamellae [1]. Infection is considered to be related to the mobility of the fragments and stability is considered to be the best protection against infection, this is because movement in the presence of foreign bodies has been associated with infection as well as pseudoarthrosis [7].

Complications can also be the result of the treatment itself. The usage of metallic plates and screws have had significant rates of hardware removal for size and profile related morbidity, [5,14,6,8,15,16]. This includes issues such as palpability where hardware must be placed in areas that have thin overlying soft tissues. The large deformations and sliding of the soft tissues of the face over the hardware can also result in erosion of the tissues and subsequent exposure [5]. The use of metal hardware often results in temperature sensitivity and can require reoperation to alleviate symptoms [15]. Concerns also exist with the persistence of metal implants due to issues of migration of the hardware possibly penetrating sensitive regions such as neural tissue and disturbing natural development of adolescents [17].

Although ORIF has shown to be successful, because of issues such as hardware failure and the need for removal of hardware after successful osteosynthesis, the latter which occurs in approximately 12% of cases, there is interest in developing improved treatment modalities. Most notable is the relatively recent introduction of resorbable hardware, made of a biodegradable polymer called poly-l-lactic acid. However, due to the lower stiffness of the polymer, the plates are more bulky than metal plates. Because of the softness of the material, tapped holes are required for the screws meaning their use is limited because certain regions of the CF skeleton are ill suited for tapping [17].

Due to donor site morbidity inherent in autografting techniques and the occurrence of resorption with native bone tissue, considerable interest has been expressed in the development of adequate bone substitute materials for skeletal defects, such as tissue-engineered scaffolds. This would present a superior alternative to autologous bone grafts by avoiding the need to source the graft from the individual, which is limited in amount and availability. Research on tissue scaffolds for craniofacial applications has emphasized developing an understanding of craniofacial biomechanics as a necessary condition critical to developing successful treatments [18,19]. However, to date little work has been dedicated to such characterization [20] despite interest from scaffold developers [18,19] that identify an uncertainty in the minimum target load bearing requirement for such scaffolds, instead opting for the local elastic modulus of bone as an indication, which has been shown to vary widely [19,21].

2.2 Craniofacial Anatomy

2.2.1 Craniofacial Skeleton

The human craniofacial (CF) skeleton is a distinct bony structure of the axial skeleton and can be separated into upper and lower regions (Figure 2-1, 2-2) [22]. The lower region includes the occlusal and masticatory structures of the mandible and maxilla. The upper skeleton, which is a static structure, is composed of many separate bones and includes the upper maxilla, zygomas, orbits, naso-orbital ethmoid complex and the bones of the calvarium (frontal, parietal, temporal, occipital). All the bones of the craniofacial skeleton with the exception of the mandible are joined by static articulations called sutures, which are thin cartilaginous joints important during craniofacial skeletal development. However, in adults sutures are calcified resulting in increased rigidity. The morphology of the various CF bones is complex and highly irregular when compared to long bones such as the femur, ulna, tibia, fibula and ribs. Variability in the size and shape of the CF skeleton is a major contributor to the distinctness of the individuals. The effect of such variability on the function of the skeleton is not yet understood and may have significant implications in treatment planning.

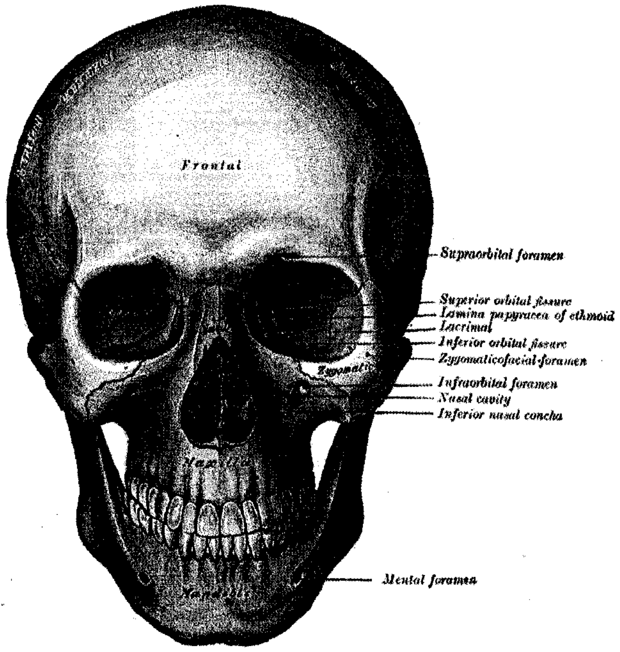

Figure 2-1 - Coronal view of the anterior craniofacial skeleton (Adapted from Gray's Anatomy 1918) [87].

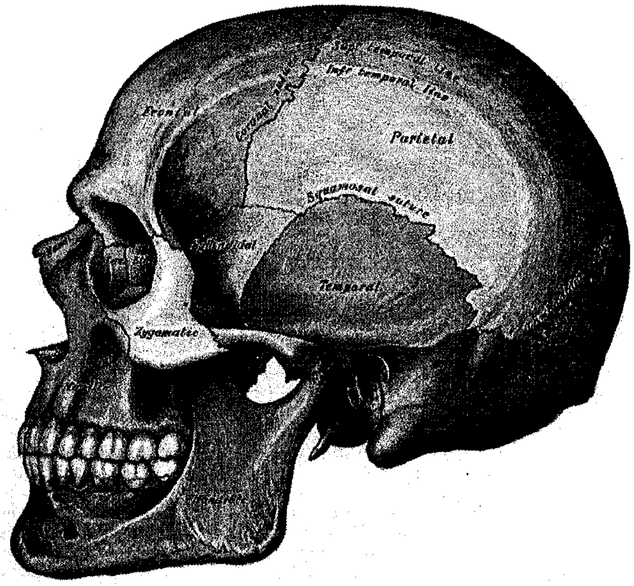

Figure 2-2 - Sagittal view of the external craniofacial skeleton (Adapted from Gray's Anatomy 1918) [87].

In addition to external shape, the morphology of CF bones also exhibits variation in bone composition, specifically the distribution of cortical and trabecular bone. The majority of bones are composite layered structures with porous trabecular bone at the centre bounded by relatively rigid and thin cortical bone [22]. In the CF skeleton, the exceptions are the maxillary sinuses (Figure 2-3) and certain portions of the temporal bone that are composed of only thin cortical bone. There also exists variability in the individual type of bone where local cortical thickness varies throughout the craniofacial skeleton and certain regions of trabecular bone can be very dense appearing to be of similar radiological intensity to cortical bone. The implications of the distributions of bone types in the biomechanics of the CF skeleton will be discussed further in section 2.8.

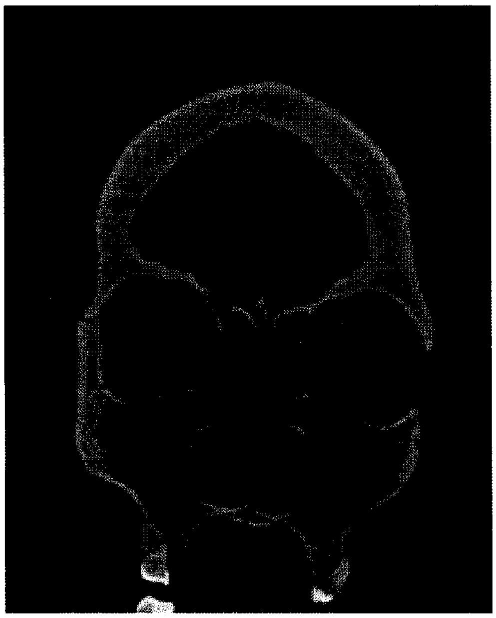

Figure 2-3 - Maxillary sinuses as imaged using CT.

2.2.2 Craniofacial Musculature

The craniofacial skeleton as with most other bones serves as the attachment location of various muscle groups. Contraction of muscle groups results in movement of the bones or soft tissue to which those groups are physically attached. The origin of a muscle is on the stationary bone and the insertion of a muscle is on the bone that moves. However, some muscle groups in the craniofacial skeleton do not insert into another bone, but into the superficial soft tissues of the face, scalp and neck, which are referred to as the mimetic musculature [23]. The remaining musculature can be associated with the masticatory system or movement of the entire head.

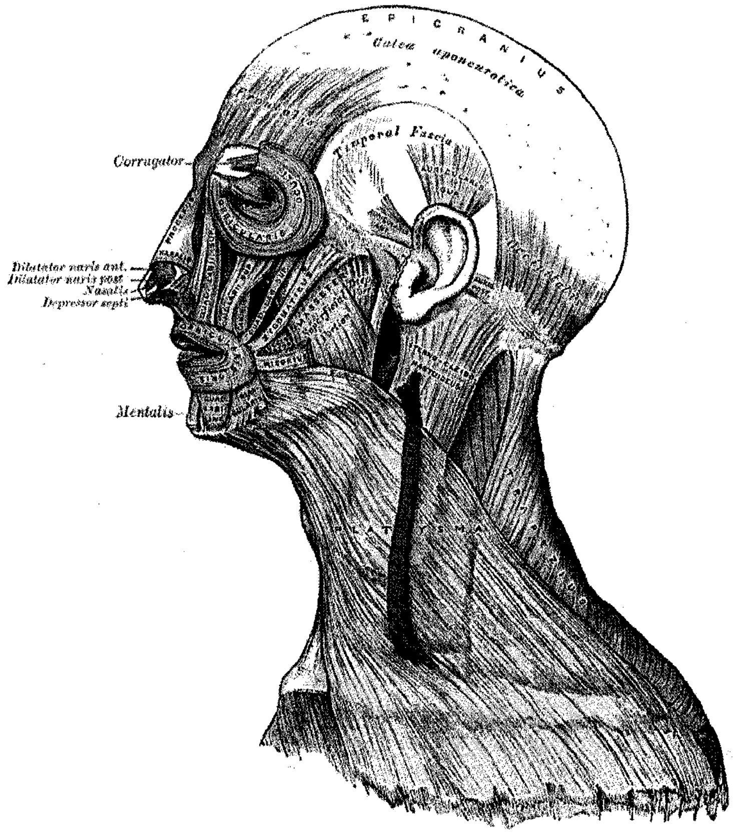

Figure 2-4 - Musculature of the Craniofacial skeleton (Adapted from Gray's Anatomy 1918) [87].

Attachment of the musculature to bones is facilitated by tendons, a dense regular connective tissue consisting mostly of collagen that is bound to the periosteum. The periosteum is a tough connective tissue that envelops all bones and is important in facilitating blood supply to bone. This underlying collagen network forms the base matrix of bone as well as providing connection between the individual muscle fibres (muscle cells). In this way a common element persists within bone and muscle providing a continuous material for load transfer.

The masticatory muscles consist mainly of the masseter and temporalis (Figure 2-4). The masseter has its origin in the underside of the zygomatic arch and inserts into the angle portion of the mandible with fibre orientation directed vertically and posteriorly (towards back). The posterior directionality is counterbalanced by the anterior (forward) fibre orientation of the temporalis, which is a fan shaped muscle that originates over a large area of the temporal and frontal bones and converges to insert into the coronoid process of the mandible [23].

2.3 Craniofacial Function

2.3.1 Mastication

The upper facial and cranial skeleton serve as a static abutment against occlusal contact with the mandible. The compressive force generated through occlusion of the maxilla and the mandible acts to cut, crush, and grind food into a bolus for easier swallowing and digestion. The contraction of various muscle groups, mainly the masseter and temporalis, act to occlude the jaws and to provide the lateral forces to grind the bolus. The forces generated by mastication musculature are the highest acting on the CF skeleton and are therefore the first concern when considering stabilization of the structure.

2.3.2 Mimetic and Soft-Tissue Loads

Additional loads are imparted on the CF skeleton by mimetic musculature. These muscles are responsible for deformations of the soft tissues of the face responsible for facial expression. It is thought that because of the relatively smaller size of these muscles that the total force generated is much smaller than those of mastication. However, the line of action of the muscles is generally not in alignment with those of mastication and as such will impart different load distributions. Because of this, treatment based on reinforcing axial load regions may incur shear loading from mimetic musculature, which conventional rigid fixation is less effective at stabilizing. In addition to the mimetic musculature, it is thought that the overlying soft tissues, which are known to place compressive loads on the skeleton, may also impart significant loads that may not be adequately resisted by considering only mastication loads [1]. At this time the significance of these loading regimes has not been studied and remains unassessed.

2.4 Form and Function

The notion of 'form and function' is a common concept in skeletal biomechanics. It is the statement that the morphology of a bony structure is dictated by its intended function. This concept was first introduced by Dr. Julius Wolff who proposed the law of bone remodeling in his treatise "Das Gestez der Transformation der Kochen" in which he states that alterations in the internal and external structure of bone occur in response to the "...stressing of the bones" [24]. Although his original attempt to present an explicit mathematical formulation has been discredited, a consequence of this notion of form fitting function is the concept of 'functional adaptation', which simply states that the structure is optimized for the required function. This is an important analytical guiding principle in many paleontological and bioarchaeological studies of skeletal material by providing a method to study the behaviour of individuals and populations [25]. More importantly it is a concept that is considered during planning for the restoration of skeletal deformities.

Many investigations propose that the mammalian appendicular skeleton is optimized for load bearing purposes, which by the same measure implies that the mammalian facial skeleton must too be optimized for countering or dissipating orthopaedic forces [26]. If bone morphology is predominantly a reflection of the loading of that given bone, then does the frontal bone, able to withstand 7,000 N of force, see that magnitude on a regular basis to explain this morphology? If so, where is this load? That such loading may exist has yet to be elucidated, but has been hinted at in the literature [27].

Studies of craniofacial form in mammals appear to provide evidence contrary to the claims of optimized load bearing craniofacial structures, which by definition would exhibit maximum strength with minimum mass [26]. In this condition, physiological function would induce relatively high and near uniform straining of the facial skeleton. Hylander et al. state that if there exist areas of the facial skeleton that incur low levels of strain with non-uniform distributions, then 'functional adaptation' would maintain that structural rigidity could be preserved with reduction in local bone mass resulting in non-optimized structures. The suggestion then is that overall craniofacial bone morphology is influenced by factors predominant over the need to satisfy functional stability [26].

Indeed, separate *in vivo* studies performed by Hylander et al. [28] of the strain levels in higher primates did not show the uniform levels of strain throughout the facial skeleton during mastication. The measurement of non-uniform strain distributions requires the presence of strain gradients and has been confirmed in similar *in vivo* studies performed on the craniofacial form of, miniature swine [29,30,31] and African green monkeys [4]. The measured *in vivo* strains provide for the most compelling counter evidence to the concept of 'form fitting function' and because these strain profiles exhibit gradient patterns, the use of this assumption in an attempt to deduce the function of the entire craniofacial architecture does not appear to be entirely accurate. Because of this a more accurate and complete characterization of functional load distribution in the craniofacial skeleton is essential before generalizations can be made regarding specific substructures when functional considerations are made for treatment regimens of bony deformities.

2.5 Modeling the Craniofacial Skeleton

In selecting a robust experimental model of the craniofacial skeleton, an *in vitro* cadaveric model most closely resembles the essential biomechanical elements of the *in vivo* condition. Because *in vivo* investigations, although representing the actual functional conditions of the anatomy, are for the most part not possible to conduct in humans, *in vitro* cadavers are a good alternative in which all the native tissue except for the regions where dissection would be required to gain access to the cortex and the relevant musculature can be preserved. Due to the complexities of the craniofacial skeleton, developing a full understanding of the intricacies of this structure using *in vitro* experimental investigations may ultimately be limited, but can provide much needed information about the CF biomechanics.

Fresh frozen *in vitro* models have many advantages over dry skulls. A dry human skull model is thought to be appropriate for studying bone strain responses to orthopaedic loading, because it provides human anatomy unmatchable by other animal models [20]. However, dry skull models include bone mechanical properties different from living or preserved bone [32] and dry skull testing omits the muscle insertions and origins introducing gross approximations of the regions and the muscle load distribution on an attachment region.

In vitro models of the CFS also require simplification in terms of the load conditions that are applied to the structure. Simplification may involve simulation of muscle activation through loading of a single muscle without regard for the combined effect of multiple muscle groups cooperating to stabilize the anatomy. However, if deformations occur in an elastic fashion where large amounts of energy are not lost through dissipation, then the effects of single muscle activation can be combined through superposition to reconstruct the same behaviour. Linearity assumptions are considered accurate for the strain regimes encountered in mechanical testing within the elastic range of bone, experimental measurement of strain will often rely on a discrete number of locations, which in addition to the inaccessibility of some sites due to functional considerations makes the interpretation of *in vitro* results sparse at best. In contrast computational models that are validated against *in vitro* testing can provide an excellent alternative for assessing the biomechanical behaviour of skeletal structures. Computational models permit controlled behaviour such as isolated and combined muscle force loadings and directions in addition to boundary restraints like tooth contact, which can be used to study both artificial and physiological loading conditions. Ultimately a validated computational model can take advantage of abundant literature about the relative recruitment of the various masticatory muscles during different masticatory or mimetic actions.

The mechanical parameters that are important to the study of bone are mainly strain. This is because validation of computational models compares numerically computed strains against strain directly measured from *in vitro* testing of bone tissue. Bone also fails in strain and the computation or measurement of strain can provide insight into the fracture risk of bone under loading [86]. Rigid fixation procedures using plates and screws may result in a stabilization where the orientation of the hardware may be such that it generates high strain concentrations at the interface between the screw and the bone which may result in local damage. This local failure could precipitate hardware loosening and ultimately possible failure of the reduction causing complications and requiring re-operation, that my result in insufficient bone quality to provide adequate stabilization requiring more advanced and risky interventions.

An FE model validated against experimental testing has great potential for providing insight into the straining of a bony structure. *In vitro* experimental strain measurement is mainly limited to sampling the mechanical environment at discrete locations on a structure. In prior *in vivo* experimental studies of animal CF biomechanics strain gauge measurement had been performed, but the experiment design could not resolve shearing, torsion and out-of-plane bending [29]. In that respect the FE method can provide information regarding stresses and strains throughout the entire volume allowing comparison of local strains against experimental measurements. Such characterization could reveal areas of interest that otherwise may not have been investigated experimentally. It has been suggested by results from experimental testing that 'functional adaptation' is not an overriding concern in the craniofacial skeleton and that function cannot completely be deduced from form. Because of this, experimental investigations could be ignorant of such regions of functional significance when considering treatment regimens.

2.6 Electrical Resistance Strain Measurement

2.6.1 The Resistance Strain Gauge

The modern resistance strain gauge may appear to be simple in appearance and principle, but is a highly sophisticated measurement tool. The technology has developed to become the most accurate, sensitive, versatile and easy to use sensor available. It is a robust sensor that is low in cost and available in a variety of configurations to suit a broad range of applications in varied operating conditions. Advances in manufacturing and instrumentation have made it the most widely used tool for experimental stress and strain analysis and it is valued for its accuracy, repeatability and reliability [33]. Alternatives to the resistance strain gauge include extensometers, capacitive, inductive and photoelectric based strain gauges. However, the resistance type gauge has the advantage in mass and size over the alternatives [34].

In 1856 Lord Kelvin first discovered that the resistance of an electrical conductor changed when it was stretched. The basic operating principle is that electrically conductive material possesses a strain/resistance relationship defined as the ratio of relative electrical resistance change of the conductor to the relative change in length. The strain sensitivity is a function of the dimensional changes that take place when the conductor is deformed elastically in addition to changes in the fundamental resistivity of the material [33]. This relationship is known as the gauge factor: $F = \frac{\Delta R / R}{\Delta l / l}$. The change in the cross-sectional dimension of a material is called the Poisson effect, which states that a change in one dimension due to strain will cause opposite strain in the perpendicular or transverse dimensions. Typically the changes in the resistivity of the material are smaller than the effect of the dimensional changes with a common gauge factor being around 2.0 [34]. Strain is defined mathematically as a differential change in length normalized against the undeformed length, often referred to as engineering strain and can be approximated for small strain as follows [34]:

$$\epsilon \equiv \frac{dL}{L} \approx \frac{L_2 - L_1}{L_1} = \frac{\Delta L}{L}$$

It is apparent from the definition of the gauge factor that if it is known, the strain can be determined directly by measuring the change in the resistance of the strain gauge. This of course depends upon equivalent transmission of strain to the gauge that is attached to a strained member [34]. The majority of modern strain gauges are typically constructed of thin metallic foils using photolithography, which etches out the desired pattern.

2.6.2 Instrumentation: The Wheatstone Bridge

Although the measurement of the output of a strain gauge simply involves measuring the resistance, upon closer examination the gauge factor equation reveals that a typical gauge with resistance of 120 Ω and a gauge factor of 2 will result in a change in resistance of 0.00024 Ω which corresponds to 1 microstrain and cannot be measured by an ordinary multimeter [34]. The more common way to measure strain is through a Wheatstone bridge where the gauge can be one or more of the arms of the bridge and a change in resistance causes an out-of-balance voltage. The most common configuration is the quarter-bridge in which one of the arms is the gauge. A change in one resistor, the gauge, will unbalance the bridge and produce a voltage that can be measured across the output terminals. Although the Wheatstone bridge is non-linear under certain conditions, when changes in resistance are small, such as the 0.00024 Ω change stated earlier, this non-linearity is negligible [35].

2.6.3 Measurement Error

Although considered to be the most accurate and robust of strain measurement systems, success depends upon proper application of the technique. Due to the configuration of the electrical strain gauge measurement system there are several possible sources of error that can impact the measurements. It is clear that any changes in the resistances of lead wires to the gauges or the resistors that complete the circuit will introduce error due to the dependence of measurement on those values. As current flows through the strain gauge, local heating occurs and the resistivity of the gauge material may change. Biological tissues such as bone have a low heat conductance resulting in reduced heat dissipation and may produce heating of the gauge and underlying material. Temperature can also cause thermal strains as the material expands. Although there are many methods by which successful bonding and sealing of the gauge can be accomplished, harsh and corrosive environments that contain a great deal of moisture can act to delaminate the gauge from the structure as well as erode the protective backing exposing the metal foil and causing shorts [33]. Biological environments present a unique challenge to strain measurement that can introduce significant error into the measurement that can be mitigated, but not always avoided. The presence of lead wires can induce noise in measurement circuits due to electric field flux from radio signals and can be mitigated by high frequency filtering.

2.7 Finite Element Analysis

2.7.1 Finite Element Method

The Finite Element (FE) method is a numerical procedure for solving complex field problems such as those found in structural mechanics, fluid flow, heat conduction and electromagnetism in an approximate manner. The FE method essentially decomposes a complex problem into simpler components whose behaviour is readily understood [36]. The original system can then be studied by rebuilding it using these basic components. The basic components in the FE method refer to the discretization of the governing differential equations that are continuous, meaning that they have an infinite number of degrees of freedom, which cannot be readily solved by classical general analytical methods [37]. The discretization of the differential equations involves approximating the solution by a polynomial over each discretization called an element. This then yields a system of linear equations that lend themselves to numerical analysis methods and can take advantage of abundant computational power [37].

In the FE method the field variable is approximated by a relevant polynomial that is representative of how the variable, in the case of structural mechanics, the displacement changes over the domain of an element. This is essentially an interpolation over the element based upon known values at certain points in the element, called nodes [37]. The specific choice for the interpolation can involve linear, quadratic and cubic polynomials, with linear being the simplest and one of the more common elements. As is the case in structural mechanics, the FE method can be applied to boundary value problems that require *a priori* knowledge of the field variable at boundary locations, so called boundary conditions [37]. In structural mechanics the boundary conditions generally represent the applied external loads that deform a structure and include predefined displacements as well. Displacement boundary conditions can either define known displacements to a structure or can restrain a structure by providing reaction forces to maintain static equilibrium. However, the FE method is not only limited to static or steady state problems.

Historically problems in structural mechanics were the first application of the FE method. Many applications in engineering require the solution of the stress and strain distributions in elastic continua that requires knowledge about the intrinsic continuum properties that define response to external perturbations. These intrinsic properties are called material properties and are chosen to reflect empirical measurement of a particular material within its elastic tolerance, which means that no energy is lost during the deformation. The concept of energy is intrinsic to the deformation of a structure much like a spring that stores energy when stretched, and it is the minimization of the energy of the structure that is at the core of various general techniques for constructing the system of linear equations that approximate the governing differential equations. Application of the FE method to a particular problem proceeds as follows:

1. The domain or geometry of the problem is defined and after selecting an appropriate interpolation, this domain is discretized by elements.
2. The constitutive material properties are defined for the material that the structure is composed of and can vary by element if such distribution of material properties is known.
3. The final component involves defining the loads that act on the structure that cause the distribution of stresses and strains which in a traditional engineering application are relevant for assessing the strength of a particular design.

2.7.2 Mindlin Deformation

There are many types of elements that one may choose when conducting an FE analysis of a structure. The choice of a particular element is determined by the application and a preliminary understanding of the behaviour of a structure and the possible numerical inaccuracies of a particular element. The Mindlin Plate finite element formulation was designed for analysis involving the bending of thin flat plates. Essentially plate bending is an extension of the classic beam to two dimensions that resist bending. Mindlin Deformation Theory assumes that a straight line normal to a plate midsurface before loading will remain straight, but not necessarily normal to the surface after loading. This is in contrast to pure bending in Kirchoff Deformation Theory that assumes that the straight line remains normal to the midsurface. In Mindlin deformation this rotation relative to the midsurface is the result of transverse shear, which is shear forces in the plane of the plate, which is not negligible in thicker plates. This makes the Mindlin formulation more general than Kirchoff alone and is useful if both deformation scenarios are under investigation in a single structure [38].

The concept of shells is common in structural mechanics. Shells can include different structures such a pressure vessels or large liquid containers that can be subject to internal pressure loads as well as transverse shear forces from reaction coupling. A shell forms a curved surface in space where the thickness normal to the shell surface is considered thin in comparison with its span. Because shells can be of complex geometry it has been convenient to model shells as a faceted surface, formed by connecting flat triangular elements together at vertex nodes [38]. In such an application the Kirchoff Triangle element is considered to be the simplest and most successful, and because the Mindlin element is simply an extension of Kirchoff triangle its accuracy is comparable. However, in certain situations it may be inaccurate if the shell under investigation approaches the thin shell limit. This limit simply put states that a thin shell analysis is accurate when the shell thickness is 1/10th the radius of curvature. Convergence studies have shown that in comparison to a tetrahedral element, the simplest solid element available, a minimum of three tetrahedrons would be required to achieve 5% accuracy against the analytical solution for a beam subject to bending. This makes the use of shell elements an attractive method for modeling the thin cortical shell present in structures such as the craniofacial skeleton. This shell element approach has been used to model cortical bone in models of the pelvis [39,40].

2.8 Bone Composition and Mechanical Properties

2.8.1 Bone

Bone is a complex composite material that displays variation in the arrangement of structures at various length scales. It performs diverse mechanical, biological and chemical functions serving as structural support, protection, storage of undifferentiated progenitor cells and mineral homeostasis. At the macrostructural scale bone can be divided into cortical, or compact bone, and trabecular, or cancellous bone [41]. Cortical bone is dense bone that forms the external surface of all bones and is composed of cylindrical units called osteons or Haversians.

These osteons contain osteocytes, bone cells that reside between concentric layers of matrix called lamellae around a central canal that houses blood vessels and nerves [23]. Trabecular bone resembles a foam-like matrix and is often distinguished from cortical bone by the degree of porosity and density. It contains numerous bars and plates called trabeculae. The cavities formed by the trabeculae are filled with fluid marrow, a specialized tissue that forms among other cells, red blood cells. In contrast to cortical bone, trabecular bone is composed of irregular, sinuous convolutions of lamellae [41]. The classification of bone as cortical or trabecular is usually based on porosity, which is the proportion of volume occupied by non-mineralized tissue. Compact bone porosity can vary from 5-30 percent, while trabecular bone porosity may range from 30-90, however the distinction between very porous cortical and very dense trabecular bone is somewhat arbitrary [42]. The microstructure of bone involves essentially two phases, the mineralized matrix and the fluid filled cavities. The solid phase involves organic fibers such as collagen, an inorganic mineral matrix composed of calcium hydroxapatite crystals and non-collagenous proteins [41].

2.8.2 Bone Mechanical Properties

A great amount of work has been done on characterizing the mechanical properties of bone. A variety of testing protocols have been employed often resulting in different values for the mechanical properties depending on the method. Bone is normally treated as an elastic material although it has been shown to have viscoelastic behaviour at very high loading rates in more fluid filled porous bone [32,42]. The Young's modulus, which is the linear portion of a stress/strain profile, has been determined through tensile testing of cortical specimens has been found to vary between 14-20 GPa, while micro-bending of cortical specimens was found to be 5.4 GPa [41]. Additionally, nano-indentation testing of lamellar bone produced a Young's modulus of 22 GPa [41]. Ultrasound propagation has also been employed to determine the mechanical properties of cortical craniofacial bone [21,43-45].

The ultrasound propagation method, which measures the propagation of ultrasound waves at various orientations, revealed that the elastic modulus of the bone depends upon the direction. The directional variation is known to correspond with anatomical axes in the appendicular skeleton and is assumed that the axis of maximum stiffness corresponds to that of anatomical loading. For example in the femur the highest elastic modulus corresponds with the axial direction corresponding to compressive body weight loads. However, such orientations are not found in the craniofacial skeleton that does not have apparent anatomical landmarks nor is the direction of maximum loading trivial [21].

Detailed elastic property measurement of craniofacial bone has been accomplished for the human dentate maxilla [43], cranial vault and zygoma [21] and mandible [44,45]. These studies tracked many parameters for the mechanical properties of craniofacial cortical bone including, apparent density, cortical thickness, and Poisson ratios. These studies found elastic moduli ranging from 9.1 GPa to 15.6 GPa for various sample points on the maxilla [43] and values ranging from 10.4 to 19.6 GPa for locations on the zygoma and cranial vault [21]. The anisotropy of the bone was limited to orthotropy, which essentially defines different elastic modulus in three orthotropic directions. This formulation is more specific than general anisotropy due to constraints on the constants between the directions. These studies performed by the same investigators reveal several important outcomes. The maximum stiffness direction was always in the plane of the cortical bone. The minimum stiffness direction was always perpendicular to the plane of the cortical bone in all the bony locations stated earlier. This suggests that cortical bone is less resistant to loading perpendicular to the cortical surface and more resistant to stresses in the plane of the cortical bone.

2.8.3 Radiographic Density Correlation

Carter and Hayes [42] originally proposed correlating the elastic modulus of trabecular bone to its apparent density. The main advantage of this approach is that as an approximation it allows the treatment of trabecular bone as a continuum and not as a meshwork. This notion is based on the similarity of trabecular bone to engineered cellular solids that have in empirical testing shown an elastic modulus dependence on apparent density. Additionally, it has been shown that the apparent density varies widely with anatomical location [46]. The work of Carter and Hayes resulted in the now classic cubic relationship of the form:

$$E = A\rho^b \qquad [42]$$

However, various empirical relationships between bone apparent density and elastic modulus have been reported. Variability and the small correlations between the experimental data and the fitted curves can be attributed to differences in the mineral content of the bone and anisotropies due to trabecular orientation, which would result in different moduli depending upon the direction of loading of the trabecular bone. This is because the data was determined from cores of trabecular bone that may not have been loaded in anatomical loading directions [42,46]. Although bone is a two-phase structure (solid and liquid) the interaction between the two phases was found to depend on the strain rate or rate of loading due to the viscous flow of the marrow only at very high strain rates of 10.0 per second and that the effect of strain rate was small compared to apparent density. The implications are that the trabecular bone is not strengthened by hydraulic pressure generated during deformation of the meshwork under physiological loading rates and that simpler elastic approximations for bone are valid [42].

This discovery permits the definition of a unique elastic modulus depending upon the local apparent density of bone by a continuum approximation. This method then lends itself to the finite element method where the domain of the trabecular bone is populated by continuum elements. One can imagine that within the domain of a single element several trabeculae may exist and that their behaviour can be approximated as a function of the apparent density. Currently computed topography (CT) scans are a convenient source of bone geometry and it has been shown that the attenuation coefficient of the material, measured by CT in Hounsfeld units (HU), can be related to the apparent density of bone [47]. It was Zannoni et al. [48] that first presented a method for assignment of material properties to finite element models of bone structures using CT data that is transformed to an elastic modulus using the empirical relations. This method was later refined to be more numerically accurate through an integration scheme [47].

2.8.4 Factors Affecting Mechanical Properties of Bone

The use of preserved tissue in mechanical testing is attractive because the stable tissue would facilitate sufficient time for preparation when the decomposition of soft tissues is considered. Studies on the mechanical properties of living versus dead bone conclude that the differences are few and that dead bone presents a valid alternative to living bone [32]. In the case of a preserved (formalin 10% buffered) specimen, the mechanical properties of the bone are expected to change from fresh cadaveric tissue. However, studies comparing fresh frozen to embalmed human cortical bone tissue showed that the modulus of elasticity increased by only 4.3% and was not considered to be significant. Additionally, similar testing of bovine cortical bone revealed changes of the elastic modulus by –1.3% in tension and –6.3% in compression [32]. The changes in the mechanical properties of the bony tissues would then be expected to have little impact on the overall response of the bone and a preserved *in vitro* model could be a reasonable approximation to *in vivo* conditions. However, CF biomechanics relies on more than just bone and the preservation of the soft-tissues such as the facia, musculature and sutures can drastically alter their mechanical properties due to the cross-linking effect of formalin that may induce stiffening in tissues whose roles are not yet understood completely [88].

2.9 Skeletal Biomechanics Models

2.9.1 Skeletal FE Modeling

The finite element (FE) method is a powerful computational tool used extensively in the analysis of traditional engineering problems. The FE method has been widely used in biomechanical studies of bony structures. The purpose of many such models varies widely and the literature is abundant. Most FE investigations of bone first began with models of femurs and pelvises where a great deal of interest has been shown in terms of implant development and surgical technique. Given that approximations in terms of material properties, geometry and boundary conditions must be made, validation of FE models against mechanical testing is important to any biomechanical study, because it assesses the accuracy in a very specific, detailed and quantitative way.

FE models have been successfully validated in many studies of various human bone structures such as the femur [49], pelvis [39,40], scapula [50,51], and metacarpal [52]. Such validation can only be achieved through comparison of the model against direct measurement of either mechanical strain or physical displacement. Methods that have been used to experimentally measure the strain on a physical model have included foil strain gauges and digitizing 3D points. However, the most common method used is strain gauges because of the excellent accuracy afforded by this method. Although displacement measurement is also a valid approach it suffers from accuracy problems when the displacements become very small.

2.9.2 Craniofacial FE Models

The FE method has previously been applied in biomechanical studies of the human craniofacial skeleton. There have been many models developed to understand stress and strain distribution changes due to implant geometries and as such isolate the analyzed geometries to alveolar bone regions directly adjacent to the tooth locations. A detailed list of such studies can be found in [53]. Although the mandible is a prominent biomechanical component and FE models have been developed, it falls outside the scope of this work. FE models that include the entire craniomaxillofacial skeleton have been used to study many different surgical procedures including simulating the effect of surgical maxillary expansion [54-60] protraction [61-63] and retraction [64]. Other models have also been developed to study craniofacial biomechanics due to physiological occlusal forces [65,66]. However, the common limitation of the aforementioned models with the exception of [60,67] is the lack of validation against mechanical testing data. Such validation is considered to be fundamental to FE analysis especially in biomechanical studies were there is much uncertainty in the material properties of the tissue and boundary conditions. The study by Provatidis et al. [60] assessed validation by comparing the displacement of 4 points located on the anterior surface of the lower maxilla and achieved a correlation of 0.90. However, this study also found that a model that considers non-linear mechanical properties of sutures was more accurate than a linear approximation so that the validation was more of the macroscopic response of the entire structure not of actual local bone strains. Also, because the purpose was to study a certain surgical method the models did not consider loading from musculature and are not interested in the physiological function of the CFS.

The study by Nagaso et al. [67] developed a model to understand the effect of maxillectomies on the resulting load distribution and compared their FE models to surface strain measurement with excellent agreement (r^2=0.989). This model used dry skulls affixed by the cranium and a metallic post placed in the molar region to serve as the point of load application. Then vertical and transverse loads were applied to the implant and the resulting strains of the maxillary region. The FE model isolates the facial portion of the skeleton and did not include the complete craniofacial skeleton by omitting the posterior zygomatic arches and the entire cranium. It also did not attempt to account for load imparted by musculature. The strain measurement areas were also concentrated in the lower maxilla providing for a validation of a small portion of the anatomy that of the central maxilla using 6 gauges. No validation of zygomatic, orbital or temporal locations was conducted simply because these areas where of little interest to the study. The model itself was approximated by relatively few elements in comparison with other CF models and no mesh density convergence was reported.

The FE method presents considerable effort in terms of development and can quickly become a complex exercise requiring the introduction of assumptions and uncertainties in the modeling requiring testing to resolve. The alternative to the FE method has in the past involved the approximation of the biomechanics of bony structures by analytical representations easier to define and analyze, which often can function as a preliminary working approximation. Specifically, the mandible has been treated as a two-dimensional cantilever beam for the purposes of elucidating the anatomical distributions of the tensile and compressive stresses for pre-surgical assessment of treatment strategies [3]. However, a comparative study performed by Rudderman and Mullen [3] of beam mechanics against finite element models revealed inadequacies with the simplified approach because of the potential for incorrect predictions. Rudderman and Mullen identified that the models could not predict the behaviour because they could not capture the complex morphology in terms of the variations in mandibular thickness, bone mineral density heterogeneities and geometries such as the condyles and coronoid processes. Additionally, *in vivo* strain measurement by Rafferty et al. [4] of the zygomatic arch in miniature swine during masticatory function confirm those findings [28,30] in that the zygomatic arch is not a simple beam-like element and that the approximation of this substructure by beam mechanics would be oversimplified and prone to misleading conclusions.

2.10 Tomographic Imaging and Anatomical Reconstruction

2.10.1 Objectives

Modeling of subject-specific geometries requires information about the morphology of the structure under investigation. In the case of the craniofacial skeleton, computed tomography (CT) imaging is a common diagnostic tool used in assessing craniofacial pathologies and is a convenient source of geometric information. CT imaging is particularly sensitive to bone because of the radiographic properties that make it distinct in terms of contrast from surrounding soft tissues. The delineation of anatomical structure from medical imaging modalities is referred to as segmentation and is by nature an ill defined problem because of ambiguity in establishing absolute definitions of tissue boundaries. Segmentation is a challenging task and despite the abundance of various methods and algorithms there is no single approach to segmentation [68].

2.10.2 Strategies

All imaging modalities are susceptible to random noise, which manifests itself in medical images as irregular speckle. Specifically in bone imaged with CT, the Hounsfled units (HU) of the image are directly related to the x-ray attenuation coefficient and to the apparent density of the tissue. More accurately CT measures the electron density of the tissue so that identification of bone relies on the contrast relative to soft tissues. However, often it is found that the lower end of the range for voxel (3D pixel) intensities for bone often overlap with the upper end of soft tissue. Because of this property a thresholding method that simply extracts those voxels in a user specified range produces segmentations that are disrupted by 'islands' that require manual user interaction to condition for geometry generation.

Successful segmentation always involves identifying structures using intrinsic properties interpreted from images. The problem of noise has been addressed by smoothing filters that implement a large variety of algorithms. However, most smoothing algorithms blur the image in order to impose a more continuous image across voxels and this destroys information at edge boundaries where the transition from soft tissue to bone is high. One particular algorithm has solved this by means of anisotropic or edge preserving smoothing. This class of filters is called anisotropic diffusion filters because the smoothing is defined as a diffusion process where the image is considered a temperature field and the smoothing involves heat transfer towards equilibrium conditions. The edge preserving nature of these filters is a result of a variable conductance term that essentially scales the rate of heat transfer by local information about the severity of the gradient magnitude of the image. Because of this fine internal structures are smoothed preferentially over the sharp edges that occur at anatomical boundaries of interest [68].

Such edge preserving smoothing used in combination with region growing methods present a robust first approach to image segmentation. The anisotropic smoothing suppresses noise but preserves edges and homogenizes solid regions so that a connected component algorithm can more effectively segment bone. Connect components or 'magic wand' is a constrained thresholding method that begins the segmentation from a seed and grows by adding all adjacent voxels that fall within a user defined range until no new voxels can be added [68]. The smoothing in addition to the connect components scheme reduces the spurious external voxels that require laborious intervention to remove.

2.10.3 Level-Set Methods

Level-set based methods are a class of computational image processing methods that are based on a specific numerical algorithm that has many advantages for application image segmentation problems [69]. Such active contours or deformable models essentially track anatomical boundaries by embedding the curve within a higher dimensional function of which the 0 crossing or level set represents the boundary of interest. The general concept involves propagating a curve by means of a velocity normal to the curve depending upon image-derived properties such as gradient and curvature. The multi-dimensional level set approach provides the advantage of allowing topology change without complex tracking schemes where independent regions undergoing evolution can merge or separate without knowledge of the number of structures in the scene [69].

One implementation of the level-set based method is the Geodesic Active Contours [69]. This method extended the shape detection algorithm by adding an advection term to the speed computation that projects the gradient field onto the level-set normals to act as a doublet term that reduces overshoot of the curve due to propagation and curvature. The level set based methods allows differential weighting of different control terms that define the speed of the curve at any particular point. The curvature scaling acts to smooth the curve, which acts to suppress irregularities in the curve due to discontinuities in the speed or propagation influence [68]. The deformable models depend upon curve characteristics at any time, and are unstable at large step sizes making them well suited for making small improvement to an existing coarser segmentation generated with more efficient methods. This means that the Geodesic Active Contours method is appropriate for the segmentation of thin shell like structures that can be unreliably defined using simple thresholding methods.

Chapter 3: In vitro Craniofacial Model

3.1 Introduction

In skeletal biomechanics *in vitro* models may provide conditions similar to the *in vivo* environment and so can serve as an adequate platform for investigation of function. However, inherent practical limitations of both *in vivo* and *in* vitro models encourage alternatives to be sought particularly with craniofacial anatomy. Although the FE method presents a more controllable and versatile alternative for studying skeletal biomechanics, uncertainties in the intrinsic properties of biomechanical systems require validation of the method against an experimental reference to determine accuracy. The FE method imposes an abstract representation of reality and is deterministic by nature and confidence in its predictive power depends upon validation of outcome parameters. Such information can be gathered by direct physical measurement of the system under consideration. Thus, measurements taken from *in vitro* skeletal biomechanical models are often used as a basis for FE model validation.

Within the context of skeletal biomechanics, *in vitro* refers to isolation of a particular musculoskeletal mechanism from the rest of the human body, and the use of cadaveric specimens. The use of cadaveric tissue necessitates accommodation for the natural process of decomposition that denatures the tissue. This denaturing involves changes in the mechanical characteristics of tissue that has incurred disruption in the molecular bonding of the cellular and matrix components. Because of this, adequate preservation is required and most commonly facilitated through fixation by formalin or freezing. Although the mechanical properties of bone are not significantly affected by formalin [32], there is a well-known cross-linking effect in organic polymers of soft tissue matricies that alters their mechanical properties [88]. As such, in studies which incorporate soft tissues such as musculature and facia a fresh frozen cadaveric skeletal model can provide a superior choice for *in vitro* mechanical testing. The effects of repeated and extended freezing on the mechanical properties of bone are limited, however, the temperature and hydration in the case of porous bone has been shown to significantly affect mechanical properties [32]. Soft tissues may be disrupted by the formation of ice crystals which can act to cut and therefore damage cellular and extracellular components.

The objective of this study was to develop a mechanical testing protocol to extract surface cortical bone strains from an *in vitro* fresh frozen model at various locations around the facial skeleton using tensile loads applied through preserved masticatory muscle origin sites. The study sought to simulate the effect of the activation of individual muscle groups without balancing site activation in such a manner that the nature of the loading and equilibrium restraint was known with high degree of confidence thereby permitting replication in computational models. The measured strains provide the gold standard for comparison with a computational model for calibration and validation.

3.2 Methods and Materials

3.2.1 Specimen Preparation

One fresh frozen cadaveric head was obtained from the University of Toronto Anatomy department subsequent to Sunnybrook Research Ethics Board approval for the study. The specimen consisted of a complete human head including all soft tissues, musculature and organs (brain, eyes) severed at the third cervical vertebrae. An incision was made to the left side of the head extending from the frontal bone, around the temporalis to the ear, then down towards the base of the neck (Figure 3-1). The soft tissue flap was retracted and removed to provide access to the bone and musculature. The adipose (fat) tissue overlying the zygoma, orbit, temporalis and masseter was removed with the periosteum. Extraneous soft tissues around the masseter such as loose adipose, the periosteum, and salivary glands were removed to isolate the masseter (Figure 3-2). The left masseter muscle was released from the insertion into the angle of the mandible using a surgical elevator (flat surgical instrument). The masseter was then raised to expose the temporalis insertion into the coronoid. A surgical chisel was used for a controlled fracture of the base of the coronoid (Figure 3-3). The insertion of the temporalis into the remaining coronoid fragment was preserved for load transmission during mechanical testing. After exposure of the musculature all remain soft tissues were removed in order to expose the surface of the bones. The periosteum was dissected away from the left maxilla, nasal bones, orbit and zygoma.

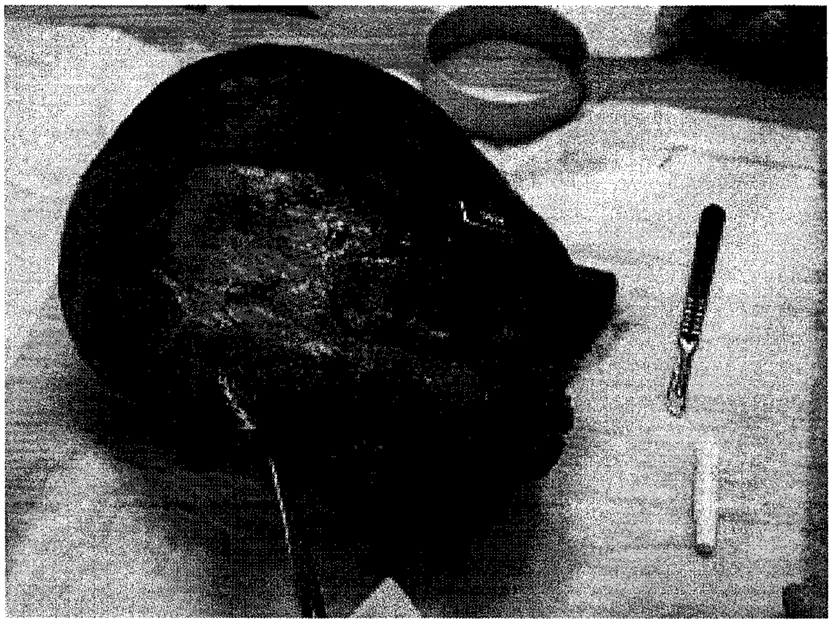

Figure 3-1 – Initial incision into the left facia. Soft tissue was detached anteriorly.

Figure 3-2 - Completed dissection showing the exposed cortical bone (periosteum removed) and masseter dettached from the mandible.

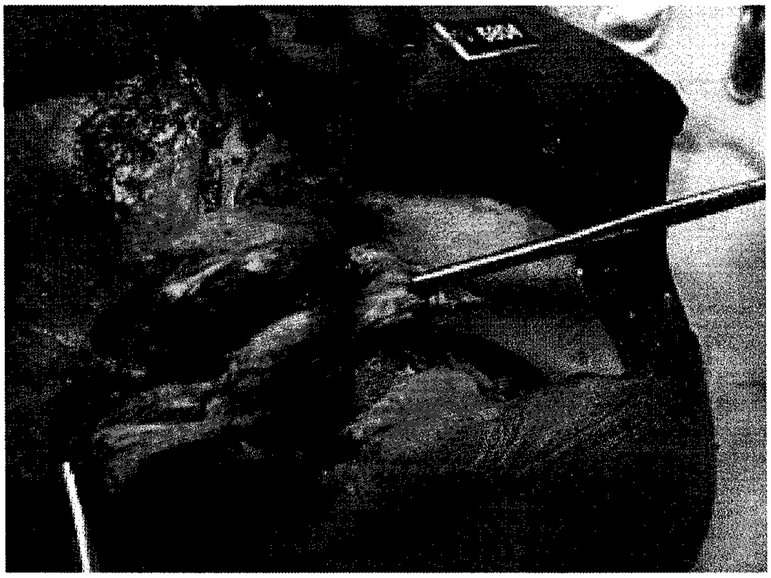

Figure 3-3 – Masseter (left most instrument) elevated to gain access to the coronoid fragment with temporalis origin preserved.

The presence of amalgam filling required accommodation for radiological concerns. Amalgam fillings cause x-ray scatter and result in artifacts when scanned using CT imaging (Figure 3-4). Such artifacts obscure all structures within the x-ray source-detector plane and elimination of this required removal of all fillings. Amalgam fillings were removed using a standard Dremel tool with a countersunk engraving bit with a coarse fluting. A finer tool became quickly obstructed by the relatively malleable filling material. The individual filings of the filling material were removed using generous hydration, however, very fine particulate matter become embedded in the soft tissues of the oral cavity. A subsequent CT scan of the specimen revealed the fine particulate matter to produce minimal scatter. Before scanning the radio-opaque fiducial markers were affixed to three linearly independent positions in order to provide a 3D coordinate system for subsequent data processing. The locations were at the root of the zygomatic arch in the temporal bone and, the front of the maxilla directly above the incisors and at the bridge of the nose just under the orbit (Figure 3-6). Radiopaque fiducial markers were applied to the skull at various locations to aid translation of strain gauge positions to the FE models. Computed tomography images (0.523mm x 0.523mm x 0.8 mm) were acquired of specimen on a clinical scanner (Philips Brilliance Big Bore, Amsterdam, The Netherlands).

Figure 3-4 - Example of artifacts caused by amalgam fillings in CT scans. Artifacts act to obscure bone in the x-ray plane that includes the fillings.

3.2.2 Loading

Mechanical testing of structures involves applying known boundary conditions to stress and strain the structure. Reaction forces must resist any load applied to a structure in order to maintain static equilibrium, a balance of loads that results in no net acceleration. Testing of conventional mechanical constructs applies loads in directions and magnitudes representative of operational reality. If an *in vitro* model is to recreate the operational conditions then it would have to be subject to physiological loads. In the CF skeleton the most significant physiological loading is experienced during mastication.

The complex morphology of the CF skeleton and the various directions of the musculature make application of physiological load conditions impractical. However, because the purpose of this *in vitro* model is to provide a validation of an FE representation physiological loading is not necessary as long as the boundary conditions are apparent and can be applied to the FE and *in vitro* models. Although arbitrary loads can be applied to any mechanical structure, it is convenient to apply loads through natural mechanisms, the musculature, for loading of the craniofacial skeleton. Muscle tissue is characterized as compliant relative to bone and has distinct fiber orientations of the muscle cells and the connective matrix between them in the direction of primary force generation. This gives the muscles in the CF skeleton constrained directions of loading and therefore the line of action of the force can be deduced.

The two muscle groups chosen for this study were the left masseter and temporalis. These two muscles are primarily responsible for generating the compressive occlusal forces used to cut, grind and crush a food bolus. They are the largest by mass of all facial musculature and therefore are responsible for generating the highest loads experienced by the CF skeleton. The reason such high loads where desired for this study was to ensure that regions of high strain are present and similar to physiological strains to increase the confidence on the computational models in replicating high strain regions that clinically relevant. These two muscle groups are also much easier to access than some internal muscle group like the pterygoid or digastrics whose primary role is to provide transverse stabilization required for crushing and motion required for grinding.

Aluminum interface plates were affixed to the dissected masseter and temporalis muscles using Ti-Cron 1-4 metric sutures (Syneture Inc., Tyco Healthcare, Mansfield, MA) threaded through the body of the muscles. These interface plates provided for load transfer from an actuator to the body of the muscle in an approximate direction of native loading. The masseter interface plate was manufactured to distribute the applied load across the whole body of the masseter (Figure 3-5). A similar procedure was applied to the temporalis, however, because it converges to essentially a point the interface plate was made smaller and sutured to the temporalis body and the coronoid fragment that was preserved with the insertion (Figure 3-6). A wound stainless steel 500 lb test wire provided a link between the interface plates of the masseter and temporalis and the tensile force actuator. This construct then allowed tensile forces to be applied through the musculature to the CF skeleton.

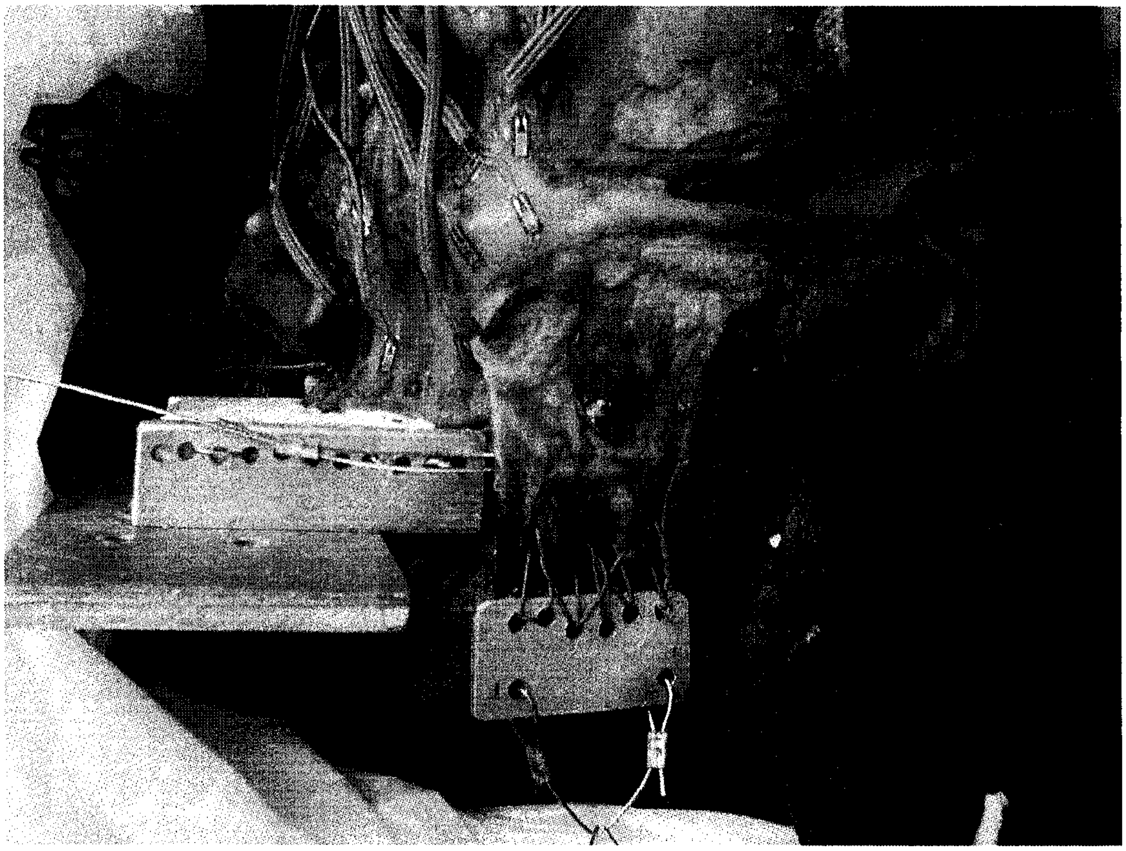

Figure 3-5 - Masseter interface plate configuration. Showing multiple hole arrangement for suturing.

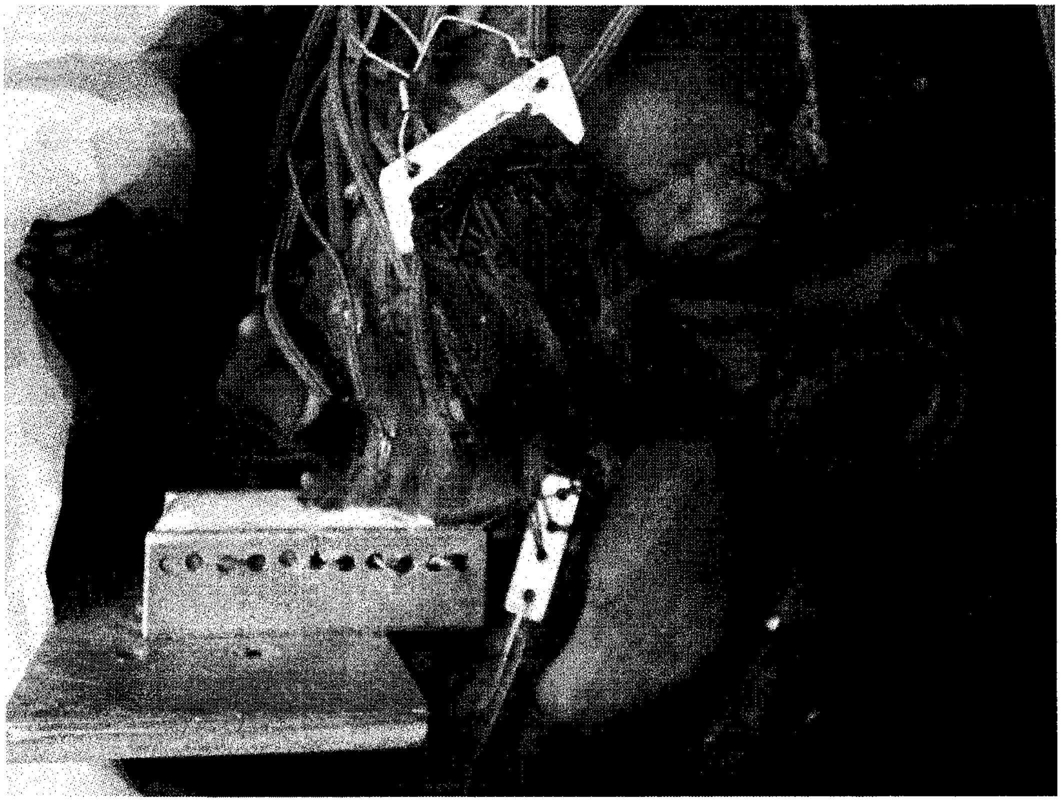

Figure 3-6 - Interface plate configuration for temporalis origin into the dislocated coronoid fragment.

An MTS Bionix (MTS, Eden Prairie, MN) mechanical testing system applied a maximum tensile force of 100N to the masseter and the temporalis. The magnitude of the force was derived from a study by Raadsheer et al. [70] of human bite force, which reported a mean force of 383.6 N for females (same sex as that of the specimen), and in assuming dual side activation a force of 100 N was chosen as a conservative value for testing. The loads were applied to each muscle independently of each other. The exact value of this load is not crucial to the test because as stated earlier physiological loading is not the goal. This value, however, was a good compromise between typical loads that the muscles generate and the need to minimize damage to the muscle after repeated trials. With the opening and closing of the jaw the orientation of the masseter changes more than the temporalis, which converges, to a point. To capitalize on this flexibility two different directions of the loading were chosen to provide additional data points to increase the confidence in the numerical model validation and also to investigate the effect of such directional variation on the strain patterns (Figure 3-7).

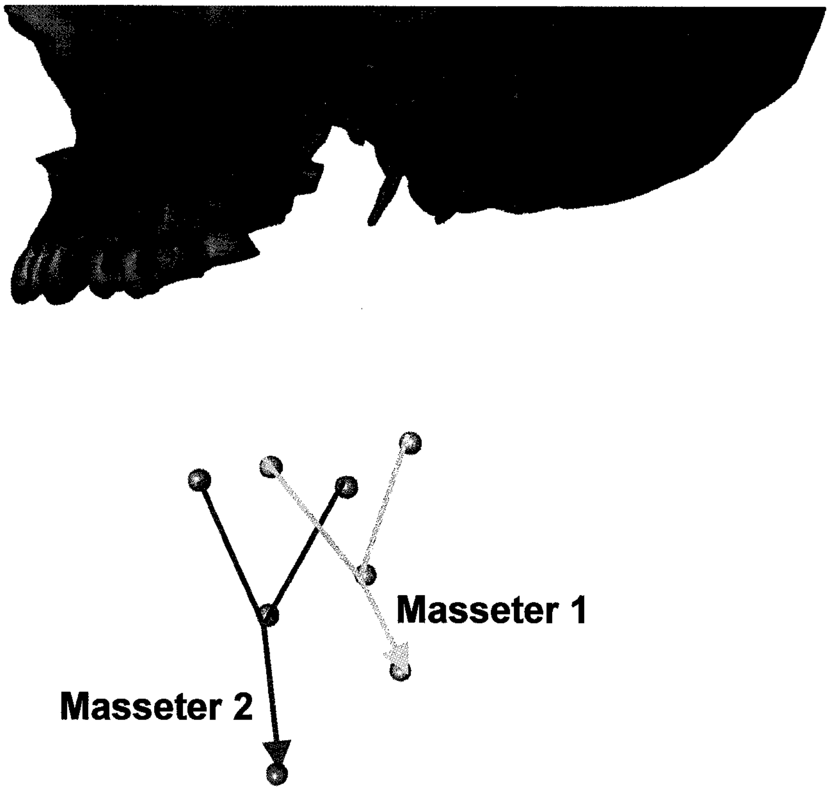

Figure 3-7 - Schematic showing the landmark points measured from the in vitro model for the masseter 1 and masseter 2 load orientation relative to the skull geometry.

3.2.3 Boundary Conditions

The boundary condition serves to maintain static equilibrium under applied load. Occlusion was chosen as the restraint position and a fixture was constructed that would provide a rigid base. The rigidity of the fixture is important because it represents complete control over the load condition for translation to FE modeling. To provide restraint of the CF skeleton at the dentate against the loads from the musculature, several load types must be resisted.

Physiologically the teeth come into contact directly or through a food bolus and resist only compressive and transverse forces. The mechanical testing applied a tensile load to a single muscle on only one side of the CFS. This loading is not symmetrical about the sagittal (side) plane and so any restraint at the teeth would see a compressive force and transverse force in the plane of the occlusion in addition to a moment. The designed restraint would have to accommodate this in order to provide essentially a rigid fixation of the teeth. The occlusal restraint is also important because, although there are alternatives to such an arrangement that would provide a valid loading to validate an FE model, a validated FE model is really only definitely accurate at the discrete locations on the *in vitro* model from which the measurement is taken and assumed to be valid in all other regions. Occlusal restraint therefore would reveal the mechanical behaviour of the structures of the facial skeleton where there is more complexity and interest. This increases the confidence of the validation in the regions of the maxilla, nasal bones, orbits and zygomas, which are the regions of primary clinical interest in this work.

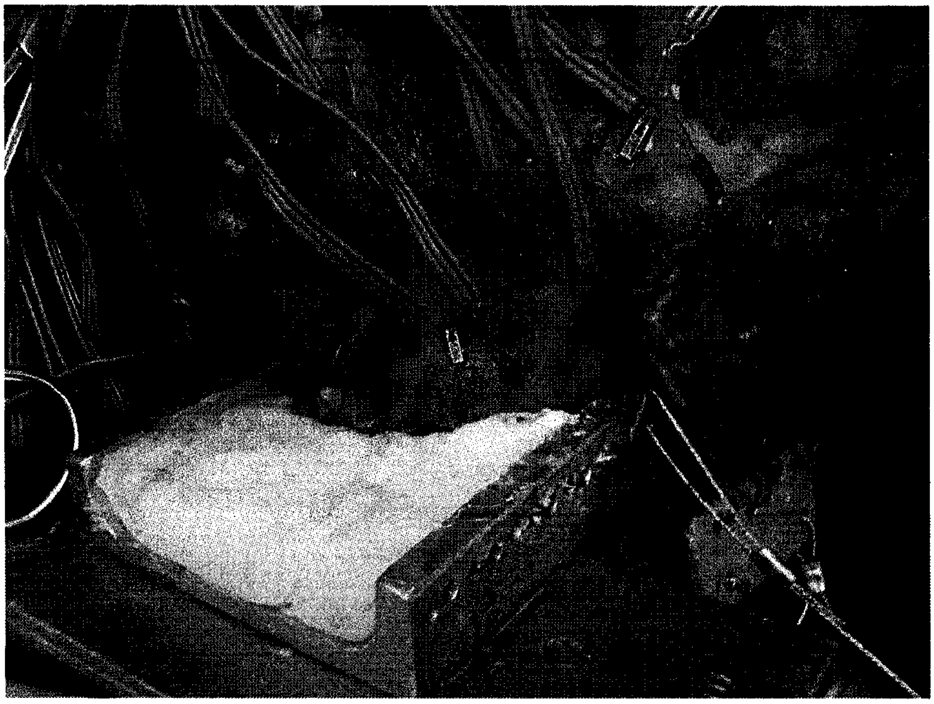

Figure 3-8 - Occlusal restraint imposed on the upper teeth by steel wire and PMMA casting. Also shown are the gauge positions located on the facial portion. Gauges 1,2,7 and 8 not shown being out of the picture range.

The rigid fixture designed to provide the occlusal restraint (Figure 3-7) uses fixation elements that provide a tensile and compressive resistance to load. A 500lb test steel wire was threaded in between the teeth to resist tensile loads caused by the moment arm and also served to center the teeth on the C channel. Tension was applied to the steel wire and polymethylmethacrylate (bone cement) was poured into the channel to fully immerse the teeth and steel wire, thereby embedding them in the bone cement. Once cured, the cement becomes brittle and rigid. The reason for elevation of the CF above the base is to provide space for force redirection pulleys to be affixed to the base plate of the fixture. Because force was transmitted using steel wire, pulleys were be used to redirect the force from the hydraulic actuator in the approximate native direction of the masseter or temporalis, thereby providing control of the direction of loading. The pulley was affixed to a rigid steel bar that allowed for freedom of placement of the pulley underneath the muscles thereby defining the direction of loading. Two different loading orientations were employed in the study for the masseter muscle (Figure 3-8) and landmark points were acquired to reconstruct the force orientation for translation to the computational model.

3.2.4 Strain Gauge Instrumentation

A total of 14 uniaxial strain gauges, with a resistance of 120-ohm (FLA-3-11-3LT, Tokyo Sokki Kenkyujo Co. Ltd., Tokyo, Japan) were bonded to the cortical surface at various locations around the zygomatico-temporal complex (Figure 3-7). Preparation of the gauge locations involved complete removal of the periosteum from the bone with a scapel. The location for a particular strain gauge was cleaned with alcohol and degreased with acetone. The location was roughened using 400-grit dry use sand paper. The chemical cleaning and mechanical abrasion served to improve the bonding between the strain gauge and the underlying bone. A strong bond ensures that the actual strain is transmitted to the strain sensitive element of the gauge. The strain gauges were affixed to the bone using the M-Bond 200 Adhesive Kit (Vishay Intertechnology, Malvern, PA). Cyanoacrylate was applied to the prepared location and excess was removed with gauze. The backing of the gauge was brushed with the M-Bond catalyst and the gauge was applied to the location with hand pressure applied for 30 seconds. The gauges were sealed using 5 coats of M-Coat A Polyurethane (Vishay Intertechnology, Malvern, PA) to protect against mechanical damage and chemical infiltration. The coordinates of the strain gauges and the fiducial markers were digitized using a Microscribe 3DX (Immersion Corp., San Jose, CA) digitizer. The position and direction of the gauges was asserted by acquiring points at the ends of the gauge using the orientation markers on the gauge.

3.2.5 Testing and Data Acquisition

The specimen was mechanically loaded through the masseter in two distinct directions and through the temporalis. The loading profile involved a steady ramp of the load through displacement control to a maximum load of 50 N, 75 N and 100N. To compensate for relaxation of the muscle tissue, which results in a decrease in load, the displacement of the hydraulic actuator was adjusted continually to maintain a constant load; although relaxation of the load was within 5N over the testing period. Under loading the direction markers were digitized from the fixture using a Microscribe 3DX (Immersion Corp., San Jose, CA) digitizer. A constant load was maintained for 40 seconds at a strain measurement-sampling rate of 25 Hz to acquire 1000 data points and then unloaded. This load profile was repeated for each load magnitude and direction 5 times.

The strain or change in resistance of the 14 strain gauges, one per multiplexed channel, was measured using a 2-wire quarter bridge configuration. The bridge circuit was completed using either 350 Ω or 120 Ω high precision resistors. The two resistances used are due to the availability at the time of testing. This did not effect the measurement of the strain only the scaling factor that converts the output voltage to the physical strain sensed by the gauge. The Wheatstone bridge was shunt calibrated at the gauge using a 59 KΩ resistor simulating 957 microstrain. The strain was measured using a data acquisition system (DAQBOOK/2000a - signal conditioner w/ a DBK43a - strain measurement module, IOTECH, Cleveland, Ohio) with the minimum excitation voltage of 1500 mV and a scaling gain of 800.

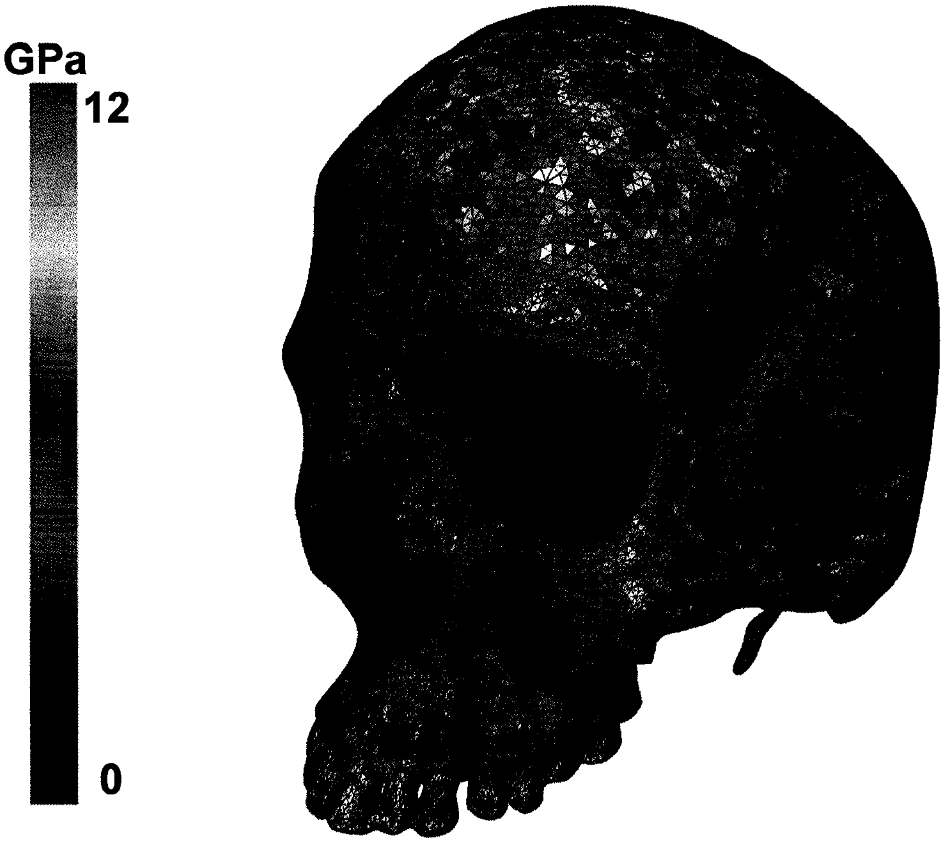

Figure 5-5 - Elastic modulus distribution mapped to the tetrahedral grid. Contour range is between 0 and 12 GPa. Note effect of partial volume averaging which results in elastic moduli of approximately 6 GPa for surface tetrahedra.

5.2.3.2 Shell Element Mesh

A hybrid solid-shell mesh was developed for the FE model based on the recognition of the thin cortical bone structures of the CF skeleton and the mesh density requirement for tetrahedra in approximating bending as discussed in Chapter 2. The linear triangular Mindlin element from the IDEAS 10 NX library were used to represent the cortical shell of the CF skeleton and the meshing was derived directly from the surface triangulation generated from the segmentation. As per the previous implementations of the hybrid mesh [39,40] the triangular element geometry defines the midline of the element and an offset was specified to establish the geometry of the shell element as the top surface, creating an overlap region of

3.2.6 Data Processing

The result of shunt calibration produced a scaling parameter that was used to convert the output voltage of the Wheatstone bridge into the equivalent microstrain based upon the resistors used in the bridge. This new gauge factor is dependent on the configuration of the Wheatstone bridge, excitation voltage and the scaling gain. The strain values were extracted from the data by identifying a time range for the plateau of the loading profile during which the measured voltage corresponds to the constant load condition for 1000 consecutive data points. The mean and standard deviation of the each channel for each trial for each load direction and magnitude where computed and converted into the equivalent strain using the shunt calibration gauge factor.

3.3 Results

The results of the *in vitro* testing are shown in Figures 3-9, 3-10 and 3-11. These figures show the mean strain measured by each gauge over the 5 trials for each magnitude and direction. For each trial the mean and standard deviation was computed for the 1000 data points extracted from the plateau region of the strain profile that corresponds temporally to the loading profile. The error bars represent the mean of the standard deviations of the 5 trials.

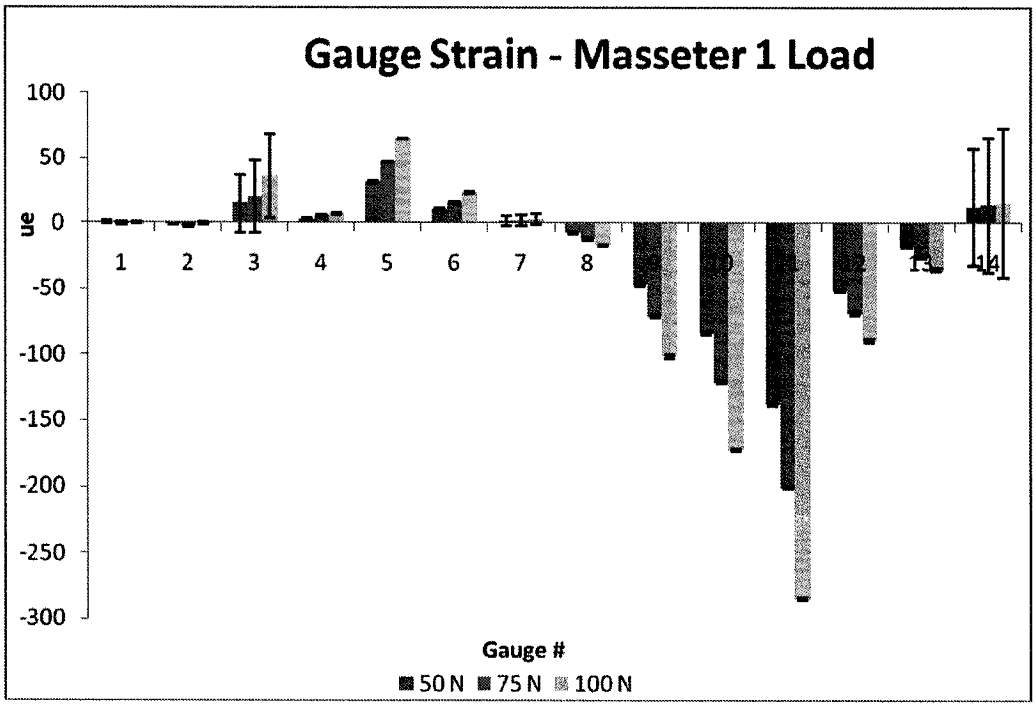

Figure 3-9 - Gauge strains for the masseter load 1 for 50 N, 75 N and 100 N tensile loads. Error bars represent one standard deviation for 5 trials for each load magnitude.

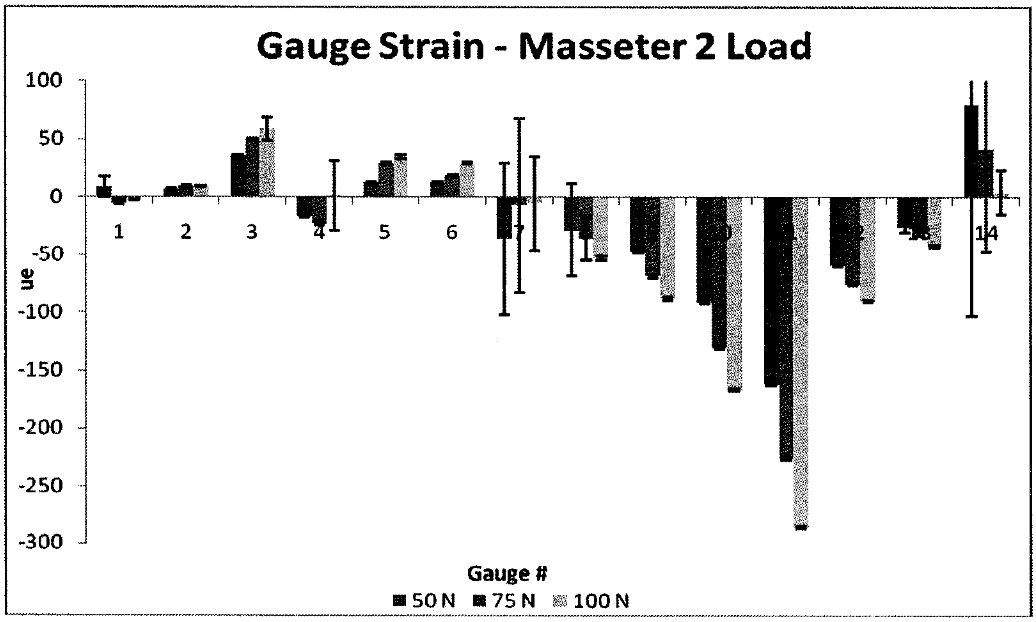

Figure 3-10 - Gauge strains for the masseter load 2 for 50 N, 75 N and 100 N tensile loads. Error bars represent one standard deviation for 5 trials for each load magnitude.

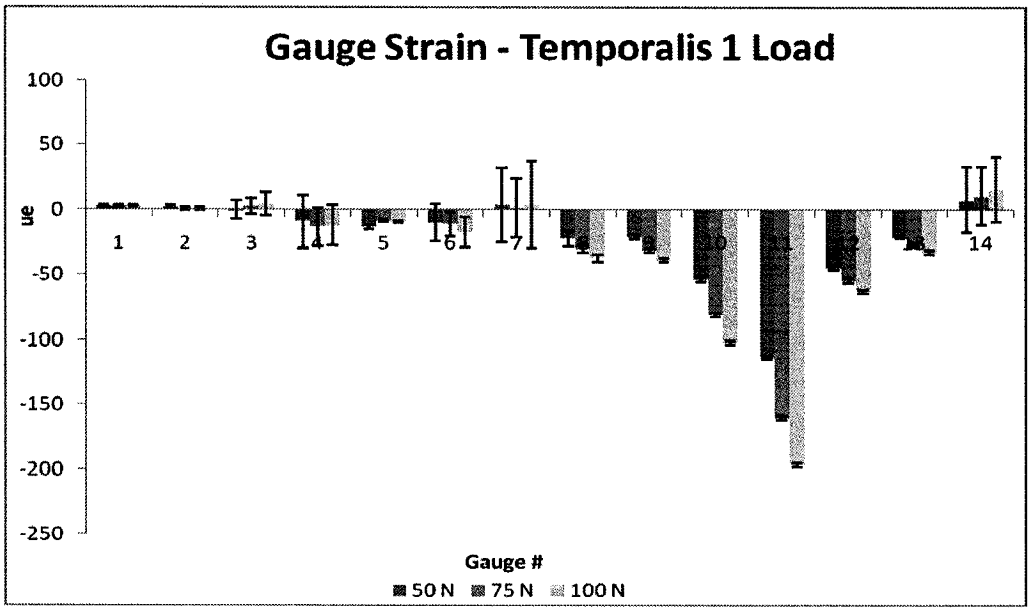

Figure 3-11 - Gauge strains for the temporalis loading for 50 N, 75 N and 100 N tensile loads. Error bars represent one standard deviation for 5 trials for each load magnitude.

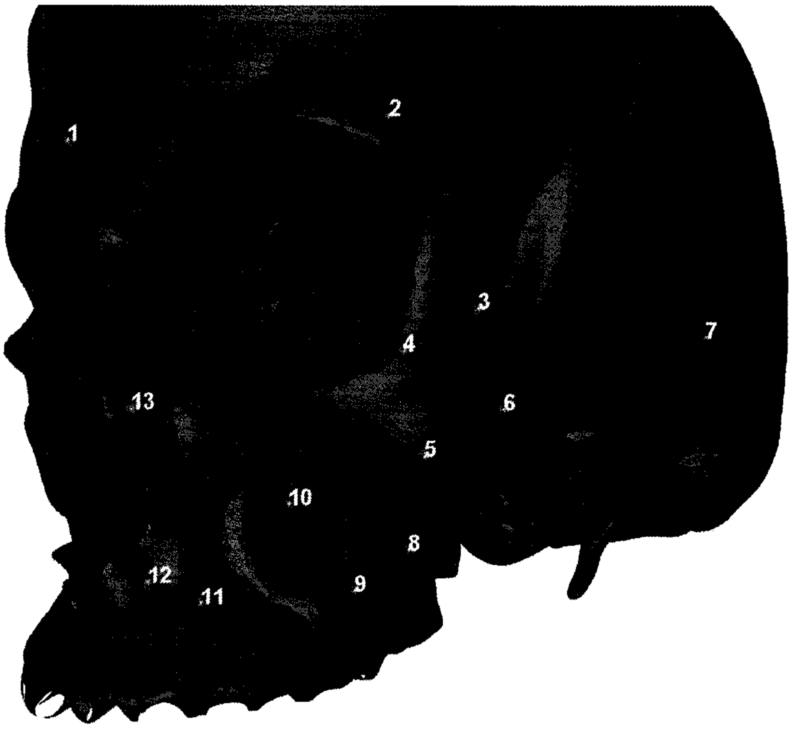

Figure 3-12 - Schematic showing the relative positions of the strain gauges on the cortical surface of the cadaveric specimen.

3.4 Discussion

The results of the mechanical testing reveal several important issues regarding the *in vitro* data (refer to Figure 3-11 for gauges positions). First consistently across all the trials, loads and directions, gauge number 14 exhibits large signal variation and no plateau region corresponding to the constant load and therefore confidence in the data from this gauge is low. Therefore, this gauge was omitted from the data to be used in the validation of the FE models. Gauge 7 also exhibits significant variability in masseter 2 and temporalis loading but because the strain at that location was consistently low across all loads it was considered still viable for validation. In contrast the other gauges show very small variability between trials except at gauge 3, which exhibits variability in masseter 1 and temporalis loading. Gauge 4 also shows variability but only in the temporalis loading case. The position of this gauge is on the zygoma, which is not in a direct path of load transfer when considering load from the temporalis and a high strain in this region is not expected. The temporalis loading was the last loading case tested and gauge 4 variability could be due to partial unbonding that cause result from fatigue and compounded by moisture infiltration.

The choice of testing the same load direction at various load magnitudes also reveals information about the material properties of the CF. Although bone is often considered a linear elastic material at low strain regimes the presence of other structures such as sutures or other extraneous fibrous tissue, which are not necessarily linear elastic, that are present around the craniofacial skeleton can impart nonlinear behaviour to the structure. The data shows that for the gauges that do not suffer from excessive noise the strain at a particular gauge increases linearly with load application. This confirms any assumptions that may be made in modeling of the CF skeleton regarding the linearity of the bone material properties under the strain regimes encountered *in vitro*. This also has implications on physiological loading because the *in vitro* experiment load of 100 N was chosen to be physiologically relevant. As such it appears assumptions regarding material property linearity also hold for typical loading that may be encountered physiologically in the CF skeleton.

Comparison of the gauge strains across the three different load cases reveals similarities in terms of the distribution of strain magnitudes. Across all load cases gauge 11, which is located on the anterior maxilla, exhibits the highest strain and is very similar for both masseter loads and lower for the temporalis load. This shows that this gauge has very high strains and in the *in vitro* testing it was important in bearing the applied loads. The high strains are also present at the location adjacent to gauge 11 and suggest that the anterior portion of the maxilla facilitates the preferred load path. This result is counterintuitive because of the off centre nature of the load application that would suggest the generation of large moments that would be born by the maxillary buttress region closer to the molars. However, because the molars were removed for radiological concerns about amalgam fillings, they did not participate in bearing load. This still presents a valid loading scenario, which required attention during application of the boundary conditions in the computational model.

Comparison of the masseter loading cases reveals very similar patterns across all the strain gauges. One difference occurs in gauge 5, which is adjacent to the anterior portion of the masseter origin where the measured strain suggests that the masseter load 1 produced a greater strain, and therefore load distribution in this region. The strain due to masseter 1 loading was 65.4 microstrain and due to masseter 2 loading was 34.9, however, comparing this value against the strains from the 50 N and 75 N load magnitudes reveals that the 100 N strain does not fall on a linear line which would suggest that for the 100 N masseter 2 load case the gauge was in error and the true strain would be high and therefore the difference for gauge 5 at 100 N between masseter 1 and masseter 2 load was less than 50%. Previous *in vitro* mechanical testing of cadaveric bone did not report the use of several different load magnitudes. Even though bone is considered linear elastic the only other study that measured cortical bone strains in the maxilla did not demonstrate testing at different magnitudes. Regardless, it was important to demonstrate that nonlinear behaviour such as plastic deformation or buckling modes of the very thin maxillary sinus, where not present under the applied loads.

3.5 Conclusions

The measured strains exhibit low variability and excellent reproducibility over a majority of the load directions, magnitudes and positions. As such the confidence in the measured strains is high. One important outcome of this study was the demonstration of the linear relationship between the strain measured at a particular location and the load applied for a majority of the strain gauges. This suggests that the bone, at those locations at least displays a linear elastic behaviour. This confirms the validity of the notion that because of the advanced age of the specimen (74) that the sutures between the various bones are calcified which makes the material properties of those sutures similar to the properties of bone and that approximating the sutures as bone would be a valid approach. The restraint chosen provides a rigid reaction system against the applied loads and can be accurately represented in the computational modeling. The presented method provides for an accurate measurement of the tension load application to the musculature, which permits translation of the forces to the computational model.

Chapter 4: Craniofacial Skeleton Segmentation

4.1 Introduction

Subject-specific finite element models that attempt to predict *in vitro* strains require accurate reconstruction of the skeletal geometry. Computed tomography (CT) scanning is a common imaging modality used clinically to assess skeletal pathologies. It provides insight into the internal structure of the skeleton by measuring the x-ray attenuation coefficient of a spatial location, which can be correlated to tissue type and is best suited for skeletal imaging because of the difference in the radiological properties between bone and soft-tissue. As such CT imaging can provide unparalleled morphological information about the human craniofacial skeleton for geometrical reconstruction.

Medical imaging provides information that forms the basis of many clinical diagnoses. However, the interpretation of imaging data is not easy, requiring trained personnel to correctly interpret the data generated by these systems, because of inherent limitations. The limitations of CT cause ambiguity in defining the boundaries between adjacent tissues and between different types of tissues, a concern that is compounded by noise. The requirement for human interpretation can be a time consuming process that is subject to human error and subjectivity in the delineation of the structures of interest. The identification of tissues from medical images is commonly referred to as segmentation.

In order, to improve image interpretation considerable interest has been invested in computational processing of medical image data to reduce human intervention and increase the repeatability of segmentation. The field of medical image processing is a rapidly growing field that has seen many new algorithms developed for common segmentation tasks.

Segmentation is such an important field that the National Institutes of Health has provided funding for the development of the Insight Toolkit (ITK) (Kitware Inc., Chapel Hill, NC), an open source software package developed for the specific purpose of image processing and segmentation. ITK contains many robust and proven algorithms for segmenting medical images. The purpose of this study was to use ITK algorithms to develop a methodology to semi-automatically segment craniofacial skeletons and differentiate between cortical and trabecular bone from computed tomography images for the development of subject-specific geometries to be used in the construction of finite element models for validation against *in vitro* mechanical testing. It is hypothesized that CT intensity and gradient information can be used to delineate between cortical and trabecular structures with semi-automated computational methods.

4.2 Methods

4.2.1 Introduction

Computed tomography images are grayscale images where the voxel intensities (in Hounsfeld Units HU) can be used to extract bone structure. A simple processing technique, called thresholding, can be used to identify those voxels that fall within a user-defined range of values. However, at the lower limit voxel intensities for bone can overlap into values that occur for soft tissue, thereby erroneously confusing the identification of soft tissue as bone. This problem is mainly caused by partial volume averaging, where structures that are smaller than the resolution of the scan have a low intensity. This partial volume averaging occurs in thin bone regions of the sinuses of the craniofacial skeleton and also in trabecular bone. Trabecular bone resembles a sponge-like porous structure with rods and plates of bone that are often much thinner than the resolution of the CT. It is for these reasons in addition to inherent noise in CT scanning due to non-linear effects like artifacts due to metals and micro-motion of the skeleton that can make thresholding an unreliable approach. However, change in intensity between adjacent tissues also provides information about the location of the boundaries where gradient magnitude information can also be used to segment the structures.

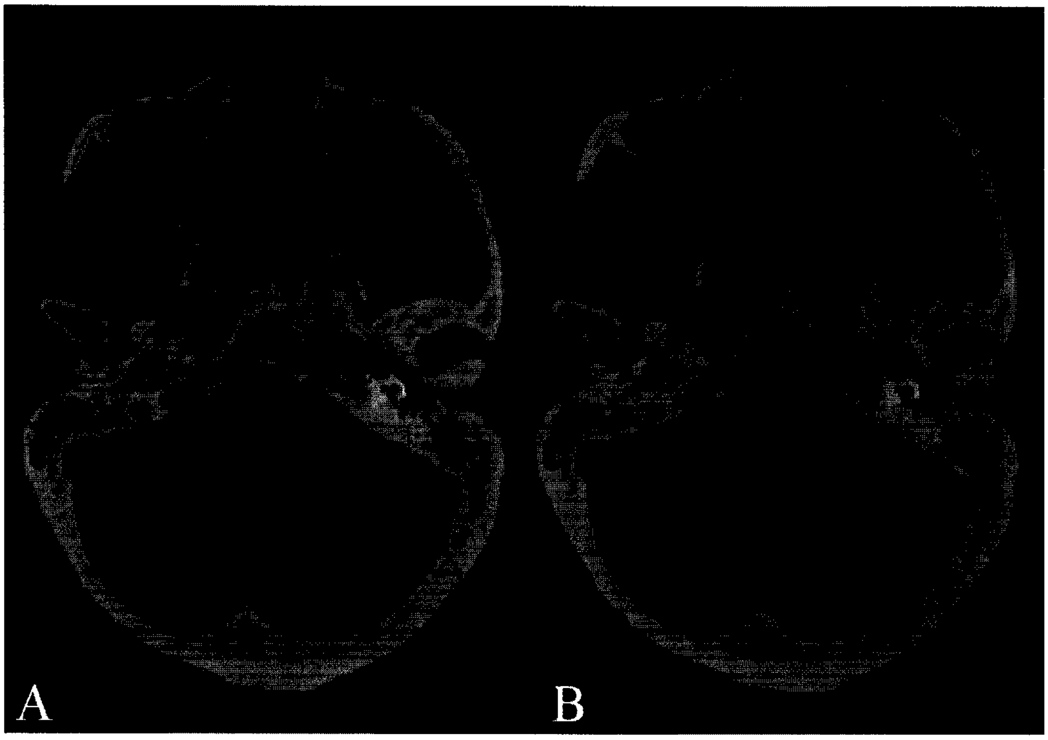

Figure 4-1 – A) Single CT slice of fresh frozen skelton. B) CT after anisotropic smoothing.

4.2.2 Skeletal Segmentation

A CT scan of a preserved craniofacial skeleton (10% buffered formalin) was acquired at a slice thickness of 0.6mm with an in-plane resolution of 0.488mm. Segmentation methodology was initially developed for the preserved specimen. A CT scan of the craniofacial skeleton was also acquired of the fresh frozen cadaver used for *in vitro* strain measurement at a slice thickness of 0.8mm with an in-plane resolution of 0.523mm. Both scans were resampled to an isotropic resolution matching the in-plane resolution (preserved = 0.488mm, fresh = 0.523mm) using a Lanczos filtering kernel. This isotropic resolution was required for subsequent image processing routines. All following methods, except where stated, were applied to both the preserved and fresh frozen craniofacial skeletons.

An anisotropic filter was applied for 10 iterations to smooth the image (fresh frozen specimen data presented) in order to reduce the noise and homogenize trabecular bone regions (Figure 4-1b). This filter is an anisotropic diffusion filter (ITK::CurvatureAnisotropicDiffusionFilter) that preserves the sharpness of the external cortical boundary while smoothing internal regions. A common interpretation of this scheme is that the output at any time point is the solution to the heat diffusion equation that defines a variable conductance that is based upon gradient information. This is in contrast to a Gaussian smoothing algorithm that acts to blur edges while denoising noise and was deemed inappropriate for this study because of the interest in accurately defining the boundaries between bone and soft tissue.

A thresholding method can be applied to the smoothed scan, but such an approach is non-specific and would still include structures external to the bone. However, a constraint can be placed on thresholding that ensures the developed segmentation is of a continuously connected structure. This functionality is facilitated by a connected components scheme (ITK::ConnectedComponents) that requires a seed voxel to be defined by the user. The algorithm begins at this voxel and searches all adjacent voxels for those that fall within the user defined threshold range and continues the segmentation until no additional voxels are identified. This algorithm was applied to the smoothed scan with a seed, which is a single voxel from which the algorithm grows the segmentation, index of 130, 340, 100 (fresh frozen specimen) which is located on the thickest cortical bone of the occipital bone. The threshold range selected was from 150 HU to 3200 HU (the maximum). An aggressive threshold, meaning one that has a lower end for the range means that more bone will be correctly segmented. The upper limit of the threshold range is fixed because only bone and artifacts caused by metal produce such high intensities and therefore is always the same.

The resulting segmentation required manual user intervention in order to fill holes that were not captured by the segmentation; this occurred mainly in the trabecular centrum of the maxilla, zygoma and orbits. The automatic hole filling function (Amira) could not be used on all slices of the CT because the craniofacial skeleton has many sinus void regions that would be incorrectly segmented by a hole filling method. Because of this, manual selection of holes in the segmentation was performed using Amira's interactive segmentation tool. Also the developed method is unable to identify the thin sinus bones because of partial volume averaging which required manual user segmentation using the brush tool available in Amira. Internal sinus bones of the upper nasal airway and eye orbits were not segmented manually. This omission was considered acceptable because of the small role those sinus regions are expected to play in physiological load bearing.

4.2.3 Cortical Bone Segmentation

Preliminary studies of the craniofacial FE model revealed the high sensitivity of the surface cortical strains to the assignment of a uniform local cortical bone thickness. A model developed of the pelvis revealed the highest correlation with *in vitro* data of models that included measurement of local cortical thickness [39]. However, in that study, a manual segmentation (procedure not presented) was performed on cortical bone and was the basis of cortical thickness measurements. The same problem with using a thresholding approach for segmenting bone in general persists in segmenting cortical and trabecular bone. Thin sinus cortices have low intensities overlapping that of trabecular bone and regions of very dense trabecular bone exhibit intensities overlapping with cortical bone. To address this problem a class of filters known as level set filters were considered for segmenting the cortical-trabecular boundary.

Level-set based computational image processing algorithms operate on the basis that the user is interested in knowing the position of a boundary and that this boundary can be identified by structural information such as the magnitude of the gradient of the image. The level set algorithms track the evolution of a contour that represents the boundary of interest, where the evolution of this contour is influenced by the shape information. Generally, transition between homogeneous regions involves a gradient at the transition zone that defines an edge or boundary. This occurs in the craniofacial skeleton both at the external cortical boundary and at the cortical-trabecular interface.

The level-set algorithms available in the ITK are best suited for small adjustments of a coarse segmentation to provide a more accurate estimate of a boundary. The Geodesic Active Contours Level-set Image Filter (ITK::GeodesciActiveContourLevelSetImageFilter) was chosen to perform the segmentation of the cortical bone mainly because craniofacial cortical bone is a shell structure and segmenting it requires very fine adjustments with high accuracy. Because the external cortical segmentation was already developed it provided an excellent initial starting position for the level-set filter.

The level-set filter requires a speed image that defines the speed of the contour representing the boundary. The main idea is that the speed image has a value of 0 at the locations that the curve is desired to stop and 1 at locations where the boundary is to evolve quickly. An analogy is the propagation of a wave formed by a drop of water hitting a pond. The speed at which the wave travels from the location of impact is the same everywhere, which results in the typical circular shape of the wave. The speed image in contrast allows the speed of the wave to be different at every location and permitting it to take on an almost arbitrary shape for structures with irregular boundaries.

The cortical-trabecular boundary can be located by a gradient magnitude, but so can the external cortical surface. However, the gradient across the cortical-trabecular boundary is smaller than the external cortical surface and formed the basis for constructing the speed image. A band pass filter was constructed by two sigmoid filters that assigned a high speed to both low gradient homogeneous regions and the high gradient external cortical surface while assigning low speeds for the mid-range gradient magnitudes of the cortical-trabecular boundary. The sigmoid transformation ($y=1/(1-e^{-x})$) normalizes the gradient magnitudes to a range of 0 to 1 around a specified location, which is required by the level-set method. The speed image was based upon a Gaussian smoothed gradient magnitude image of the CT scan. The kernel size for the preserved specimen was 0.035. For the speed image one sigmoid was constructed at a gradient magnitude of 3000 with a relaxation of -750 (gradient $< 3000 \approx 1$) and the second at a magnitude of 6000 with a relaxation of 1000 (gradient $> 6000 \approx 1$). The kernel size for the preserved specimen was 0.05. For the speed image one sigmoid was constructed at a gradient magnitude of 3000 with a relaxation of -750 (gradient $< 3000 \approx 1$) and the second at a magnitude of 6000 with a relaxation of 1000 (gradient $> 6000 \approx 1$).

Pilot studies were conducted examining curve evolution parameters (propagation, curvature and advection) for identifying coarse parametric ranges suitable for further refinement. The three parameters control the relative influence of the different terms of the curve evolution equation. Optimization of the level-set segmentation was performed using automated analyses (+1000) that varied the control parameters and evaluated the outcome against a manually user defined gold standard segmentation of the cortical-trabecular boundary using a volumetric concurrency (VC) metric that is defined as the average value of the ratios of the volume of the intersection region between the automated and manual segmentations and individual volumes, as follows:

$$VC = \frac{\frac{Vol_{intersection}}{Vol_{Manual}} + \frac{Vol_{intersection}}{Vol_{Automatic}}}{2}$$

Manual segmentation of cortical bone in the craniofacial skeleton was limited to the facial skeleton. This segmentation was not required because the cranial vault does not play a role in the facial biomechanics that involve the mastication muscles and structures involved in mastication that was the focus of this study.

4.3 Results

4.3.1 Skeletal Segmentation

The external cortical boundary of the fresh frozen craniofacial specimen was segmented using the developed technique (Figures 4-2). The developed method reduced the amount of manual intervention required to remove spurious external voxels called islands that would be abundant with a thresholding only method. The most time consuming method is the manual user intervention and with the developed algorithm segmentation of craniofacial specimen was achieved in approximately 3 hrs.

Figure 4-2 – Complete segmentation of craniofacial skeleton using the proposed method of anisotropic smoothing, connected components and manual intervention.

4.3.2 Cortical Bone Segmentation

The automated level-set segmentation technique produced a volumetric concurrency of 0.904 for the facial region of the preserved skeleton with a concurrency of 0.936 of the maxilla and 0.719 for the facial region of the fresh frozen specimen with a concurrency for the maxilla of 0.846. The maxilla was considered separately because it was qualitatively the best segmented structure for both specimens for the optimized level set parameters. Representative slices of the outcome of the automated segmentation against the manual definition are shown for the preserved and the fresh frozen skeletons (Figure 4-3). The best-fit scaling parameters for the preserved specimen were: propagation=1, curvature=1.5 and advection=1. The best-fit scaling parameters for the fresh frozen specimen were: propagation=1, curvature=1.5 and advection=0.5.

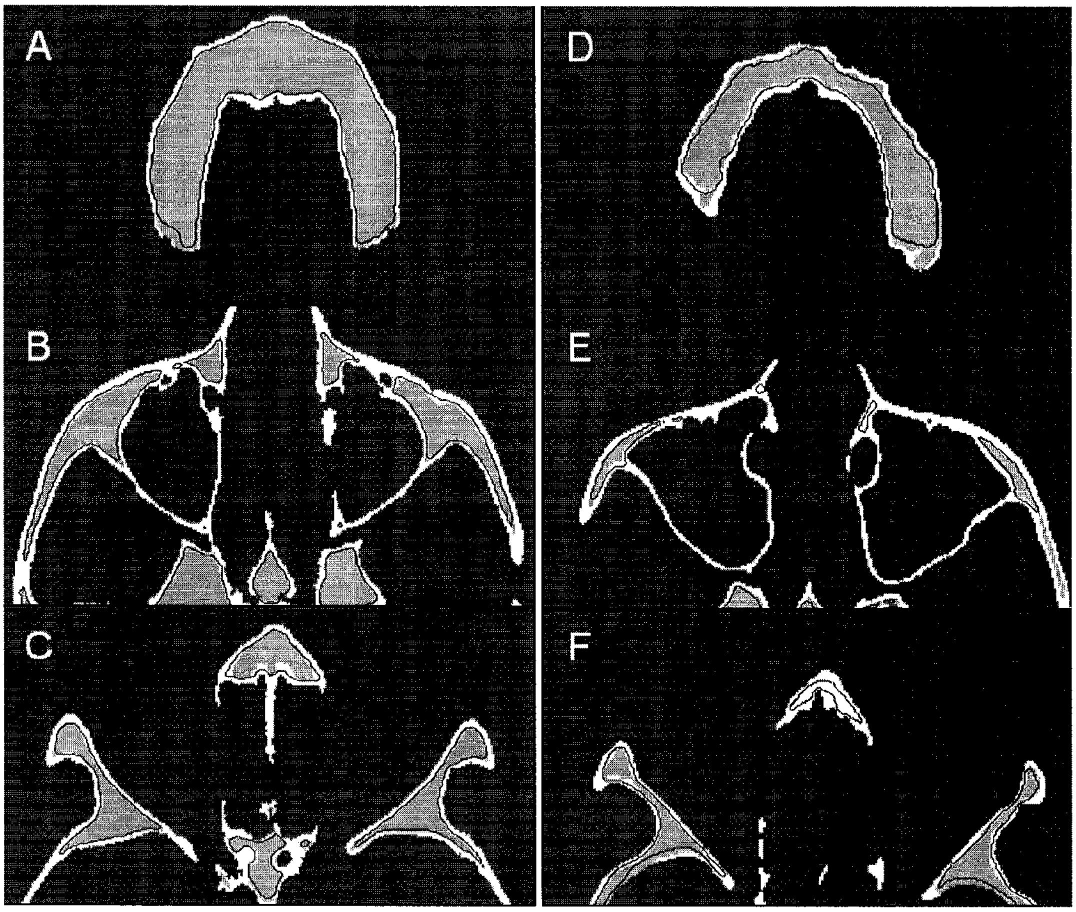

Figure 4-3 – The black contour represents the automated segmentation in all cases. White is cortical bone and light grey is trabecular that was manully segmented. A) Preserved specimen maxilla, B) Preserved specimen zygomas, C) Preserved specimen orbits. D) Fresh frozen specimen maxilla, E) Fresh frozen specimen zygomas, F) Fresh frozen specimen orbits.

4.4 Discussion

4.4.1 Skeletal Segmentation

The developed methodology that uses edge-preserving smoothing and a connected components constrained thresholding method provided a CF segmentation that required less manual intervention than would a straight thresholding technique by allowing for a more aggressive threshold to be used. A threshold of 150 HU is required to include as much material as possible, but inevitably results in the inclusion of voxels external to the region of interest. Removal of these points of noise requires the use of Amira's island removal method. As such the large number of islands that remain after a simple thresholding are reduced with the developed method. This in turn requires less review of the segmentation by the user for the purpose of assessing the need for further island removal. With thresholding more noise is included at lower thresholds and the resulting holes in the trabecular bone are irregular and numerous. The same threshold used with the connected components scheme on the smoothed image includes virtually no noise and fewer holes (Figure 4-4). Neither the thresholding technique nor the proposed technique can create a continuous segmentation of the thin sinus bones, however, the latter substantially reduces the islands in the nasal sinuses.

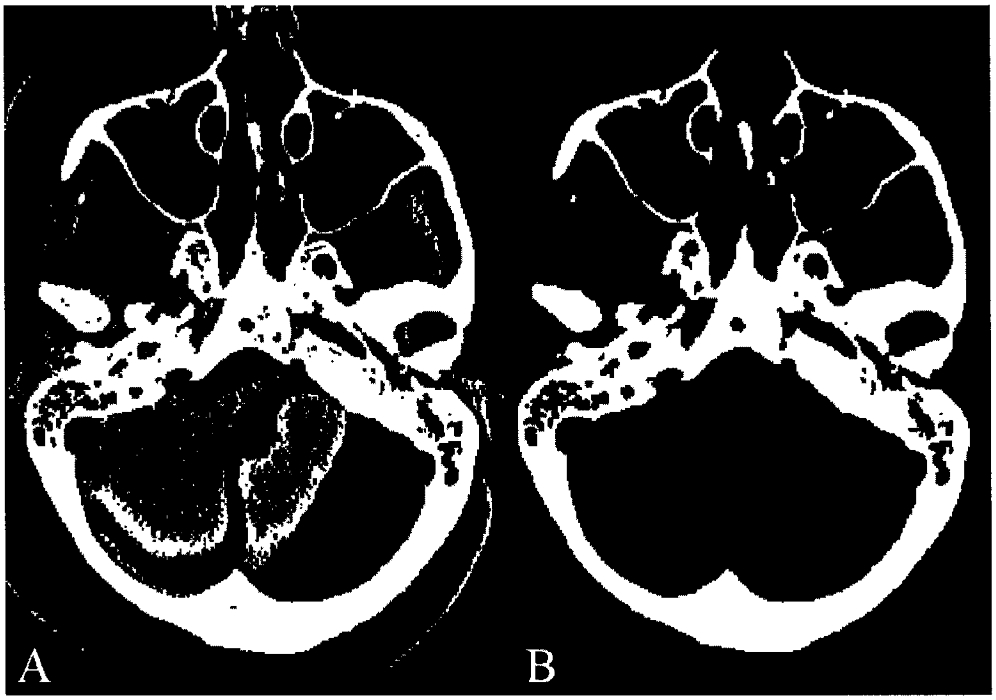

Figure 4-4 - A) Segmentation using threshold and B) Segmentaion using smoothed CT and connected component. Both using a lower threshold of 150 HU.

The craniofacial skeleton is an extremely complex structure consisting of large variation in curvature and distribution of cortical and trabecular bone. Thin bone regions are difficult to segment using thresholding and the developed smoothed thresholding techniques due to partial volume averaging effects. Future work could seek to implement an algorithm presented by Descouteaux et al.[71] specifically for segmenting the thin sinus bones of the craniofacial skeleton.

4.4.2 Cortical Bone Segmentation

The level-set segmentation scheme developed for this study was able to provide a segmentation of the cortical-trabecular boundary. The sigmoid band-pass filter succeeded in establishing high speed in the high gradient regions of the external cortical bone. This is important because the initial position of the contour was on the cortical boundary and high speeds are needed in order to induce the contour to evolve towards the cortical-trabecular boundary.

Parametric sensitivity studies reveal that the curvature scaling parameter causes the boundary to become smoother and prevents the curve from developing cusps and corners due to local noise that may produce high speeds. However, a high curvature scaling reduces the local speed of the evolving boundary thereby requiring more iterations and therefore computational effort to complete the segmentation. Additionally, too high of a curvature scaling will decimate fine details that may be the true nature of the structure and so a fine balance must be sought that economizes smoothness with accuracy. Smoothness is imposed on a segmentation because, although the differentiation between cortical and trabecular bone is somewhat arbitrary, at the chosen level bone is assumed to be smooth with no discontinuities.

The segmentation algorithm achieved an overall concurrency metric of 0.904 for the preserved and 0.719 for the fresh frozen specimen. Visual inspection reveals that the approximation of the boundary was best in the maxilla region for the set of parameters identified as resulting in the best segmentation (propogation =1, curvature=1.5 and advection =1) and the solution converged after 100 iterations. However, the approximation of the boundary was poorer for the regions of the zygoma and orbits. Although the differences between the manually and automatically defined boundaries are on the order of 1 voxel this equates to a thickness difference of approximately half a millimeter. The scan resolution is ultimately the detection limit for any structure and is simply a limitation of the CT scan and not the method. The difference in agreement and the zygomas and orbits suggests that globally defined parameters are insufficient to effectively segment the cortical bone of the entire craniofacial skeleton. Due to the number of sensitivity runs conducted (1000+) the concurrency metric was chosen as the goodness-of-fit parameter rather than evaluating the fit in separate regions of the CFS. The level-set methods in general address an ill-defined problem with numerous parameters that can be varied to achieve the desired goal. Future work will have to determine the most appropriate parameters by evaluating the performance of the algorithm against individual regions; for example separately assessing the evolution for the maxilla, zygomas and orbits, the structures most important in craniofacial biomechanics. The same non-uniform behaviour was observed in the level-set segmentations of the fresh frozen model where the maxilla was segmented automatically with high accuracy resulting in a concurrency for that specific region of 0.846.

The effectiveness of the level-set algorithm is limited by the resolution of the CT scan used. In both cases the resolution was set at the maximum resolution achievable (preserved = 0.488mm, fresh frozen = 0.523) in that two different scanners were used between the specimen therefore causing the change in resolution. The differences in the concurrency metrics is related to the resolution difference between the two scans which differ by approximately 7% in each dimension for an overall difference of approximately 22.5% in the volume of each voxel. The implication of this difference is that the same amount of volume is represented by fewer voxels and so the metric is more sensitive to the voxels that are not common between the manual and automated segmentations.

Issues related to insufficient contrast at the cortical-trabecular interface for the fresh frozen specimen are related to the morphological variation seen between the two craniofacial skeletons in addition to the resolution. The differences exist mainly in the zygomatic region where the preserved skeleton has more mass and greater contrast between the trabecular and cortical bone that in the zygomatic regions of the fresh frozen skeleton, which is much thinner with the trabecular centrum of the zygomatic arch indiscernible from the cortical bone resulting in low gradients.

Although some regions of the skeleton are more difficult to segment using the automated technique, overall a level-set based approach presents a good method for several reasons. The methods as implemented in ITK are best for small changes to an existing segmentation as required for the thin cortical bone of the craniofacial skeleton. The level-set methods implicitly allow the evolving contour representing the boundary to merge and split while maintaining bulk connectivity and smoothness. The region splitting is important in areas of the external cortical segmentation such as the thin sinus bone and regions of the temporalis were there is no trabecular centrum or it is not evident from the CT scan.

4.5 Conclusions

The segmentation of the cortical-trabecular interface is important to the biomechanics of the craniofacial skeleton and an automated method is required to make the segmentation process repeatable and semi-automatic to eliminate or reduce the laborious process of manual segmentation. The developed method has reduced the amount of user intervention required to complete the segmentation of the craniofacial skeleton by denoising the CT scans and using a connected components scheme to segment bone.

The developed level-set segmentation method shows higher correlation with a manual segmentation for the maxillary region for both craniofacial skeletons used for this study and highlights the need for a multi-region approach to segmenting cortical bone in the craniofacial skeleton. Additional segmentation algorithms may be investigated for use on the extremely thin sinus bone regions. Overall the level-set approach presents a method that is capable of the accuracy required in thin cortical bone regions thereby making such important measurement repeatable and objective.

Chapter 5: Finite Element Model Development and Validation

5.1 Introduction

Finite element (FE) modeling is a versatile and robust platform for developing a better understanding of craniofacial biomechanics. It can provide a complete characterization of the stresses and strains that a human craniofacial skeleton must bear when subject to physiological or non-physiological loading. The FE method presents an alternative to *in vitro* mechanical testing for understanding load distribution in the craniofacial skeleton (CFS), however, the accuracy of the FE method in predicting the response to loading must be assessed before clinical interpretations of load distributions can be made. Both the FE method and the *in vitro* approach are simplifications of *in vivo* conditions in that not all the components of the true system are necessarily represented (such as the complete physiological loading encountered). However, many practical limitations prevent a complete knowledge of the response of the CFS from being understood in an *in vivo* model. The FE method provides the ability to apply multiple loading scenarios to understand their effects. In terms of clinical relevance, the FE model provides unlimited freedom to recreate pathologies and their treatment, to understand effectiveness as well as providing definite quantitative information about the mechanical conditions that tissue fixation and replacement technologies require to ensure successful osteosynthesis in a deformity.

It is clear that within the human anatomy there exist structures that bear morphological similarity, but that there exists variation in size and shape from person to person. The FE method has been employed to understand the general response of a class of structures in the human skeleton (i.e. vertebrae, femurs) [72,73]. The craniofacial skeleton is unique, however, because of the large morphological variation and distinctiveness that exists between individuals. Assessing the accuracy of a FE model against *in vitro* mechanical testing requires that the model be constructed to reflect the characteristics of the specimen and is referred to as subject-specific. The power of a single subject-specific model for providing insights into the biomechanics of all craniofacial skeletons is limited and basing clinical decisions on a single model would be irresponsible. Therefore the methodology would have to be demonstrated for a sample of the population that would include such morphological variation. It is unclear what factors influence craniofacial biomechanics, but by constructing models of multiple anatomies the mechanical response of each can be compared to determine if correlations exist between functional outcomes and morphological characteristics.

The development of a FE model on the subject specific level is an exercise in reverse engineering. However, in many cases the uncertainty in the level of detail required and in the empirical measurement itself of material and geometrical properties of skeletal structures requires additional scrutinization of those values that most significantly impact the intended outcomes. One could understand this as investigating the sensitivity of our abstract representation, the FE model, to limited information. Such studies can elucidate new needs for more precise information about certain parameters, which can change in a dynamic system like organic tissue and vary from subject to subject, as well as pathologies that may arise due to changes from the baseline. Such parametric studies can reveal their importance for the purpose of determining the accuracy of the FE models and establishing the sensitivity of the models to various geometrical, material and load-based factors. Sensitivity studies provide information and insight into how a system is affected by changes in underlying characteristics and impact on function that may be clinically significant.

The objective of this study was to develop a methodology for constructing subject-specific finite element models of the human craniofacial skeleton and validating the model by assessing the accuracy through comparison against measured strains from *in vitro* mechanical testing. The developed methods sought to incorporate subject-specific estimates of bone geometry and spatial variation of material properties derived from imaging data. This sought to evaluate the importance of using subject-specific cortical thickness measurements and the sensitivity of the developed model to the variability demonstrated by empirical estimates of the material properties of craniofacial bone.

5.2 Methods

5.2.1 Mesh Generation

5.2.1.1 Triangulation

A CT scan of a cadaveric specimen was used to produce a segmentation of the CF skeleton that described the external surface of the bone (see Chapter 4). The segmentation approximates tissue structure as a stepwise boundary contour that is smooth and continuous yet sometimes ambiguous, an artifact caused by the resolution limitation of CT. Although the voxel-wise segmentation lends itself easily to voxelated meshing, the discretization of the geometry from a voxel definition is limited by the fact that the stepwise nature of the surface would provide stress concentrations that are numerically manifest as singularities which numerical inaccuracies. As such, an alternative method is required that imposes smoothness on the boundary definition because of the dependence of the validation of the FE model on surface strains.

Reconstruction of the external cortical surface of the CF skeleton was performed using the SurfaceGen module in the commercial software package Amira (Mercury Computer Systems, Chelmsford, MA). The segmentation was used to compute a surface triangulation representation, which is a faceted surface composed of triangles, surrounding an empty core. The principles of the algorithm can be decomposed into two stages. First the method identified the boundary between different regions either inside, outside or between adjacent tissues. In the case of the developed CF model this includes regions defined as teeth, trabecular and cortical bone. The boundary was seeded by points in space and then the individual triangles were computed by a tangent sphere method using the Amira software. It constructed individual triangles by finding three points that would be coincident with an imaginary sphere traversing the surface. The seeding of the mesh points on the intersection of the voxels of the segmentation without smoothing resulted in a surface with similar stepwise structure as the segmentation.

5.2.1.2 Refinement and Smoothing

The reconstruction of the geometry required imposing smoothness constraints on the methodology. The smoothness can be controlled by the seeding of the boundary points. While the smoothness of the initial surface can be improved, the smoothing algorithm takes liberties in regions such as the sinus bones that are very thin relative to other structures (Figures 5-1). The reconstruction of the CF with smoothing would omit the sinus bone regions, which would not be included in the model and was therefore deemed ineffective.

Figure 5-1 - Result of SurfaceGen (Amira) using smoothing for the resonstruction. Note the lack of geometry in sinus regions due to the smoothing and the intersection of the tooth roots with the external surface.

The surface generation was performed without any initial smoothing (Figure 5-2); however, smoothing of the surface was performed through subsequent processing by a combination of triangle density reduction and shape modification. Because the triangulation is dependent on the resolution of the segmentation, the resulting surface was densely populated with triangles above that which was necessary or practical to implement. The computed triangulation produced a surface with over 2 million triangles. To reduce this density, adjacent coplanar triangles are removed by successive removal of the most coplanar triangles until the target mesh density has been achieved. This was done iteratively because the process of simplification combines nearly coplanar triangles into a new larger triangle that encloses the domain of previous triangles. This process naturally creates triangles that deviate from an equilateral shape.

Figure 5-2 - Surface generation without inital smoothing. Note compared to Figure 5-1 that the sinus bone regions are preserved and continuous.

The simplification of the surface proceeded in increments to the desired mesh density with smoothing of individual triangles performed at each increment to adjust the triangles towards an equilateral shape. This incremental method produced a surface triangulation with a drastically reduced mesh density that was smooth (Figure 5-3). In between the iterations of simplification of the surface, individual faces were smoothed through 2 iterations of the SmoothFaces method in the Amira Surface Editor. This is distinct from the smoothing triangulation, as region joining and splitting is not allowed using the SmoothFaces method. A total of 9 triangle densities were defined from the initial number of +2 million to 250,000. Only two iterations in between surface simplification iterations were used because of fast convergence of the method beyond which there was no benefit from the additional computational expense.

Figure 5-3 - Result of the iterative surface simplificaiton scheme with intermediate surface smoothing (Amira).

5.2.1.3 Tetrahedral Mesh Generation

The triangulated intermediate surface provides the initial condition for generating the internal discretizations of the geometry using tetrahedral elements. To generate the 3D elements the Delaunay mesh generation algorithm was used (Amira). This method used the triangulation as the initial front from which layers of tetrahedra are constructed towards the centre of the object. The density of the mesh is dependent upon the density of the surface triangulation. Tetrahedral density was determined by several surface triangulations that varied the surface mesh density (Table 5-1). Each tetrahedral mesh was generated by successive reductions in the numbers of surface triangles by the described surface simplification and smooth faces methods.

5.2.2 Mesh Density Convergence

Finite element mesh density is important, as the quality of the solution to the governing partial differential equations is dependent on the coarseness of the mesh. To address this concern a mesh density convergence study was conducted. Mesh density convergence refers to the computational efficiency of the mesh at providing the desired accuracy with the minimum amount of computational effort. It is determined by tracking standard outcome parameters of a model that are related to the purpose of the models. Convergence is a matter of subjectivity in that the theoretical behaviour should be an asymptote where the increasing density improves the approximation of the 'true' solution and an acceptable level must be assessed by the investigator. Several different surface mesh densities and tetrahedral mesh densities were generated (Table 5-1). Convergence was assessed by identifying the density at which further increases did not produce significant change in the outcome variables due to diminishing returns.

For this study the local strains from the FE models averaged over the same area that is representative of the strain gauge were chosen as the outcome parameters to assess convergence. Mesh density convergence should only depend upon the geometry and discretizations and so an arbitrary load can be used to assess this. However, to ensure convergence for a loading scenario similar to the *in vitro* testing a uniform vertical load of 100N was applied to the masseter origin surface attachment for all mesh densities. The local strains are of primary interest in the models and it is important to demonstrate the density at which strains become stable. Global parameters such as mean stress and strain and total strain energy are valid if global behaviour is of interest. However, maximum stresses and strains are subject to singularities, which cannot be eliminated by a higher mesh density, and would produce irregular patterns even though convergence may have been achieved. The maximum displacement of the model was also used to investigate global convergence behaviour. The mesh density at which all gauge strains become stable was chosen as the baseline model for comparison against the *in vitro* mechanical testing and sensitivity studies of model input parameters. Stability was defined as a change in the gauge strain of not more than 10% or a change of less than 10 microstrain.

Table 5-1 - Meshes used for mesh density convergence study.

# Triangles	# Nodes	# Tetrahedra	Tri/mm^2
40,000	25,638	94,152	0.207
60,000	46,397	187,768	0.309
82,500	73,428	315,505	0.425
100,000	92,506	402,433	0.514
125,000	127,546	573,242	0.645
150,000	161,502	737,433	0.770
200,000	230,831	1,072,820	1.028
250,000	370,066	1,819,667	1.280

5.2.3 Material Property assignment

5.2.3.1 Tetrahedral Elements

The geometry of the subject-specific model of the CF skeleton was based on the specimen CT scan. The intensity of the CT scan also provided information as to the distribution of bony material properties within the CF skeleton. Local apparent density in bone has been shown to correlate with both CT image intensity in Hounsfeld units (HU) and elastic modulus. A method for incorporating element specific material property assignment was incorporated into the models using the Bonemat method described by Taddei et al. [48] the algorithm produced a mapping of the average CT scan intensity of the voxels that are within the domain of each element (Figure 5-4). The intensities, which are defined per element, were then scaled to the apparent density of the element using an empirical calibration curve for the particular CT scanner and scanning parameters. The apparent densities were transformed into an elastic modulus using the empirical relation: $E=2017.3\rho^{2.46}$ [39] to produce a heterogeneous distribution of elastic moduli (Figure 5-5).

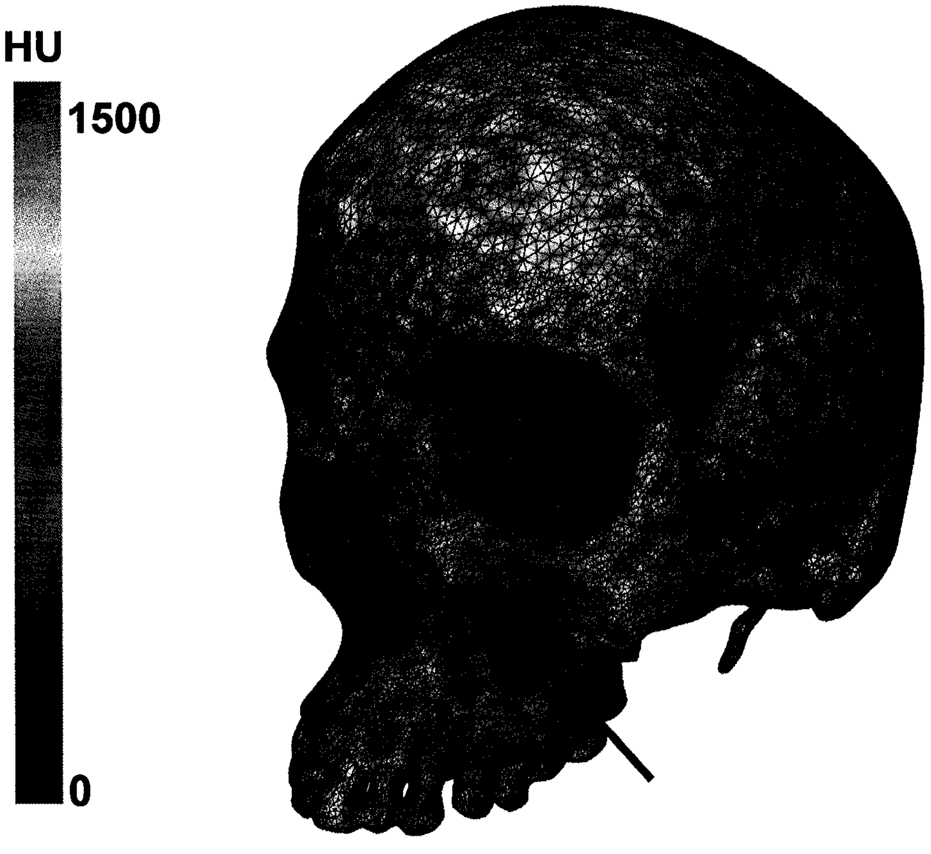

Figure 5-4 – Hounsfeld unit (HU) intensity mapping on the the tetrahedral grid. Partial volume effects are evident on the surface tetrahedra as cortical bone usually has a value of 1200+ HU. Contour plot ranges between 0 (water) and 1500 HU. Note the extremely low intensity approaching that of water at the sinus region (denoted by arrow).

The CT derived material properties assign a unique value to each element. In a model that can include hundreds of thousands of elements, having a separate material definition for each element require a great deal of memory and computational effort. Such detail may not be necessary to capture the behaviour of a system in which there may be only small differences between adjacent elements. As such elements that have very similar assigned properties can be described by a common material definition thereby dramatically reducing the number of material definitions while still approximating the established distribution. The grouping of the elements was performed by dividing the range of elastic moduli values into segments or bins of identical width. A search of the mesh was used to assign elements into each particular bin. The grouped elements were then assigned an identical single elastic modulus that was chosen to be the mean of the range for a particular bin. The range of elastic values is bounded at the upper limit and therefore the number of bins created is dependent on the width or range of each bin. As such, because the material properties of all the elements in a particular bin were changed to the mean of the bin, the error between values assigned by the image and that assigned by the binning decreases as the bin width decreases. Zannoni et al. [48] demonstrated that 600 material property bins represent the saturation point beyond which further decreases in bin width did not appreciably affect bony model outcome values. The baseline bin width chosen was 50 MPa, which produced approximately 600 material property bins.

one shell thickness over the tetrahedral elements with exposed external faces corresponding to the surface triangulation (Figure 5-3).

The shell element mesh also helps resolve inconsistencies with a pure CT based assignment of material properties. Partial volume effects are caused by the limited resolution of CT that results in voxels that are partially occupied by a structure and produce artificially low image intensities due to averaging over the whole voxel. As such the material property assignment underestimates the stiffness of surface tetrahedra that are affected by partial volume effects. This problem is compounded by the mesh density used in that the assignment of the average intensity for a single element also depends upon its size and therefore large elements can potentially be assigned artificially low intensities because they may span a region of various intensities. Although this produces a smoothing effect it can become problematic if the tetrahedra become too large. This underestimation occurs in the sensitive boundary region, which is the region of primary interest in validation of the FE model. Applying the shell element mesh to the model enforces the cortical bone stiffness to the surface.

Qualitative review of CF morphology revealed a heterogeneous distribution of cortical shell throughout the skeleton. The individual shell elements were thus assigned a location specific cortical thickness measured from segmentation of the CT scan (Figure 5-13). The cortical bone was manually segmented because of insufficiency in the developed segmentation algorithm for the fresh specimen (Chapter 4). The measurement of local cortical thickness was implemented using a stepwise normal distance measurement. The measurement was made by translating along the inward normal of each triangular shell element until the current position was outside the segmentation of cortical bone. The corresponding shell element was then assigned the distance from the triangle centre to the trabecular bone segmentation (Figure 5-13). To reduce the number of unique material property definitions shell elements were grouped using a binning procedure as for tetrahedral elements with a bin width of 0.01mm. All shell elements were assigned an offset value of half the thickness associated with that element. This ensured that the top surface of the element was coincident with the surface triangulation. Much like a beam the midplane is defined by the triangle and the offset makes the top of the beam, which is a virtual geometry, match the external surface by setting the midplane to reside half a thickness inside the first layer of tetrahedral elements.

The shell thickness measurement determines the stiffness of each particular element. This is analogous to a thick beam being more resistant to bending than a thinner beam. However, this element still requires a material property definition. The material of the cortical shell element was assumed to be linear elastic and isotropic with an elastic modulus of 12 GPa and a Poisson's ratio of 0.3. This is in accordance with the published values for the experimentally measured elastic modulus of cortical bone [21,43,45].

The hybrid shell-solid mesh results in an overlap of one cortical shell thickness because the surface triangulation corresponds to the external faces of the surface tetrahedral elements. Because of this the tetrahedra in the overlap region must be adjusted to compensate for the double stiffness that would occur if the tetrahedrons were assigned the CT based material properties regardless of the partial volume effects. The elastic modulus of the interface layer consisting of the tetrahedrons with one side on the surface of the model was chosen to be 300 MPa, representing the average value [39] for the elastic modulus of trabecular bone to provide connectivity and therefore load transfer between the cortical and trabecular bone. However, because of the two orders of magnitude difference between the cortical bone and trabecular bone elastic modulus the load distribution is assumed to occur largely throughout the cortical bone.

5.2.4 Sensitivity Studies

The strains at the gauge locations measured from the *in vitro* model as computed by the FE model are dependent, in addition to the FE mesh density, on the material property assumptions that define the degree of deformation for a given load. As such, uncertainty in the material properties, such as the image derived elastic modulus, the cortical bone elastic modulus and the shell element thickness, will impact the accuracy of the FE predictions. Sensitivity studies of model input parameters will provide information regarding the importance of various material property assignments in determining the biomechanical response of the CF skeleton and accuracy with respect to the *in vitro* strain measurement.

For all the subsequent sensitivity analyses a sensitivity outcome measure was defined as per Anderson et al. [39] as the ratio of the percentage change in the calculated regression slope to the percentage change in the input parameter from the baseline model. For the cortical thickness sensitivity the percentage change was calculated between the constant cortical thickness values.

5.2.4.1 Material Property Assignment

The hybrid shell-solid mesh requires the definition of a relatively low material property for the tetrahedral elements that are adjacent to the surface triangle shell elements. Previous models have used either 0 MPa [39] or 0.0001 MPa [51] for this interface layer (note: the latter model did not use 0 because the commercial FE software did not allow such a value). The value chosen for this study was 300 MPa and is based upon the reported average modulus of trabecular bone to provide connectivity between the cortical surface and bulk trabecular bone, however, due to the values presented in the literature a sensitivity study was performed to assess the effect of this value on the standard outcome parameters used in the mesh density, material property and shell thickness binning studies. The baseline model was altered by setting the modulus of the interface layer to 0.001 MPa. (IDEAS software also does not permit a 0 elastic modulus to be defined).

In a similar manner sensitivity studies were conducted on the elastic modulus and the Poisson's ratio of the cortical shell elements. The study was based on values reported in studies that measured the elastic modulus of craniofacial cortical bone at various positions throughout the human craniofacial skeleton [21,43,45]. Sensitivity models were all based upon changing a single parameter at a time in the baseline model. Models were generated for elastic modulus values of 10, 12, and 17 GPa and Poisson's ratios of 0.2, 0.3, and 0.4. The purpose of this study was to assess the global cortical bone modulus that would produce the best agreement with the *in vitro* testing results to determine the sensitivity of these parameters to provide an assessment the of accuracy required to calibrate the models.

5.2.4.2 Shell Thickness Sensitivity

The shell thickness associated with the cortical shell elements will change the effective material properties of those elements. Because shell thickness is measured and subject to error it is important to assess the sensitivity of the model to this parameter. A baseline model was constructed in which the local cortical thickness was derived from the segmentation of the specimen CT as described in section 5.2.3.2. Error in the thickness measurement is related to the resolution of the CT image. In this study an image resolution of 0.52 mm was used after resampling the axial slices from a distance of 0.6mm. The segmentation must identify each voxel as either belonging to cortical bone or not, thus the minimum thickness measurable is on the order of the voxel dimensions. Hence, the confidence in correctly identifying structures that are on the order of or smaller than the CT scan resolution (0.52mm) is low. Additional models were developed to assess whether local cortical thickness was more accurate than assuming a uniform thickness for the cortical shell throughout the facial skeleton. Models were developed using uniform thickness values of 1.0, 1.5, 2.0 and 2.5 mm. These values are representative of the range of values reported by Dechow et al. [21,43,45] for various CFS locations for cortical bone.

5.2.5 Boundary Conditions

5.2.5.1 Load Application

The loads applied to an FE model represent the external perturbation that acts to deform a structure. In order to validate the FE model the loads applied must be equivalent to those applied in the mechanical testing. As discussed in Section 3.6 several points on the loading apparatus were digitized and transformed to the coordinate system of the FE model. The transformation was facilitated through the measurement of fiducial markers on the cadaveric specimen and identifying those markers in the CT scan. The transformation between the *in vitro* and CT positions was computed using the *computeRigidTransform* function in Amira. These points were the basis for computing the line of action of the forces applied to the origin areas of the masseter and temporalis.

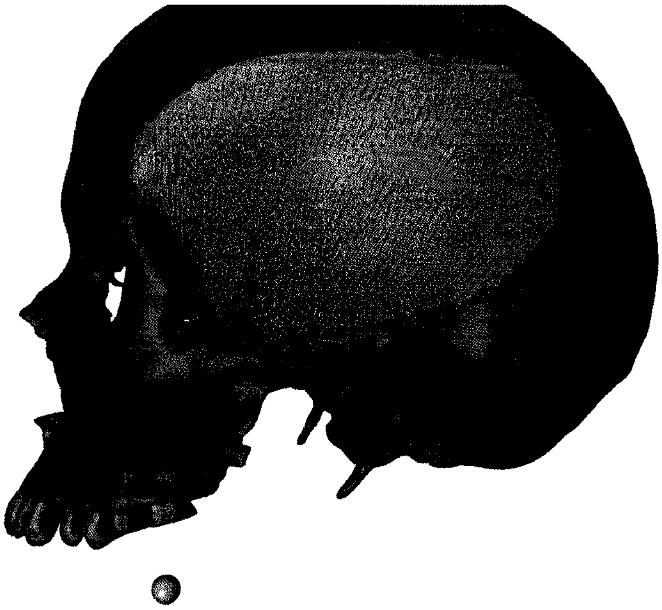

Figure 5-6 - Temporalis orgin (green) with individual nodal force vecors assigned and directed towards the single point landmark measured from the in vitro testing and transformed to the model co-ordinate sstem

The 100 N forces transmitted to the origins of the masseter and temporalis muscles from the hydraulic actuator were modeled as a collection of forces applied to the FE model nodes belonging to the identified insertion of the muscles. This method permits a unique line of action to be defined per node. The algorithm for computing the force vector on a particular node used the digitized points from the masseter and temporalis interface plates. In the case of the temporalis the muscle fibers converge to essentially a point and so the vector from a surface node was directed from the node to the digitized point (Figure 5-6). The magnitude of one nodal force was determined by dividing the total force (100 N) by the number of nodes belonging to the insertion. Additional constraints were applied to the load vector calculation because of a special requirement of the temporalis. After each force vector was computed a check for intersection with the surface triangulation was performed to determine if the vector penetrated the surface of the model. This is because in the case of intersection, the muscle fibers and therefore the direction of load are oriented tangent to the surface and so assigning a force from a temporalis node towards the force landmark would produce a vector that would then penetrate the surface. This is not the true situation so a method was devised that if an intersection was found then the vector at that node location was projected onto to the intersecting triangle by: 1) computing the cross product of the intersecting vector with the plane normal to get a vector tangent to the plane and 2) computing the cross product of the tangent vector with the normal to find the new force vector that is tangent to the surface, but also preserves the original orientation towards the digitized force landmark without penetrating the surface. This procedure was necessary because the temporalis attaches to a curved surface and intersection is common when computing the vector from nodes to the interface landmark.

The same procedure of nodal force magnitude was applied to the masseter insertion but the direction of an individual nodal force vector was based upon the two points of the masseter interface plate that define the perpendicular line to the load direction (Figure 5-7, 5-8). The direction of a particular nodal vector was defined as a vector perpendicular to the line formed by the two digitized interface plate points. However, a constraint was placed on the vectors to be directed towards the line segment formed by the two interface points. This meant that if the computed vector did not intersect the interface plate line segment it was adjusted to point towards the closest end of the line segment. Any intersections found were eliminated as described for the temporalis.

Figure 5-7 - Masseter origin surface shown with interface plate loading points transformed to the FE coordinate system. Nodal load vectors for the masseter 1 load are shown computed by the developed algorithm and directed towards the line segment formed by the landmark points.

Figure 5-8 - Masseter origin surface shown with interface plate loading points transformed to the FE coordinate system. Nodal load vectors for the masseter 2 load are shown computed by the developed algorithm and directed towards the line segment formed by the landmark points.

The identification of the masseter and temporalis muscles is not trivial. During dissection the insertion of the muscles was uncovered and the contours defining the boundaries of the origins were digitized. These contours consisted of consecutive points providing a linear piecewise approximation of the origins. The origins of the muscles corresponding to the FE model were determined by again transforming the contours to the coordinate system of the model. Using these contours the origin of the masseter and temporalis were extracted manually from the surface triangulation of the specimen. The nodes of the origin surface were then used in the force vector assignment already described. Two different load distributions were applied with the perpendicular vector method described relying on the digitized interface plate landmarks for the masseter. The force landmark for the temporalis was a single point to which all the forces from the temporalis nodes converged.

5.2.5.2 Restraint Assignment

The restraint applied to a FE model acts to resist the imposed loading in order to maintain static equilibrium. In the *in vitro* testing the specimen was restrained by embedding the upper teeth in PMMA in order to prevent motion in all directions. The fixture was constructed out of aluminum and the PMMA quantity was chosen to be significant in comparison with the teeth to make the fixation more rigid than the teeth thereby restricting their motion. The equivalent situation in FE modeling was to impose full restraint of all the nodes of the teeth embedded in the cement with an assigned zero displacement boundary condition on the embedded teeth. Two teeth of the left side were excluded because they were removed prior to embedding in the PMMA in order to eliminate scatter effects of their fillings. The experimental fixture was specifically defined to fully restrict tooth motion because of the high certainty in replication of such a condition in the FE model. Subsequent, investigation of the developed occlusal restraint revealed that the left two bicuspid teeth had not been properly embedded in the PMMA. Although a visual inspection exhibited PMMA flow up against the front surface of the teeth, it had failed to flow behind all the teeth in order to provide a secure restraint. This was attributed to too viscous a mix for the PMMA and future investigations should be careful to ensure full submersion of the teeth in the cement.

5.2.6 Post Processing

The FE models were solved with IDEAS (EDS, Plano, Texas) to produce the stress and strain distributions over the entire model. The strain field is a tensor-valued field that has six distinct components that define the state of strain over each element. The strain tensor for a particular location is unique in the global coordinate system. In order to compare the FE strain values with the mechanical testing results the local computed strains must represent the axial strain gauge data. At each location in a structure the strain is a tensor, but the strain gauge measures the strain in a single direction, which corresponds to a single component of the strain tensor at that location. Therefore in order to compare against the experimental strains, the FE strains at the corresponding locations were transformed into the gauge direction.

The strain gauge is of finite dimension and measures the strain over the entire active element of the gauge. Because of this the strain gauge effectively measures the mean strain over the area of the gauge. Comparison of the strains required a method to normalize the FE strain at a particular location over the representative area of the strain gauge. This is important because strain is defined inside a particular shell or solid element and is discontinuous between adjacent elements. As such averaging over a gauge representative area reduces the sensitivity of the FE strain to discontinuities and sharp gradients that may exist and would impact the agreement with the experimental data. The strains extracted from the FE model were averaged over a circular region of 2 mm radius. The mean gauge strain was computed from the element strains that were first averaged to the nodes found within the circular region in the direction of the gauge using the following relation: $\varepsilon_{gauge}= u^T\varepsilon u$, where u is the unit direction vector of the axial strain gauge and ε is the strain tensor for a particular element within the averaging radius. The transformed strains are then averaged to produce the gauge strain for comparison against the mechanical testing. The maximum and minimum strains for the circular gauge region were also extracted.

The strains for each gauge position and direction were computed and compared against the measured strains for those gauges. The agreement between the experimentally measured strains and the extracted FE strains was assessed by a linear regression analysis. For the baseline and sensitivity models the slope, offset and r^2 were calculated.

5.3 Results

5.3.1 Reconstruction

The reconstruction of the subject-specific geometry of the cadaveric specimen successfully produced a closed surface triangulation with no self-intersections. A closed non-intersecting surface triangulation is a critical requirement for the tetrahedral mesh generation algorithm required to construct the individual finite elements. The final surface was smooth and the external thin sinus bone regions were preserved intact (Figure 5-3). Some breaching of two boundaries in the thin bone regions occurred in situations where the bone segmentation identified two adjacent voxels that share only a single corner. These breaches were present only in the internal bones of the nasal airway and occurred at distances far from the loading conditions or regions of high strain gradients, so that any error introduced was far from any gauge locations or regions of critical load bearing. The cortical thickness distribution as measured from the segmentation can be seen in Figure 5-13.

5.3.2 Mesh Density Convergence

Eight FE meshes ranging in density from 0.15 to 1.3 triangles/mm^2 were created to study convergence representing densities from 100,000 to 1.8 million tetrahedral elements with 30,000 to 250,000 surface triangles. The extracted numerical gauge strains due to the vertical load were plotted against the mesh density in terms of the number of triangles per millimeter squared. The change in numerical strain varied across all the gauge locations and directions (Figure 5-9). The performance of each gauge was considered independently and a plateau region was identified for each gauge and the variation over this region was analyzed. Strain gauges 1, 2, and 7 exhibited low strain behaviour and varied over the entire range of mesh densities by less than 10 microstrain. Gauges 3, 4, 5, 9, 10 and 11 exhibited a plateau variation of less than 10% over the final three mesh densities. Gauges 8 and 13 exhibited plateau variation of less than 15% and gauge 12 varied by less than 25% over the final three mesh densities. Of all the gauge positions considered gauge 6 did not exhibit a plateau region, but the changed over the last three mesh densities by less than 20 microstrain or 50% of its highest value.

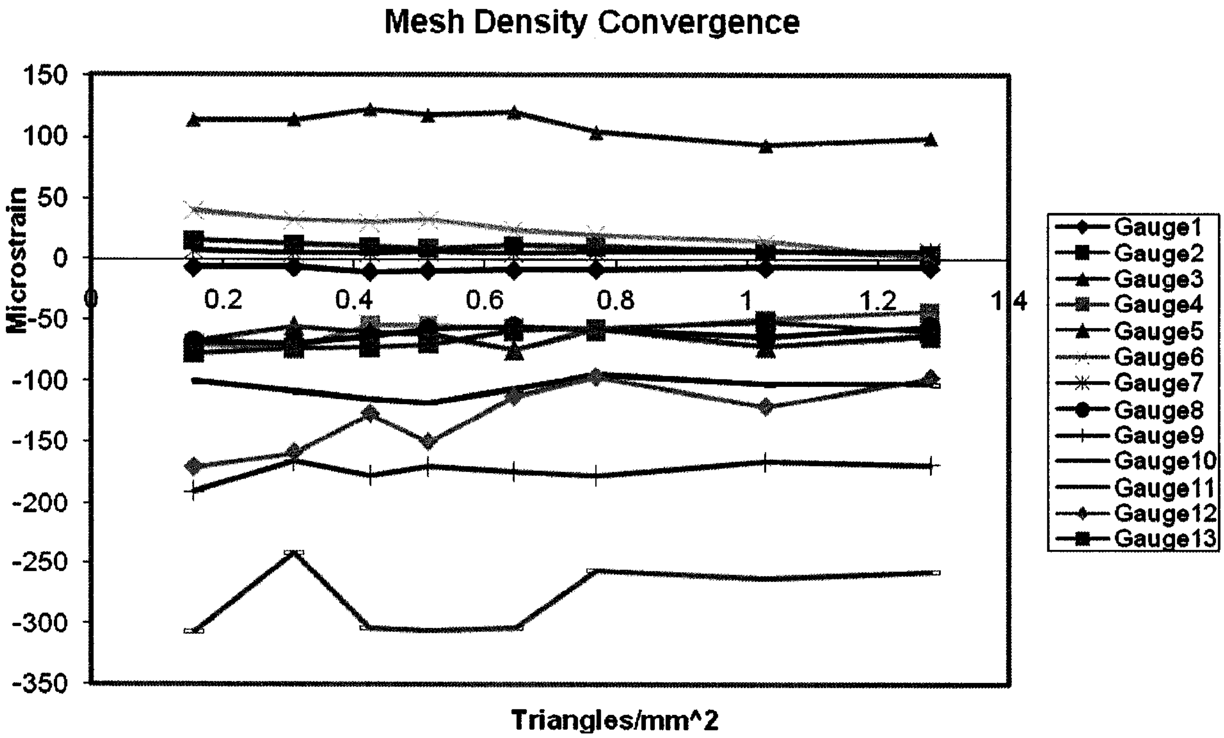

Figure 5-9 - Mesh density convergence data showing absolute strain at a particular gauge location with increasing surface triangulation density.

The majority of the high strain gauge positions displayed asymptotic behaviour at mesh densities above 0.8 triangles/mm^2. The low strain gauges displayed very little variation and consequently did not impact the assessment of convergence. The convergence was determined for the highest mesh density permissible (1.28 tri/mm^2) by the employed hardware because of high variability seen by gauge 6 and due to the occurrence of the plateau regions for all other gauges at the final 2-3 mesh densities. The convergence is not in this case a definitive assessment, but rather an estimate of the error around the chosen mesh density. This mesh density (1.28 tri/mm^2) representing 370,660 nodes, 250,000 shell elements and 1.8 million tetrahedral elements was used in all subsequent analyses. As an additional check, the maximum displacement of the model was also considered with respect to the mesh density convergence (Figure 5-10).

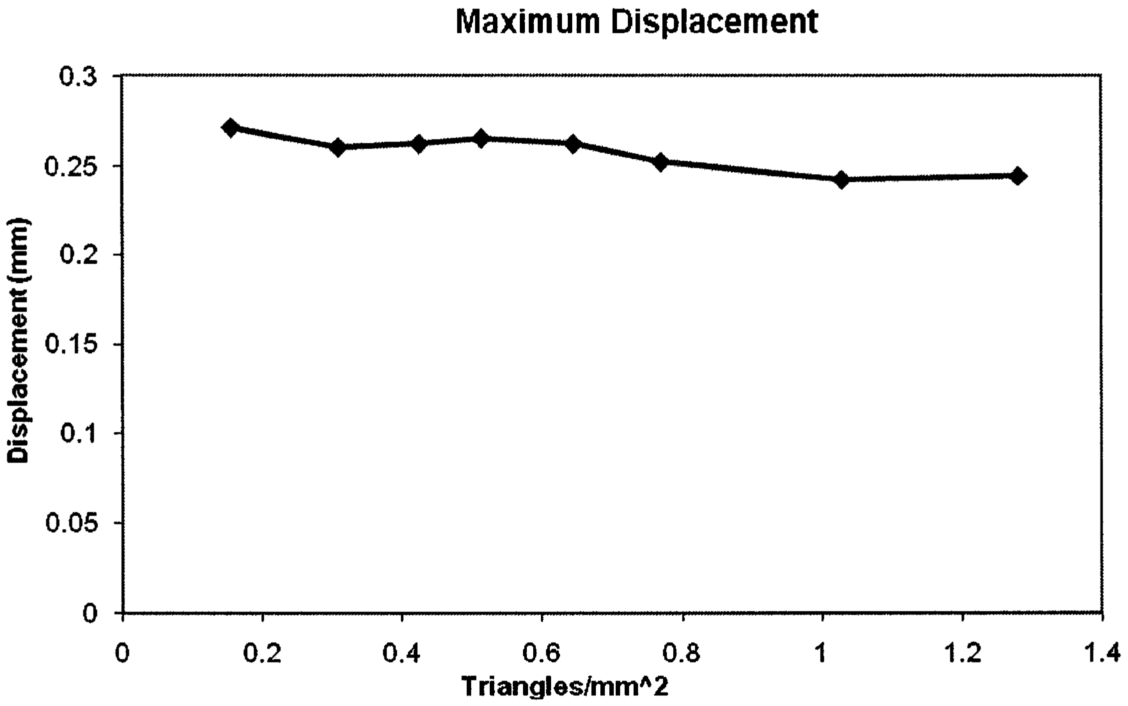

Figure 5-10 - Maximum displacement profile for mesh density convergnce study models.

5.3.3 FE Model Predictions

Comparison of the strains predicted by the FE model against measured strains from the *in vitro* model revealed strong correlations (r^2= 0.73) with a linear regression fit of y = 0.891x - 16.20 (Figure 5-11). Linear regression analysis for each individual load case produced an agreement of 0.70 for the masseter 1 load, 0.75 for the masseter 2 and 0.81 for the temporalis load. The best fit lines computed by the linear regression where for the Masseter 1 load, 0.868x - 12.60, for the Masseter 2 load, 0.862x - 13.15, and for the Temporalis load 1.059x - 18.77. The error bars represent the maximum and minimum strains over the region used for the averaging calculation.

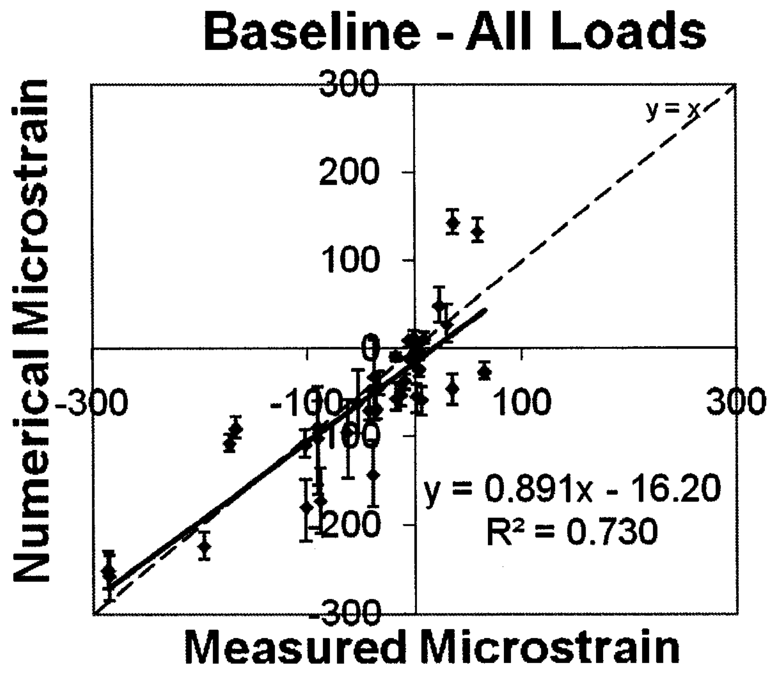

Figure 5-11 - Linear regression analysis for all three load cases of *in vitro* measured versus finite element computed numerical strains at gauge locations.

5.3.4 FE Model Sensitivity

All models that imparted variation on the subject-specific baseline model had a lower correlation with experimental data than the baseline model (Refer to Appendix A for linear regression plots per model) (summary in Table 5-2). The correlation of the baseline line model was most affected by changes in the local cortical thickness of the bone. The definition of the cortical bone elastic modulus as 10 GPa improved the slope for overall data from 0.891 to 1.020 but the correlation decreased from 0.730 to 0.708. A cortical modulus of 17 GPa improved the agreement from 0.730 to 0.738, but saw a decrease in the slope from 0.891 to 0.689. The sensitivity of the models to changes in the cortical Poisson's ratio where small with negligible changes in the slopes and correlation. However, changes to the Poisson's ratios resulted in lower correlations with experimental data. The interface parameter had the largest effect with a sensitivity of 1.357 on the slope of the fit from 0.891 to 2.100 with a reduction in the agreement to 0.659.

Table 5-2 - Linear regression fits of single parameter modified baseline model strains against *in vitro* mechanical testing. The baseline parameters were local cortical thickness, cortical modulus of 12 GPa, interface modulus of 300 Mpa and a cortical Poisson's ratio of 0.3.

Parameter/Model	Value	Linear Fit	R^2	Sensitivity
Baseline	-	y = 0.891x - 16.20	0.730	-
Cortical Modulus	10 GPa	y = 1.020x - 19.56	0.708	0.869
	17 GPa	y = 0.689x - 11.68	0.738	0.544
Cortical Poisson's Ratio	0.2	y = 0.890x - 16.39	0.715	0.0034
	0.4	y = 0.893x - 16.18	0.726	0.010
Const. Cortical Thickness	1.0 mm	y = 0.922x - 6.404	0.460	-
	1.5 mm	y = 0.751x - 3.121	0.566	0.371
	2.0 mm	y = 0.66x - 2.995	0.588	0.363
	2.5 mm	y = 0.617x - 4.560	0.597	0.261
Interface Modulus	0.001 MPa	y = 2.100x - 31.58	0.659	1.357

5.4 Discussion

5.4.1 Reconstruction

The subject-specific geometry of the cadaveric specimen was successfully generated using the semi-automated segmentation technique. The difficulty in segmenting the bony structures of the craniofacial skeleton was limited to the internal bones of the nasal and upper sinus compartments along with the thin orbital bone forming the eye sockets. In these regions of incomplete segmentation that results in discontinuities, the surface triangulation and meshing algorithm can successfully generate a viable and continuous mesh. As previously discussed the internal sinus bones have a thickness that is on the order of and smaller than the voxel resolution of the clinical CT utilized for this study (0.52mm). Due to partial volume averaging, the image intensities parallel those of soft tissue and make segmentation of those regions difficult. However, the prevailing sentiment among clinicians is that these thin sheet-like internal bones play a small role in overall load bearing when compared to the thicker sinus bones of the maxilla. Rather, the internal thin sinus bone regions are usually associated with airflow management for foreign object filtering and air moisturizing. Because of this, the same attention with manual segmentation of the external sinus bone was not applied to the internal regions. Descotueax et al. [71] present a methodology for filtering clinical CT scans using eigenvalue analysis to enhance sheet-like structures based on local shape characteristics. This algorithm has the potential to provide an automated and repeatable alternative to time consuming manual user segmentation in the internal sinus region for future models, but was not implemented for this study.

5.4.2 Mesh Density Convergence

A FE mesh density of 1.8 million tetrahedral elements was used to represent the CF skeleton. Although the strain at the majority of gauge positions varied by less than 10%, with this density there are several factors that could compound the variability of the outcome measures at the locations representing the experimental strain gauges. Gauge positions in high strain areas (such as 9, 10, 11 and 12) are particularly sensitive to changes in local strains. Slight shifts that occur due to minor changes in mesh geometry can alter the mean strain of the gauge area easily within 10% of the plateau range that at the highest gauge strain is approximately 30 microstrain. Because the strain extraction method searches for elements that fall within a spherical radius, subsequent increases in mesh density could cause a particular strain to be included in the averaging that may have just been outside the region at a lower density. This issue is also pertinent in the assessment of mesh density convergence through tracking the outcome of a single node or point that provides a repeatable reference

[74]. The meshing methodology used in this study does not permit the identification and preservation of nodes to provide this kind of fixed reference point.

The converged mesh density was assessed at 1.28 triangles/mm^2, which is higher than the mesh density chosen by Anderson et al. at 0.5 triangles/mm^2. However, in that study a mesh density study was not conducted by the authors, instead relying on a performance assessment for the required mesh density to approximate the analytical beam solution to within 5% with no further elaboration provided by the authors. The converged mesh density in the present study has a mean edge length of 1.038 mm, which is still above the minimum edge length of 0.1666 mm required for a tetrahedral only mesh to accurately capture the behaviour of the thinnest measurable (0.52mm) cortical bone due to bending modes. The bending of cortical bone is common in the CF skeleton due to the high curvature exhibited throughout the anatomy; for example, the compressive load generated by the masseter muscle on the maxillary buttress is transmitted as a moment through to the teeth and physiological loading by biting using the incisors deflects the maxilla which already has a concave shape upward. The concavity creates an off center load that imparts a moment on that curved region resulting in higher strains than a straight beam structure would experience.

5.4.3 FE Model Predictions

The linear regression fit for the baseline model (r^2=0.730) is comparable to values published for models of the pelvis (r^2=0.824 to r^2=0.728)[39] and scapula (r^2=0.806)[51] that employed a similar hybrid shell-solid mesh technique. A craniofacial model developed by Nagasao et al. [67] demonstrated excellent correlation with experimental data (r^2=0.989). That study differs from the presented work in several major aspects. Although such good correlation was reported, the number of locations used in the study was limited to strain rosettes at only two locations throughout the experimental specimen. One rosette was located in the front of the zygoma (distinct from the sinus bone region where gauge number 10 was placed in this current work), and the second gauge was placed on the front of the maxilla just above the incisors. Nagaso's study provided data at only 2 locations for comparison against testing data in contrast to this work that examined 13 different spatial locations. As such, many locations included in this study, the nasal buttress, maxillary buttress, orbits, zygoma, temporalis and sinus bones, were not considered in the study by Nagasao et al. It is important to note, that Nagano's study was interested in computing the stresses due to a titanium molar implant, however no strain gages were located on the maxillary buttress which experienced the highest stresses under load. As such, although good agreement was demonstrated, the study suffers from a low spatial variation of the measured strains in addition to a relatively small amount of data points for assessment of validation.

The study by Nagasao et al. [67] used a dry skull for the experimental validation, which presents a different situation than the fresh frozen model used in this work, where hydration of the soft tissues and bone was maintained during the experiment. Dry bone [67] omits many of the challenges that can be the source of error in fresh frozen bone strain measurement. Moisture infiltration that can cause debonding of the strain gauge is not a concern with the dry bone specimens. Local heating effects due to gauge excitation, which may be large enough to alter the gauge factor and therefore the strain measured, are less of a concern in a dry skull model because in the fresh frozen model the local moisture content, which is immobile, may contribute to accumulating heat locally. The potential for this phenomenon was mitigated by using the minimum excitation voltage achievable with the current system. Additionally, dry skulls completely omit the muscle insertions of the masseter and temporalis that were used in this study for transmission of load to the skeleton. Because of this, Nagasao et al. did not validate the models for loads applied through musculature. Nagano's testing applied a compressive load at the second molar with restraint imposed on the cranial vault in contrast to this study that was designed to fully restrain the upper teeth to resist loads applied through the masseter and temporalis muscles.

Nagasao et al. did not present data about mesh density convergence and no final mesh density statistics were stated. However, the figures presented for their models show a very coarse mesh relative to the one presented in this work (an estimate of the density would be on the order of less than 10,000 tetrahedra). This mesh density clearly does not consider the beam approximation requirement that is the basis for the development of a hybrid solid-shell mesh, which casts doubt on the overall quality of their model results notwithstanding the high correlation coefficient presented.

Looking specifically at the masseter loads in our model, it is apparent that the strains seen are very similar across the two loads although the direction of loading is different (See Appendix for bar plots of measured and FE model strains) (Figure 5-7, 5-8 for direction illustration). The strain profile at the gauge locations does not exhibit large variation due to the direction of muscle activation alone.

The linear regressions for each load scenario revealed that the temporalis load produces the best slope (1.020) and r^2 value (0.809). The two masseter loads on the other hand exhibit a similar slope and lower r^2 value. The higher correlation for the temporalis load suggests that this load case was more accurately recreated in the FE model than the two masseter load cases. This discrepancy between the temporalis and masseter load cases can be accounted for by the approximation of the load distribution over the masseter insertion regions. This is because for the masseter load cases, gauges 3, 4 and 5, which are close to the masseter loading condition exhibit the largest discrepancy between the numerical and measured strains. These results suggest that there may be an error in the FE approximation of the masseter loads as equally distributed over the entire origin surface. Under masseter loading as predicted by the FE models, the regions corresponding to gauges 4 and 5 undergo compressive vertical strains. This compression is not counter-intuitive because the masseter inserts into the zygomatic arch which, when loaded, should act like a lever. The majority of the insertion and therefore the proportion of the masseter load is born by the arch portion, this causes a downward deflection of the arch and a rotation around the location where the zygomatic arch joins the vertical orbital buttress that becomes the fulcrum. This downward rotation of the arch is counterbalanced by an upward rotation of the bone anterior to the fulcrum where compression is generated. This could cause the body of zygoma (locations of gauge 4 and 5) to rotate upward and compress against the orbital bones. This could potentially explain why gauges 4 and 5 exhibit compressive stresses (Figure 5-12). Future work will have to apply the loading in such a manner that the distribution of the load over the surface is predictable and can be recreated in the finite element models.

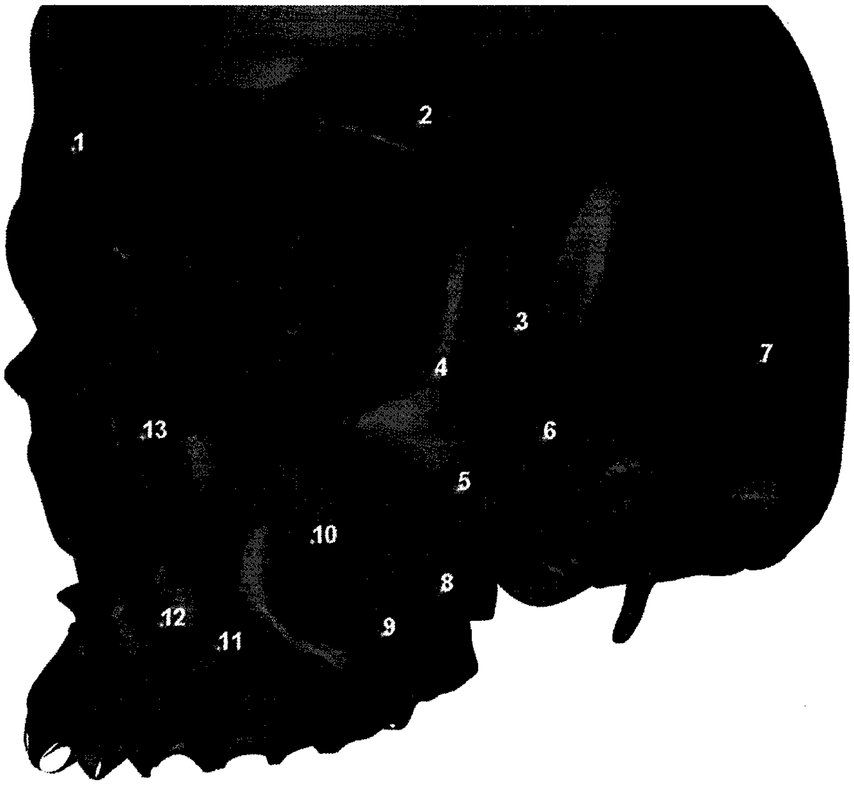

Figure 5-12 - Positions of the gauges after transformation to the FE model coordinate system.

However, the *in vitro* testing suggests that there is significant tensile strain at least at gauge 5, which was oriented parallel to the muscle orientation to capture the anticipated tensile strain. The high tensile strain seen at gauge 5 is most likely due to issues related to the hyperelastic properties of the muscle in general and the unique nature of the masseter origin itself. The masseter muscle directions chosen for the study involved small rotations away from the neutral position of the muscle. Masseter 1 was oriented posteriorly and Masseter 2 was oriented anteriorly. This rotation away from the neutral orientation causes the fibers of the muscles, which run along the axis, to become differentially stretched and because the fibers behave hyperelastically as the strain increases in a fiber the stress or force required to impart further deformation increases exponentially. This hyperelastic behaviour is essentially a strain hardening that increases the effective stiffness of that fiber relative to adjacent fibers that are experiencing lower strains.

This differential stretch across the masseter fibers is compounded by the concave masseter origin, which results in a differential length of the fibers between the arch portion of the origin and the zygoma portion. The end result of this is that the fibers towards the anterior of the origin may experience higher strains because the distance from the masseter origin to the end of the muscle is smaller. As such when the end of the muscle is displaced a constant amount the shorter fibres at the anterior portion experience higher strains than the posterior fibres. An analogy is to imagine two parallel sticks joined by ropes. If an axial load is applied parallel to the direction of the ropes then all the ropes are stretched the same amount and carry the same load, but if one stick is rotated so that it is no longer parallel then some ropes will be loaded and some will be slack. If an axial load is now applied, those fibers already loaded will have to stretch more before the slack fibers begin to bear load, but because the fibers behave hyperelastically those already loaded will only become stiffer and therefore carry a greater proportion of the load. The issue in the masseter loading likely has more to do with the differential fiber length than the rotation, because in both masseter load cases gauge 5 exhibits tensile strain, in contrast to the model prediction of compression. Because the measured strain profiles are similar between the two masseter load cases, the actual direction of loading alone does not account for the tensile strain seen at gauge 5. Future work directed at developing validated models of additional CF specimens will require a method to ensure a higher degree of confidence in the load distribution that is applied. Alternately, future models may incorporate the geometry of the masseter muscle as well as the material properties. However, a recent study that was focused in the loading of macaque skeletons through the masseter reported difficulties with lower agreement against measured strains of the zygomatic arch as a result of including the masseter geometry [75]. Future work could strive to include the masseter geometry as well as the hyperelastic material properties that may account for the differential fiber stretching which may be responsible for the discrepancy noted between the measured and computed strains.

The discrepancy of approximately 50% seen at gauge 9 is only present for the masseter load cases while the strain due to the temporalis loading case shows a difference of only 5%. This further suggests that the weaker correlation at this location for the masseter load cases is an outcome of the force distribution approximation.

Gauge 10, which was placed on the thin sinus bone region of the upper maxilla, exhibited constant discrepancy of approximately 46 % over all three load cases. This position was chosen in order to validate the ability of the model to capture the deformation of this very thin bone region that has a thickness on the order of one voxel and clinically is not believed to bear high strains. The effect of limited CT resolution on the thickness prediction of the thin sinus bone regions has been discussed and is one limitation of the developed methodology. In the case of the FE models, the predicted strains at gauge 10 are approximately half of the strain measured during the *in vitro* testing. The measured thickness at this location varied between 0.5mm and 1mm because the cortical bone segmentation must be at least one voxel thick in order to register that cortical bone is present. Anderson et al. [39] demonstrated the limitations of the approximation of structures used for reconstructions whose thickness was less than the resolution of the CT scan. The actual thickness at gauge 10 is most likely lower than that measured on the scan (voxel intensity), which potentially could account for a large change in the strain seen locally (as thickness of the shell elements defines their stiffness). Although the measured thickness of the sinus bones could be compared to the true thickness of the tissue (using excised tissue measurements), the developed CT based methodology would not be capable of matching the thickness correctly. However, local inaccuracies in measuring thickness would only affect the local strains and not the global behaviour of the craniofacial skeleton, and such a change in thickness represents an almost negligible change in the total amount of material (bone) that is mechanically loaded.

The actual role of the sinus bones in load bearing is not clear at this stage because physiological loading patterns have not been applied to the model. The outcome of the present model however provides a valuable insight into the nature of load bearing in thin bone structures. Not only does this thin cortical bone bear load in the craniofacial skeleton but small changes in the amount of local material can significantly influence the local strain experienced and provides a very fine method for controlling skeletal deformation. Future application of more complex loading to the developed model may provide insights into the role that the thin sinus bone regions play in resisting physiological loads.

The agreement of FE model strains with the measured strains may also be affected by the inherent error in the transformation of the measured gauge positions. Although the error in transforming the fiducial markers used to compute the transformation between the physical space of the cadaver and the FE model revealed error of no more than 5%, the transformed inaccuracies in the gauge coordinates even at this level may have a substantial impact on strain values. A visual comparison of the transformed positions to a picture (Figure 3-7 and Figure 5-13) of the actual positions shows that the transformed positions of gauges 4, 5, 11 and 12 deviate from their true positions on the cadaveric specimen; the transformed gauge coordinates were elevated above the surface of the cortical bone for some gauges (gauges 4,5,11,12) suggesting inaccuracy in the transformation. This transformational error can impact the elements that are found within the strain averaging region and therefore the strain calculated from the FE model. This inaccuracy is compounded when gauges reside on high gradient regions like the orbital rim (Gauge 4) and orbital bone (Gauge 3). In the case of gauge 3 the high gradients are unavoidable because the nature of the geometry naturally forces high strain gradients to be developed in order to maintain static equilibrium.

The error in the transformation of the gauge positions also affects the transformed direction of the gauge and therefore would impact the computation of the strain extracted from the FE model. This problem can be avoided by the use of rosette configuration strain gauges instead of uniaxial gauges. Whereas uniaxial strain gauges measure strain in only one direction, the rosette configuration permits the calculation of principle strains at the gauge locations, which are by definition independent of the orientation of the rosette strain gauge. This method was employed by Anderson et al. [39] for the pelvis, which has substantially larger surfaces that can more easily accommodate the large footprint of a rosette strain gauge. The highly irregular geometry of the craniofacial skeleton with small thin structures and high strain gradients are not well suited to the large area demands of rosette gauges.

The tradeoff between uniaxial and rosette gauges is also in the technical implementation. The digital acquisition system used for measuring the *in vitro* strain allowed 14 distinct channels permitting 14 separate gauge measurements to be taken at once. By using a rosette, three channels are used for a single location. In this validation experiment, uniaxial measurements were taken at multiple locations rather than rosette measurements at fewer locations. Future work should strive to better understand the error around the transformed gauge positions and direction to assess the effect of potential errors in the transformations to determine the significance of considering alternate gauge localization methodologies.

5.4.4 Sensitivity studies

5.4.4.1 Material Property Assignment

The sensitivity of the developed model to the elastic modulus of cortical bone reveals a near linear relationship between the gauge strains and the elastic modulus. If all bone was defined as a single linearly elastic material, then a 10% change in the modulus would change the local strains by exactly 10%, however, because there is a heterogeneous distribution of elastic moduli throughout bone in general, scaling changes made to the cortical elastic modulus also change its relative stiffness of adjacent material resulting in non-linear changes in the FE model strains.

Table 5-3 - Load wise comparison against in vitro data for baseline models with variation applied, to the cortical elastic modulus. E12 refers to a cortical modulus of 12 GPA and E10 refers to a cortical modulus of 10 GPa.

Model	Linear Fit	Correlation (r^2)
Baseline – E12 – Masseter 1	0.868x-12.60	0.704
Baseline – E10 – Masseter 1	1.070x -10103	0.742
Baseline – E12 – Masseter 2	0.862x-13.15	0.749
Baseline – E10 – Masseter 2	0.983x-16.01	0.735
Baseline – E12 – Temporalis	1.059x - 18.77	0.809
Baseline – E10 – Temporalis	1.204x-2.52	0.788

Overall, the models that assign a cortical elastic modulus of 10 GPa and 12 GPa are the most accurate in predicting *in vitro* strains (See Appendix A for load wise linear regression analysis for 10 GPa models) Table (5-3). The regressions reveal an interesting pattern in that for both masseter load cases the model with a cortical modulus of 10 GPa produces a better linear fit with a slope that is closer to unity. However, the agreement with a cortical modulus of 10 GPa improves for the masseter 1 load but decreases for the masseter 2 load. The 10 GPa model also shows lower correlation for the temporalis loading scenario in addition to a slope deviating away from unity. The correlation for all the load cases is higher for a cortical bone modulus of 12 GPa than for the 10 GPa model. Both of these values are within the range found in studies of the local cortical bone elastic modulus measured by ultrasound elastography [21,43,45]. The model with a cortical elastic modulus of 17 GPa, the value that provided the best agreement for Anderson et al. [39] in the pelvis, increased the agreement with the *in vitro* data only a very small amount (from 0.730 to 0.738) however this model was less accurate with a regression slope of only 0.689.

This data shows that small changes in the cortical elastic modulus can improve the results but not across all load cases and that the discrepancies between models and *in vitro* data may be due to local variations in bone material properties that are not known a priori. Although the model with a cortical elastic modulus of 10 GPa resulted in a better linear slope overall, the 12 GPa model is considered more accurate because the slope of the regression for that model for the masseter load cases is believed to be related to the masseter muscle fiber strain stiffening described in Section 5.4.2 and not inaccuracies due to material property approximations. This is because the temporalis loading case reveals a better correlation with the data and a linear slope and is not subject to the same inaccuracies that affect the masseter loading conditions. Studies of the elastic modulus of craniofacial cortical bone found this material property to be orthotropic in nature. Such material definitions could possibly improve the model agreement with experimental data; however, unlike in long bones where there is a clear axis of orientation for defining orthotropic properties, defining such properties based on anatomical landmarks may present unreasonable complexity in the craniofacial skeleton with little overall improvement in accuracy. Additionally, studies of craniofacial cortical bone showed that the orthotropic material orientation directions exhibited variation between locations as well as the elastic moduli in the different directions. The difficulty in measuring the orthotropic properties is in the destructive nature of the method that requires local bone cores to be taken in addition to resolving the orthotropic properties at model locations that were not measured. To include such specific definitions into the current model would be difficult and it appears that without such specificity sufficient agreement has been achieved.

Dechow et al. [21,43,45] also found spatial variation in the Poisson's ratios of human craniofacial cortical bone. The models from this study that changed the baseline by assigning a different Poisson's ratio reveal that the effect of such ratios on the overall agreement were small both in terms of the slope and correlation and that the baseline model that assumed a cortical bone Poisson's ratio of 0.3 was the most accurate for the values assumed (0.2, 0.4).

Previous models that have used the hybrid shell-solid mesh have assigned either 0[39] or 0.0001[51] MPa for the elastic modulus of the overlap layer between the triangle and tetrahedral elements. Effectively such low values disconnect the cortical surface triangulation from the internal tetrahedral mesh representing the trabecular bone and as a result one would not expect load transfer from the cortical bone to the trabecular core. Although the authors did not justify the choice of such a low value, the purpose of this overlap parameter was to prevent a 'doubling' of the stiffness that would occur if the tetrahedral elements adjacent to the triangular shell elements were assigned moduli on the order of cortical bone. The subsequent correlation between with the measured strain decreased from 0.730 to 0.659 and the linear fit was the worst of all developed models. This would suggest that the baseline model that assigns an interface modulus of 300 MPa, which is based upon the average elastic modulus for trabecular bone provides for a more accurate solution. It seems unreasonable to impose no load transfer from the cortical to the trabecular bone regardless of the two orders of magnitude difference in the elastic modulus and so an overlap modulus of 300 MPa is deemed reasonable for use in future investigations.

An alternative method to the single cortical overlap that requires the assignment of the interface modulus to the underlying tetrahedral element could be avoided by defining the geometry of the shells at the boundary between cortical and trabecular bone. However, this method would be limited in that it would not represent the surface topology as accurately as meshing the outer surface of the cortical bone which is important for the definition of the loads applied to the musculature. Alternatively, elements exist that are formulated using plate bending theory that have a 3D dimensional structure in the form of a pentahedron. However, the study that developed the hybrid mesh for a pelvis rejected such elements because of poor performance in predicting the tip deflection of a beam due to bending [39]. Such a meshing strategy was considered for this study but the technical implementation of such a specific geometry on the already complex craniofacial skeleton made the method less desirable and perhaps appropriate for future model refinement. Surface triangulation and tetrahedral mesh generation remains the simplest and most robust meshing strategy for highly irregular shapes and is the recommended approach for the development of FE models of the human craniofacial skeleton.

5.4.4.2 Shell Thickness Sensitivity

In all cases, the craniofacial models that assumed a uniform cortical thickness were less accurate in predicting *in vitro* strains than the subject-specific cortical thickness definition. This concurs with results from a validated model of the pelvis [39] where application of a uniform cortical thickness led to a poorer correlation with experimental data. The distribution of cortical thicknesses throughout the craniofacial skeleton ranged from 0.5mm and 4.0mm with a mean thickness of 2.13mm (Figure 5-13).

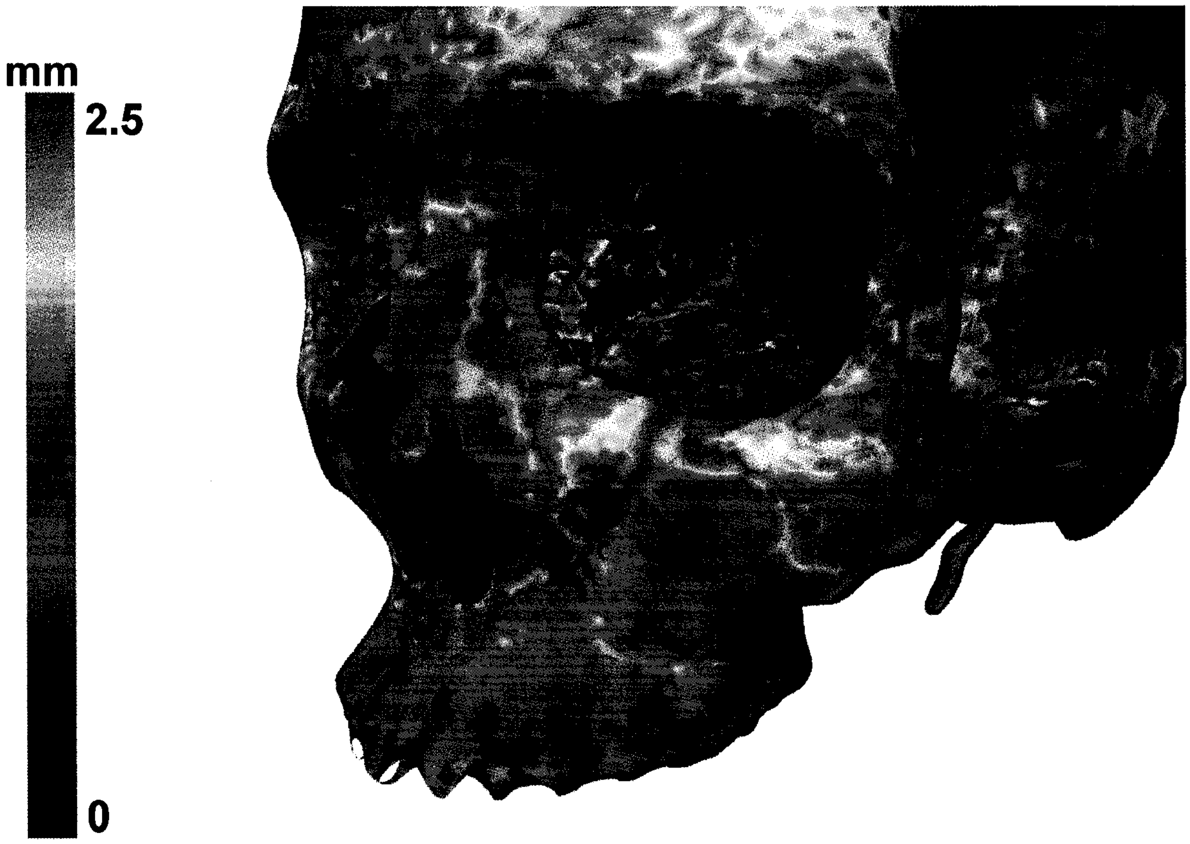

Figure 5-13 - Cortical thickness distribution within the craniofacial skeleton according to the surface normal distance measurement scheme using the manual user defined thickness cortical segmentation. Gauge positions included.

The developed FE model demonstrated high sensitivities to uniform cortical bone thickness approximation ranging from 0.371 to 0.261 (Table 5-2). Those results show that assignment of the cortical thickness is important because slight deviation of 0.5mm can impact the accuracy of the resulting strain distributions throughout the craniofacial skeleton. The maxillary region exhibits a cortical thickness between 0.5mm, the minimum measurable thickness, and 1.0mm. For all models the strains at the gauge locations for the maxillary region were lower than those for the subject-specific baseline model. Because of the high sensitivity of the models to the assignment of cortical thickness measurement, future models will need to incorporate local thickness measurements in order to ensure the accuracy of local strains.

A study of the error in thickness measurement was performed by Anderson et al. [39], which found that measurement of aluminum tubes that are thinner than the CT scan resolution used produced considerable error. However, error in measuring structures above this limit reduced rapidly to approximately 5% (for thicknesses above 0.8mm in Andersons study at a CT resolution of 0.6mm). As such, the resolution of the CT scan used to construct a model can be considered a limiting factor in determining the ability of FE model to predicting surface cortical strain in the thin bone regions (like the sinuses) although the use of aluminum tubes for thickness measurement may have not been an accurate radiological substitute for cortical bone. However, this error is localized to the region where uncertainty in the cortical bone thickness is high, meaning that small inaccuracies in measuring cortical thickness should not effect the strain distribution if the region represents a small proportion of the overall geometry. It would also not be reasonable to have a structure that is so inherently unstable that even small local changes can have significant consequences.

5.5 Conclusions

A subject-specific finite element model that incorporated position dependent cortical bone thicknesses and trabecular bone material properties was developed and successfully validated against *in vitro* experimental data. Linear regression analysis resulted in an overall slope of 0.891 with an offset of -16.20 microstrain and a correlation of 0.73 that is comparable to similar FE models presented in the literature. Linear regression demonstrated the best agreement for the temporalis loading case with a slope of 1.02 and correlation of 0.802. The masseter loading cases exhibited slightly lower correlations of 0.702 and 0.742 with slopes of 0.862 and 0.861 respectively. The lower agreement for masseter load cases may be explained by inaccuracies due to the approximation of the equal distribution of load over the masseter origin sites. No previous FE models of the human craniofacial skeleton have been validated under loading applied through musculature with occlusal restraint, nor have they considered validation over as large a proportion of the facial skeleton as was demonstrated in this study.

Sensitivity studies performed on the material properties of the cortical bone showed that assigning a cortical modulus of 17 GPa (as done for models of the pelvis [39] and scapula [51] that utilized hybrid solid-shell meshes) did not yield as good a correlation with the experimental data as the craniofacial model that was assigned a cortical elastic modulus of 12 GPa. The models were very sensitive to the assignment of the cortical bone modulus with sensitivities of 0.869 and 0.544 for models with a cortical elastic modulus of 10 GPa and 17 GPa with respect to the baseline of 12 GPa. The developed model exhibited the highest sensitivity to the interface parameter assigned to the tetrahedral elements in the overlap region; assuming an interface modulus of 300 MPa, which is representative of trabecular bone, resulted in the best agreement. The models were also found to be very sensitive to the assignment of cortical thickness with sensitivities ranging from 0.371 to 0.261 for uniform thickness assumed for the models at 1.0, 1.5, 2.0 and 2.5mm. Overall it was found that assigning local specimen specific cortical thicknesses (measured from the CT scan) achieved the best agreement with *in vitro* testing data.

Chapter 6: Summary

6.1 Conclusions

A subject-specific finite element model was developed of a human craniofacial skeleton. Cortical bone strains were measured from an *in vitro* cadaveric model under mechanical loading through the masseter in two unique directions and temporalis under a single loading direction with reaction to the tensile loads provided by restraint of the upper teeth. The developed FE model was validated against the experimentally measured *in vitro* strains. Linear regression analysis produced a slope of 0.891 with a correlation of 0.73 for all three loading cases with correlations for individual loading cases ranging from 0.702 to 0.802, which are comparable to *in vitro* validation studies of other thin bone skeletal anatomies.

A semi-automated technique was developed for segmenting the craniofacial skeleton from computed tomography images. This included the implementation of level-set based computational image processing methods for delineation of the cortical-trabecular boundary. Level-set based methods performed well in segmenting certain structures of thin cortical bone, but additional algorithmic improvements may further increase the ability of the automated method to yield more accurate cortical shell segmentations. Overall it is believed that level-set based methods are well suited to the high accuracy requirements of the craniofacial skeleton, but the limitations of CT resolution and indeed morphological variation between individuals make this job more difficult to address.

The developed FE model exhibited high sensitivities to assumptions regarding the linear elastic material properties of the cortical shell. Conversely, the model exhibited the lowest sensitivity to variations in the assumed Poisson's ratio, which empirically has been shown to vary spatially over the craniofacial skeleton. The most accurate model incorporated position dependent cortical thickness distribution throughout the craniofacial skeleton. However, cortical thickness measurement is limited in very thin cortical structures that are on the order of or smaller than the CT voxel resolution and consequently the ability of the models to capture the strain in such regions may depend upon the utilization of higher resolution imaging modalities.

6.2 Future Directions

6.2.1 Multiple Specimen Validation

The overall purpose of developing FE models of the human craniofacial skeleton is to use those models to understand the distribution of load throughout the skeleton due to physiological loading. This distribution is important because it forms the basis upon which design criteria for emerging technologies and methodologies such as engineered tissue replacements and the next generation of reduction hardware will be developed. However, the deduction of such design criteria cannot be based upon a single subject-specific model alone. Using a sample size of one is unreasonable for basing treatment requirements because the role that morphological variation between individuals has in determining the load distribution at clinically relevant locations is not understood. To detect a correlation of 0.9 compared to a null correlation of 0.4 (power=0.8, α=0.1) requires the developed validation methodology to be demonstrated for at least six specimens according to a power analysis.

The manual segmentation of the cortical bone of the craniofacial skeleton is a laborious process that is time consuming and subject to intra and inter observer variability. Ideally, an automated method would significantly improve the repeatability of the segmentation of the cortical shell, the thickness of which is crucial in determining the local strain distribution throughout the craniofacial skeleton. This study has demonstrated that level-set based methods were a reasonable first approach by succeeding in segmenting at the very least the maxillary region of two different craniofacial skeletons. However, difficulty was found to exist in imposing global control over the performance of the segmentation due to the pronounced variation in morphologies between the maxilla, zygoma and orbital regions as well as between individuals. The effectiveness of the algorithm was hampered in the fresh frozen case by a reduced resolution over the preserved model and lower contrast in general. Future work should strive to improve upon the developed method because of the potential demonstrated in the maxilla which of all the craniofacial bones has the thinnest cortical bone and is the site of significant strains whether they be physiological or not. Increasing the CT scan resolution would increase the confidence in measuring the cortical bone thickness that has been found to be influential in determining local strain patterns.

As such the development of models of multiple specimens all validated against in vitro mechanical testing is an absolute necessity if design criteria for treatment modalities of pathologies are desired. This multi-specimen validation will answer two important questions: 1) what differences exists in the load distribution between individuals? and 2) what role does morphology play in determining the distribution of load between individuals? If so why? Certainly load distribution variability due to morphological variation would require correlations to be found between clinically measurable parameters and expected load distributions in order to provide guidelines for the assessment of similar craniofacial morphologies.

6.2.2 Physiological Loading

The development of a number of subject-specific craniofacial models validated against *in vitro* testing would still be insufficient for understanding *in vivo* load distribution. To understand *in vivo* function requires the application of more complex physiological loading conditions to the validated models. The literature is rich with studies of *in vivo* bite force measurements that correlate direction, magnitude and location of occlusion with EMG measurements of craniofacial muscle groups [70,76-84]. Most importantly these studies measured the activation of multiple muscle groups involved in mastication providing data about the relative recruitment levels of the ipsilateral and contralateral masseter, temporalis and digastric muscle groups which can be used to apply physiologic loading to a validated FE model. A non-validated FE model of a macaque skull attempted such physiological loading by using data in the literature to derive the subject-specific muscle forces based upon relative recruitment levels and muscle cross sectional area for defined masticatory activities like biting, crushing and grinding [85]. The application of physiological loading scenarios to validated finite element models of human craniofacial skeletons will provide stresses and strains that will require post processing in order to extract mechanical variables that would provide clinically relevant and transferable information. Rudderman and Mullen [3] mention the notion of load paths that clinicians assume when reconstructing deformities of the craniofacial skeleton however, this is not supported by quantitative data. As such there is a clear need for the development of advanced visualization methods that can assist the clinician in determining the relative importance of craniofacial structures in bearing physiological loads.

Future models interested in understanding the strain distributions in the thin sinus bone regions of the maxilla and upper facial skeleton may require CT scanning capabilities above those afforded by conventional clinical CT. This requirement can be demonstrated by determining the true thickness of the sinus bones and comparing against imaging based measurement methods to provide an estimate of the error associated with such measurement. Sensitivity studies of the sinus bone regions could reveal the effect that modifications of the measured thicknesses based upon the error in measuring such structures below image resolution would have on the resulting strain and stress distribution in the craniofacial skeleton.

Comparison against *in vitro* mechanical testing data remains the most accurate method for assessing overall accuracy of subject-specific finite element models of the craniofacial skeleton to simulated musculature loading. Such validated models provide a versatile and robust platform for studying the biomechanics of the human craniofacial skeleton under physiological loading for normal, pathological and reconstructed skeletal anatomies. The true power of such models becomes apparent when considering that virtually any skeletal anatomy or pathology can be studied, which will be important in assessing the treatment of congenital deformities that make compiling sufficient donor tissue to provide clinically relevant results impractical, and for assessing patient specific traumatic injuries like fractures that are often as varied as craniofacial morphology.

References

[1] Anonymous *Craniomaxillofacial Reconstructive and Corrective Bone Surgery : Principles of Internal Fixation using AO/ASIF Technique.* ,1st ed.New York: Springer, 2002,

[2] K. A. Egol, E. N. Kubiak, E. Fulkerson, F. J. Kummer and K. J. Koval, "Biomechanics of locked plates and screws," *J. Orthop. Tra.,* vol. 18, pp. 488-493, 2004.

[3] R. H. Rudderman and R. L. Mullen, "Biomechanics of the facial skeleton," *Clin. Plast. Surg.,* vol. 19, pp. 11-29, Jan. 1992.

[4] O. J. Oyen, M. B. Melugin and A. T. Indresano, "Strain gauge analysis of the frontozygomatic region of the zygomatic complex," *J. Oral Maxillofac. Surg.,* vol. 54, pp. 1092-5; discussion 1095-6, Sep. 1996.

[5] J. M. Jack, D. H. Stewart, B. D. Rinker, H. C. Vasconez and L. L. Pu, "Modern surgical treatment of complex facial fractures: a 6-year review," *J. Craniofac. Surg.,* vol. 16, pp. 726-731, Jul. 2005.

[6] T. J. Francel, B. C. Birely, P. R. Ringelman and P. N. Manson, "The fate of plates and screws after facial fracture reconstruction," *Plast. Reconstr. Surg.,* vol. 90, pp. 568-573, Oct. 1992.

[7] S. Bhanot, J. C. Alex, R. A. Lowlicht, D. A. Ross and C. T. Sasaki, "The efficacy of resorbable plates in head and neck reconstruction," *Laryngoscope,* vol. 112, pp. 890-898, May. 2002.

[8] J. S. Orringer, V. Barcelona and S. R. Buchman, "Reasons for removal of rigid internal fixation devices in craniofacial surgery," *J. Craniofac. Surg.,* vol. 9, pp. 40-44, Jan. 1998.

[9] J. E. Barrera and S. G. Batuello. (2006, February 6, 2006). Fractures, mandible, angle. *2006(7/6),* pp. 1.

[10] J. A. Fialkov, C. E. Holy and O. O. Antonyshyn, "Strategies for bone subsititutes in craniofacial surgery," in *Bone Engineering* ,1st ed.J. E. Davies, Ed. Toronto: Em Squared Inc., 2000, pp. 548-556.

[11] A. S. Murthy and J. A. Lehman Jr, "Symptomatic plate removal in maxillofacial trauma: a review of 76 cases," *Ann. Plast. Surg.,* vol. 55, pp. 603-607, Dec. 2005.

[12] J. A. Girotto, E. MacKenzie, C. Fowler, R. Redett, B. Robertson and P. N. Manson, "Long-term physical impairment and functional outcomes after complex facial fractures," *Plast. Reconstr. Surg.,* vol. 108, pp. 312-327, Aug. 2001.

[13] J. A. Fialkov, C. Holy, C. R. Forrest, J. H. Phillips and O. M. Antonyshyn, "Postoperative infections in craniofacial reconstructive procedures," *J. Craniofac. Surg.*, vol. 12, pp. 362-368, Jul. 2001.

[14] J. Jensen, S. Sindet-Pedersen and L. Christensen, "Rigid fixation in reconstruction of craniofacial fractures," *J. Oral Maxillofac. Surg.*, vol. 50, pp. 550-554, Jun. 1992.

[15] D. Y. Nagase, D. J. Courtemanche and D. A. Peters, "Plate removal in traumatic facial fractures: 13-year practice review," *Ann. Plast. Surg.*, vol. 55, pp. 608-611, Dec. 2005.

[16] J. Schortinghuis, R. R. Bos and A. Vissink, "Complications of internal fixation of maxillofacial fractures with microplates," *J. Oral Maxillofac. Surg.*, vol. 57, pp. 130-4; discussion 135, Feb. 1999.

[17] R. B. Bell and C. S. Kindsfater, "The use of biodegradable plates and screws to stabilize facial fractures," *J. Oral Maxillofac. Surg.*, vol. 64, pp. 31-39, Jan. 2006.

[18] S. W. Herring and P. Ochareon, "Bone--special problems of the craniofacial region," *Orthod. Craniofac. Res.*, vol. 8, pp. 174-182, Aug. 2005.

[19] S. J. Hollister, C. Y. Lin, E. Saito, C. Y. Lin, R. D. Schek, J. M. Taboas, J. M. Williams, B. Partee, C. L. Flanagan, A. Diggs, E. N. Wilke, G. H. Van Lenthe, R. Muller, T. Wirtz, S. Das, S. E. Feinberg and P. H. Krebsbach, "Engineering craniofacial scaffolds," *Orthod. Craniofac. Res.*, vol. 8, pp. 162-173, Aug. 2005.

[20] M. C. Oberheim and J. J. Mao, "Bone strain patterns of the zygomatic complex in response to simulated orthopedic forces," *J. Dent. Res.*, vol. 81, pp. 608-612, Sep. 2002.

[21] J. Peterson and P. C. Dechow, "Material properties of the human cranial vault and zygoma," *Anat. Rec. A. Discov. Mol. Cell. Evol. Biol.*, vol. 274, pp. 785-797, Sep. 2003.

[22] van De Graaf, K., *Human Anatomy.* ,6th ed., vol. 1, New York: Mc-Graw-Hill Companies, 2001,

[23] S. Mader, *Understanding Human Anatomy and Physiology.* ,Fifth ed., vol. 1, New York: Mc-Graw-Hill Companies, 2004,

[24] J. Wolff, *The Law of Bone Remodelling.* New York: Springer-Verlag, 1986,

[25] C. Ruff, B. Holt and E. Trinkaus, "Who's afraid of the big bad Wolff?: "Wolff's law" and bone functional adaptation," *Am. J. Phys. Anthropol.*, vol. 129, pp. 484-498, Apr. 2006.

[26] W. L. Hylander and K. R. Johnson, "In vivo bone strain patterns in the zygomatic arch of macaques and the significance of these patterns for functional interpretations of craniofacial form," *Am. J. Phys. Anthropol.*, vol. 102, pp. 203-232, Feb. 1997.

[27] C. S. Goldberg, O. Antonyshyn, R. Midha and J. A. Fialkov, "Measuring pulsatile forces on the human cranium," *J. Craniofac. Surg.*, vol. 16, pp. 134-139, Jan. 2005.

[28] W. L. Hylander, P. G. Picq and K. R. Johnson, "Masticatory-stress hypotheses and the supraorbital region of primates," *Am. J. Phys. Anthropol.,* vol. 86, pp. 1-36, Sep. 1991.

[29] K. L. Rafferty, S. W. Herring and F. Artese, "Three-dimensional loading and growth of the zygomatic arch," *J. Exp. Biol.,* vol. 203, pp. 2093-2104, Jul. 2000.

[30] S. W. Herring, S. Teng, X. Huang, R. J. Mucci and J. Freeman, "Patterns of bone strain in the zygomatic arch," *Anat. Rec.,* vol. 246, pp. 446-457, Dec. 1996.

[31] S. W. Herring, K. L. Rafferty, Z. J. Liu and C. D. Marshall, "Jaw muscles and the skull in mammals: the biomechanics of mastication," *Comp. Biochem. Physiol. A. Mol. Integr. Physiol.,* vol. 131, pp. 207-219, Dec. 2001.

[32] F. G. Evans, *Mechanical Properties of Bone.* Springfield, Ill.: Thomas, 1973,

[33] G. F. Chalmers, "Materials, construction, performance and characteristics," in *Strain Gauge Technology* ,Second ed., vol. 1, A. L. Window, Ed. New York: Elsevier Applied Science, 1992, pp. 1-39.

[34] T. G. Beckwith, R. D. Marangoni and J. H. Lienhard, *Mechanical Measurements.* ,Fifth ed.Don Mills, Ontario: Addison-Wesley Publishing Company, 1993,

[35] K. Scott and A. Owens, "Instrumentation," in *Strain Gauge Technology* ,Second ed., vol. 1, A. L. Window, Ed. New York: Elsevier Applied Science, 1992, pp. 97-150.

[36] O. C. Zienkiewicz and R. L. Taylor, *The Finite Element Method.* ,Fifth ed., vol. Volume 1: The Basis, Woburn, MA: Butterworth-Heinemann, 2000,

[37] N. Ottosen and H. Petersson, *Introduction to the Finite Element Method.* ,First ed., vol. 1, Hemel Hempstead Hertfordshire: Prentice-Hall International, 1992,

[38] Anonymous *Concepts and Applications of Finite Element Analysis.* ,4th ed. ed.New York: John Wiley, 2002,

[39] A. E. Anderson, C. L. Peters, B. D. Tuttle and J. A. Weiss, "Subject-specific finite element model of the pelvis: development, validation and sensitivity studies," *J. Biomech. Eng.,* vol. 127, pp. 364-373, Jun. 2005.

[40] M. Dalstra, R. Huiskes and L. van Erning, "Development and validation of a three-dimensional finite element model of the pelvic bone," *J. Biomech. Eng.,* vol. 117, pp. 272-278, Aug. 1995.

[41] J. Rho, L. Kuhn-Spearing and P. Zioupos, "Mechanical properties and the hierarchical structure of bone," *Medical Engineering & Physics,* vol. 20, pp. 92-102, March, 1998. 1998.

[42] D. R. Carter and W. C. Hayes, "The compressive behavior of bone as a two-phase porous structure," *J. Bone Joint Surg. Am.,* vol. 59, pp. 954-962, Oct. 1977.

[43] J. Peterson, Q. Wang and P. C. Dechow, "Material properties of the dentate maxilla," *Anat. Rec. A. Discov. Mol. Cell. Evol. Biol.,* vol. 288, pp. 962-972, Sep. 2006.

[44] C. L. Schwartz-Dabney and P. C. Dechow, "Variations in cortical material properties throughout the human dentate mandible," *Am. J. Phys. Anthropol.,* vol. 120, pp. 252-277, Mar. 2003.

[45] P. C. Dechow, G. A. Nail, C. L. Schwartz-Dabney and R. B. Ashman, "Elastic properties of human supraorbital and mandibular bone," *Am. J. Phys. Anthropol.,* vol. 90, pp. 291-306, March 1993. 1993.

[46] T. M. Keaveny and W. C. Hayes, "A 20-year perspective on the mechanical properties of trabecular bone," *J. Biomech. Eng.,* vol. 115, pp. 534-542, Nov. 1993.

[47] F. Taddei, A. Pancanti and M. Viceconti, "An improved method for the automatic mapping of computed tomography numbers onto finite element models," *Med. Eng. Phys.,* vol. 26, pp. 61-69, Jan. 2004.

[48] C. Zannoni, R. Mantovani and M. Viceconti, "Material properties assignment to finite element models of bone structures: a new method," *Med. Eng. Phys.,* vol. 20, pp. 735-740, Dec. 1998.

[49] J. H. Keyak, M. G. Fourkas, J. M. Meagher and H. B. Skinner, "Validation of an automated method of three-dimensional finite element modelling of bone," *J. Biomed. Eng.,* vol. 15, pp. 505-509, Nov. 1993.

[50] N. Maurel, A. Diop and J. Grimberg, "A 3D finite element model of an implanted scapula: importance of a multiparametric validation using experimental data," *J. Biomech.,* vol. 38, pp. 1865-1872, 09. 2005.

[51] S. Gupta, F. C. van der Helm, J. C. Sterk, F. van Keulen and B. L. Kaptein, "Development and experimental validation of a three-dimensional finite element model of the human scapula," *Proc. Inst. Mech. Eng. [H],* vol. 218, pp. 127-142, 2004.

[52] D. S. Barker, D. J. Netherway, J. Krishnan and T. C. Hearn, "Validation of a finite element model of the human metacarpal," *Med. Eng. Phys.,* vol. 27, pp. 103-113, Mar. 2005.

[53] J. Mackerle, "Finite element modelling and simulations in dentistry: a bibliography 1990-2003," *Comput. Methods Biomech. Biomed. Engin.,* vol. 7, pp. 277-303, Oct. 2004.

[54] A. Jafari, K. S. Shetty and M. Kumar, "Study of stress distribution and displacement of various craniofacial structures following application of transverse orthopedic forces--a three-dimensional FEM study," *Angle Orthod.,* vol. 73, pp. 12-20, Feb. 2003.

[55] H. Iseri, A. E. Tekkaya, O. Oztan and S. Bilgic, "Biomechanical effects of rapid maxillary expansion on the craniofacial skeleton, studied by the finite element method," *Eur. J. Orthod.,* vol. 20, pp. 347-356, Aug. 1998.

[56] J. Miyasaka-Hiraga, K. Tanne and S. Nakamura, "Finite element analysis for stresses in the craniofacial sutures produced by maxillary protraction forces applied at the upper canines," *Br. J. Orthod.,* vol. 21, pp. 343-348, Nov. 1994.

[57] C. Holberg and I. Rudzki-Janson, "Stresses at the cranial base induced by rapid maxillary expansion," *Angle Orthod.,* vol. 76, pp. 543-550, Jul. 2006.

[58] C. Provatidis, B. Georgiopoulos, A. Kotinas and J. P. McDonald, "On the FEM modeling of craniofacial changes during rapid maxillary expansion," *Med. Eng. Phys.,* vol. 29, pp. 566-579, Jun. 2007.

[59] X. Pan, Y. Qian, J. Yu, D. Wang, Y. Tang and G. Shen, "Biomechanical effects of rapid palatal expansion on the craniofacial skeleton with cleft palate: a three-dimensional finite element analysis," *Cleft Palate. Craniofac. J.,* vol. 44, pp. 149-154, Mar. 2007.

[60] C. Provatidis, B. Georgiopoulos, A. Kotinas and J. P. MacDonald, "In vitro validated finite element method model for a human skull and related craniofacial effects during rapid maxillary expansion," *Proc. Inst. Mech. Eng. [H],* vol. 220, pp. 897-907, Nov. 2006.

[61] K. Tanne, J. Hiraga, K. Kakiuchi, Y. Yamagata and M. Sakuda, "Biomechanical effect of anteriorly directed extraoral forces on the craniofacial complex: a study using the finite element method," *Am. J. Orthod. Dentofacial Orthop.,* vol. 95, pp. 200-207, Mar. 1989.

[62] K. Maki, N. Inou, A. Takanishi and A. J. Miller, "Modeling of structure, quality, and function in the orthodontic patient," *Orthod. Craniofac. Res.,* vol. 6 Suppl 1, pp. 52-8; discussion 179-82, 2003.

[63] H. S. Yu, H. S. Baik, S. J. Sung, K. D. Kim and Y. S. Cho, "Three-dimensional finite-element analysis of maxillary protraction with and without rapid palatal expansion," *Eur. J. Orthod.,* Jan 11. 2007.

[64] K. Tanne, J. Miyasaka, Y. Yamagata, R. Sachdeva, S. Tsutsumi and M. Sakuda, "Three-dimensional model of the human craniofacial skeleton: method and preliminary results using finite element analysis," *J. Biomed. Eng.,* vol. 10, pp. 246-252, May. 1988.

[65] M. D. Gross, G. Arbel and I. Hershkovitz, "Three-dimensional finite element analysis of the facial skeleton on simulated occlusal loading," *J. Oral Rehabil.,* vol. 28, pp. 684-694, Jul. 2001.

[66] P. M. Cattaneo, M. Dalstra and B. Melsen, "The transfer of occlusal forces through the maxillary molars: a finite element study," *Am. J. Orthod. Dentofacial Orthop.,* vol. 123, pp. 367-373, Apr. 2003.

[67] T. Nagasao, T. Nakajima, A. Kimura, T. Kaneko, H. Jin and T. Tamaki, "The dynamic role of buttress reconstruction after maxillectomy," *Plast. Reconstr. Surg.,* vol. 115, pp. 1328-40; discussion 1341, Apr 15. 2005.

[68] L. Ibanez, W. Schroeder, L. Ng and J. Cates. (2005, *ITK Software Guide.* (Second ed.)

[69] V. Caselles, R. Kimmel and G. Sapiro, "Geodesic Active Contours," *International Journal of Computer Vision,* vol. 22, pp. 61-79, February 1997. 1997.

[70] M. C. Raadsheer, T. M. van Eijden, F. C. van Ginkel and B. Prahl-Andersen, "Contribution of jaw muscle size and craniofacial morphology to human bite force magnitude," *J. Dent. Res.,* vol. 78, pp. 31-42, Jan. 1999.

[71] M. Descoteaux, M. Audette, K. Chinzei and K. Siddiqi, "Bone enhancement filtering: application to sinus bone segmentation and simulation of pituitary surgery," *Comput. Aided Surg.,* vol. 11, pp. 247-255, Sep. 2006.

[72] C. E. Tschirhart, J. A. Finkelstein and C. M. Whyne, "Biomechanics of vertebral level, geometry, and transcortical tumors in the metastatic spine," *J. Biomech.,* vol. 40, pp. 46-54, 2007.

[73] D. M. Estok 2nd, T. E. Orr and W. H. Harris, "Factors affecting cement strains near the tip of a cemented femoral component," *J. Arthroplasty,* vol. 12, pp. 40-48, Jan. 1997.

[74] P. Krimbalis, "A validated finite element study of blunt trauma to the human maxilla," 2004.

[75] K. Kupczik, C. A. Dobson, M. J. Fagan, R. H. Crompton, C. E. Oxnard and P. O'higgins, "Assessing mechanical function of the zygomatic region in macaques: validation and sensitivity testing of finite element models," *J. Anat.,* vol. 210, pp. 41-53, Jan. 2007.

[76] C. C. Peck and A. G. Hannam, "Human jaw and muscle modelling," *Arch. Oral Biol.,* vol. 52, pp. 300-304, Apr. 2007.

[77] C. F. Ross, R. Dharia, S. W. Herring, W. L. Hylander, Z. J. Liu, K. L. Rafferty, M. J. Ravosa and S. H. Williams, "Modulation of mandibular loading and bite force in mammals during mastication," *J. Exp. Biol.,* vol. 210, pp. 1046-1063, Mar. 2007.

[78] J. C. Nickel, L. R. Iwasaki, R. D. Walker, K. R. McLachlan and W. D. McCall Jr, "Human masticatory muscle forces during static biting," *J. Dent. Res.,* vol. 82, pp. 212-217, Mar. 2003.

[79] N. G. Blanksma, T. M. G. J. vanEijden, L. J. vanRuijven and W. A. Weijs, "Electromyographic heterogeneity in the human temporalis and masseter muscles during dynamic tasks guided by visual feedback," *J. Dent. Res.,* vol. 76, pp. 542-551, 1997.

[80] N. G. Blanksma, T. M. G. J. Van Eijden and W. A. Weijs, "Electromyographic Heterogeneity in the Human Masseter Muscle," *J. Dent. Res.,* vol. 71, pp. 47-52, 1992.

[81] D. S. Strait, B. G. Richmond, M. A. Spencer, C. F. Ross, P. C. Dechow and B. A. Wood, "Masticatory biomechanics and its relevance to early hominid phylogeny: An examination of palatal thickness using finite-element analysis," *J. Hum. Evol.,* Feb 20. 2007.

[82] T. M. G. J. Van Eijden, P. Brugman, W. A. Weijs and J. Oosting, "Coactivation of jaw muscles: Recruitment order and level as a function of bite force direction and magnitude," *J. Biomech.,* vol. 23, pp. 475-485, 1990. 1990.

[83] T. M. G. J. Van Eijden, "Jaw Muscle-Activity in Relation to the Direction and Point of Application of Bite Force," *J. Dent. Res.,* vol. 69, pp. 901-905, 1990.

[84] H. J. Schindler, S. Rues, J. C. Turp, K. Schweizerhof and J. Lenz, "Activity patterns of the masticatory muscles during feedback-controlled simulated clenching activities," *Eur. J. Oral Sci.,* vol. 113, pp. 469-478, Dec. 2005.

[85] C. F. Ross, B. A. Patel, D. E. Slice, D. S. Strait, P. C. Dechow, B. G. Richmond and M. A. Spencer, "Modeling masticatory muscle force in finite element analysis: sensitivity analysis using principal coordinates analysis," *Anat. Rec. A. Discov. Mol. Cell. Evol. Biol.,* vol. 283, pp. 288-299, Apr. 2005.

[86] D. L. Kopperdahl and T. M. Keaveny, "Yield strain behavior of trabecular bone," *J. Biomech.,* vol. 31, pp. 601-608, Jul. 1998.

[87] H. Gray, *Gray's Anatomy of the Human Body.* ,Twentieth ed., Philadephia, PA: Lea & Febiger, 1918.

[88] H. R. Elden, "Effect of cross-linking by formaldehyde on the contraction-relaxation of rat tail tendon," *Nature,* vol. 183, pp. 332-333, Jan 31. 1959.

Appendix A - Finite Element Model and In Vitro Strain Comparisons

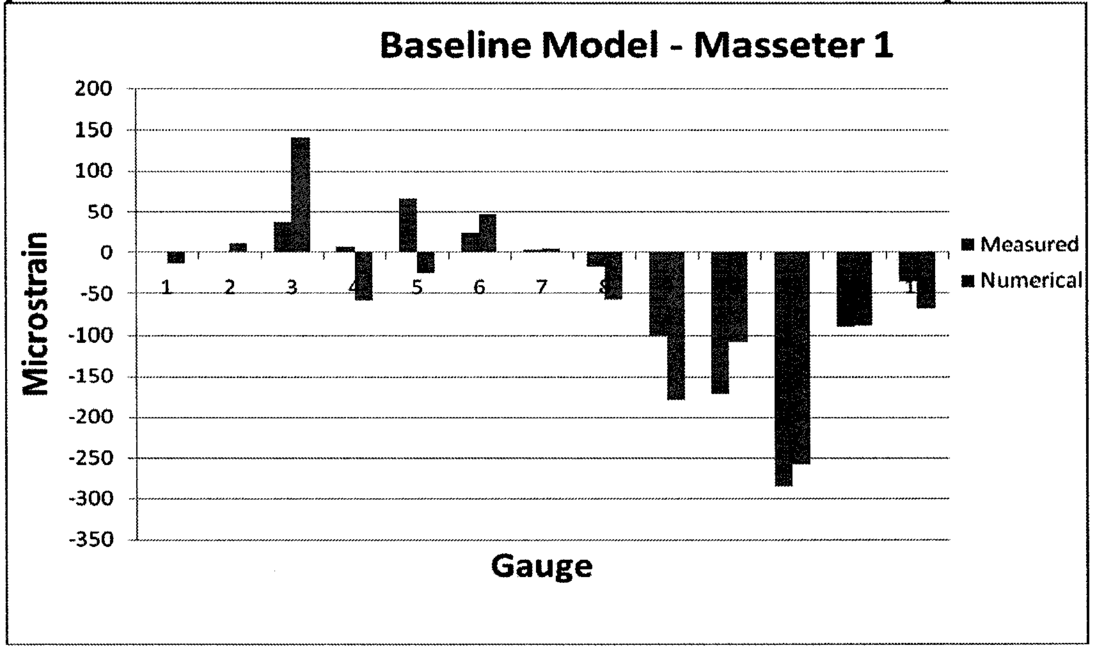

Figure 6-1 – Comparison of measured and numerical strains for the masseter 1 load.

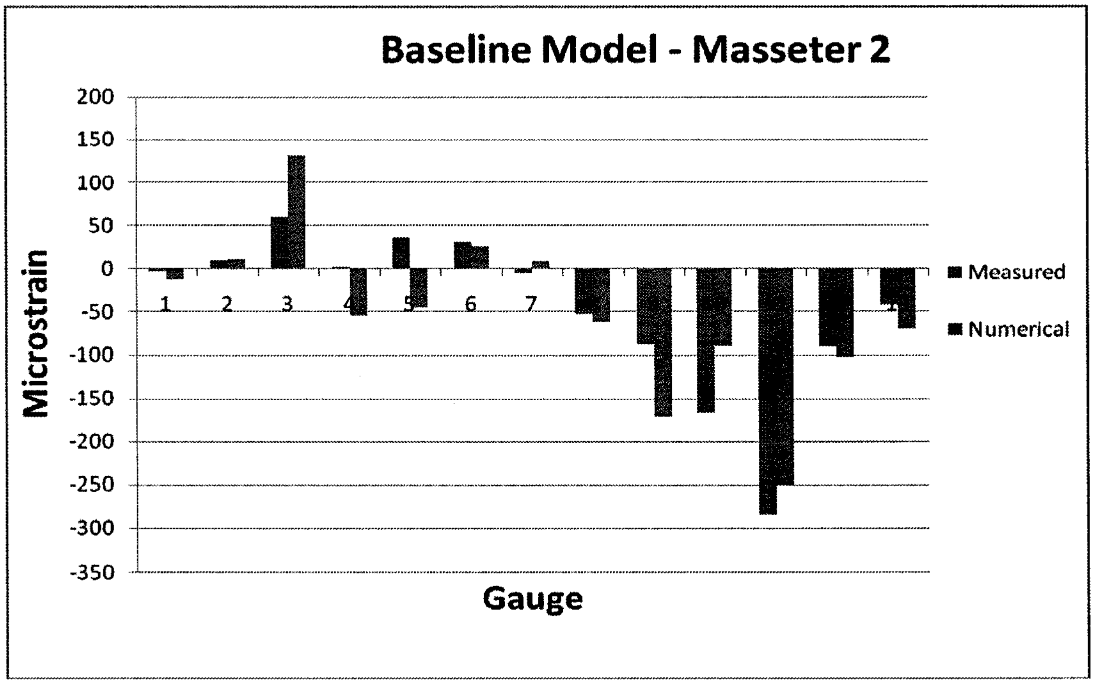

Figure 6-2 - Comparison of measured and numerical strains for the masseter 2 load.

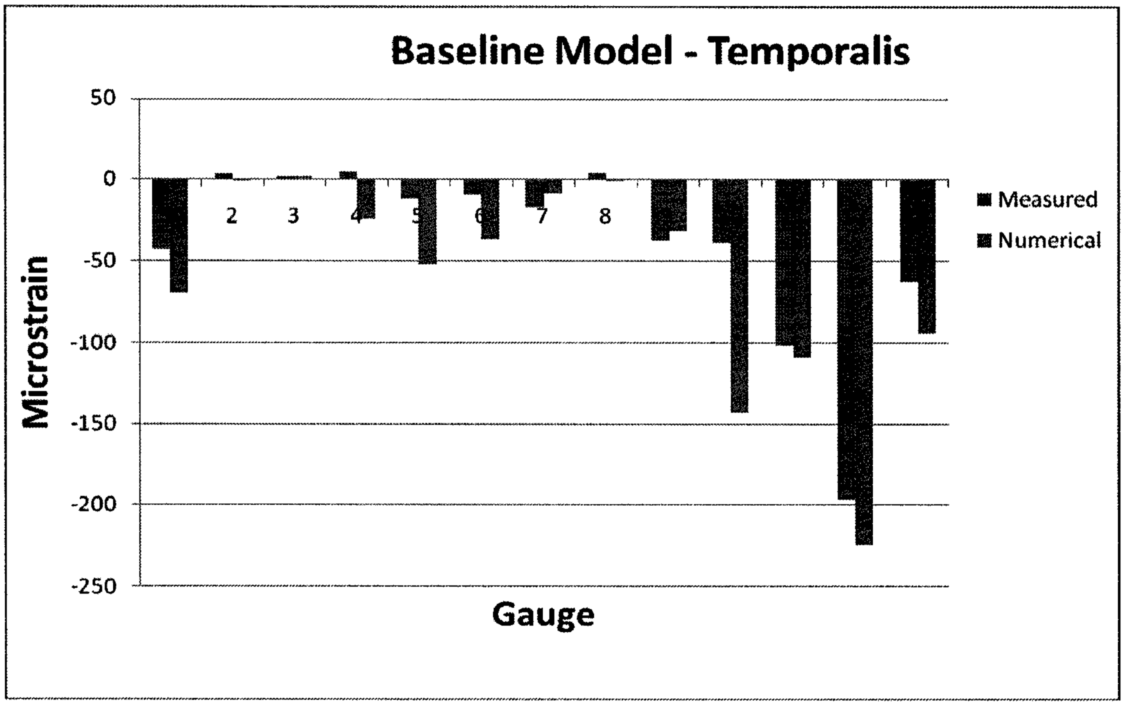

Figure 6-3 - Comparison of measured and numerical strains for the temporalis load.

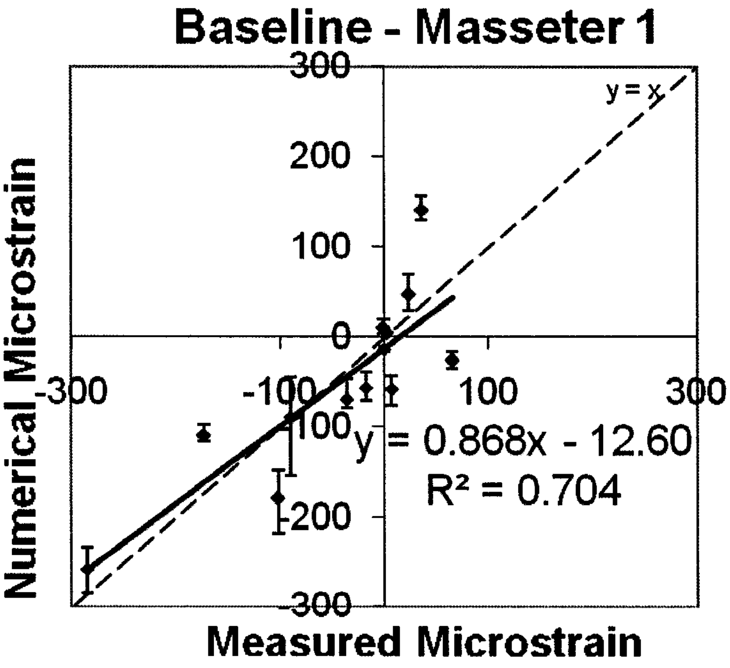

Figure 6-4 - Linear regression analysis for baseline model subject to masseter 1 load case.

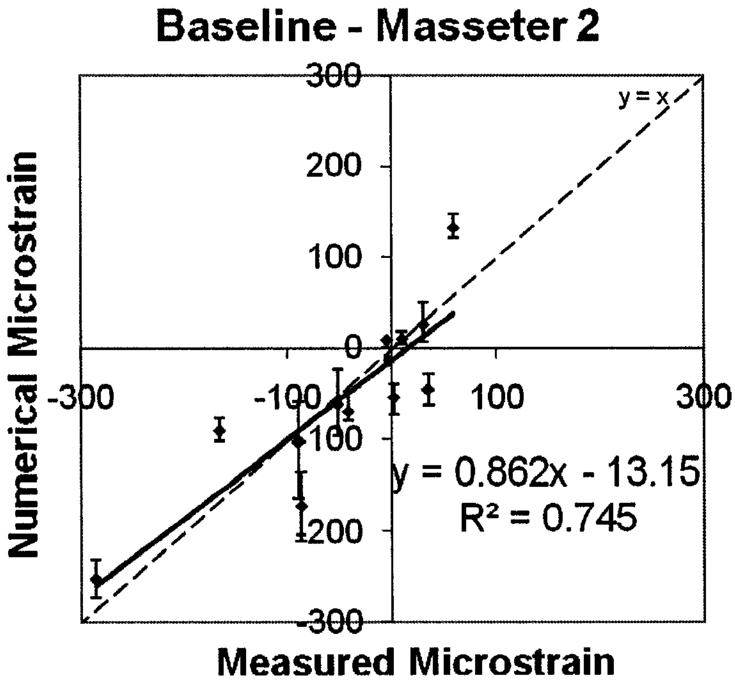

Figure 6-5 - Linear regression analysis for baseline model subject to masseter 2 load case.

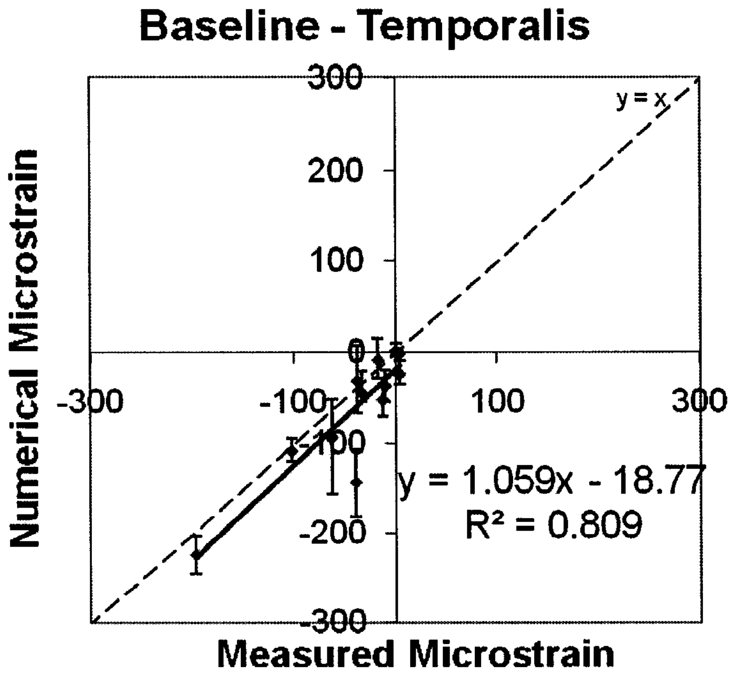

Figure 6-6 - Linear regression analysis for baseline model subject to temporalis load case.

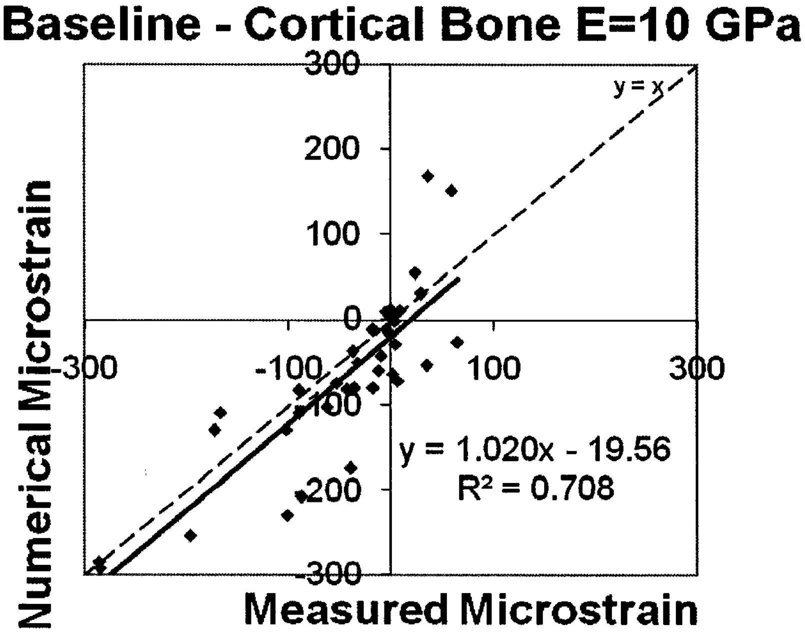

Figure 6-7 - Linear regression analysis for model with cortical modulus of 10 GPa, all load cases.

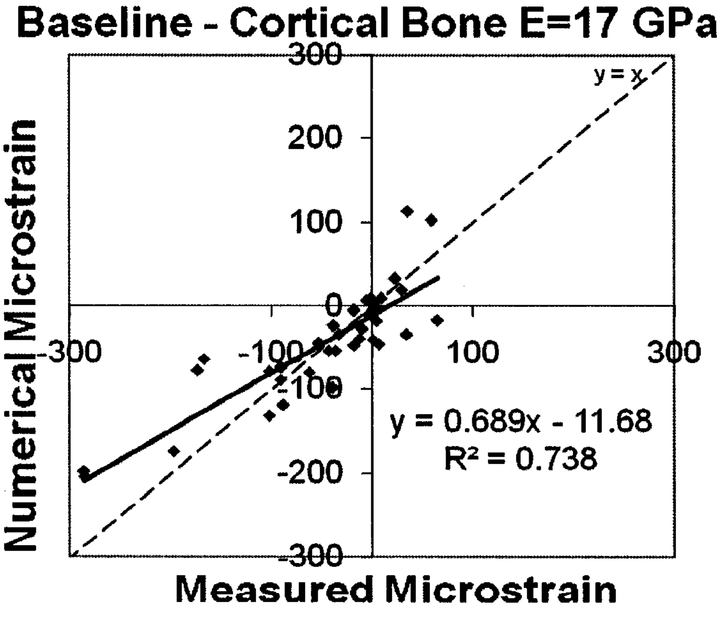

Figure 6-8 - Linear regression analysis for model with cortical modulus of 17 GPa, all load cases.

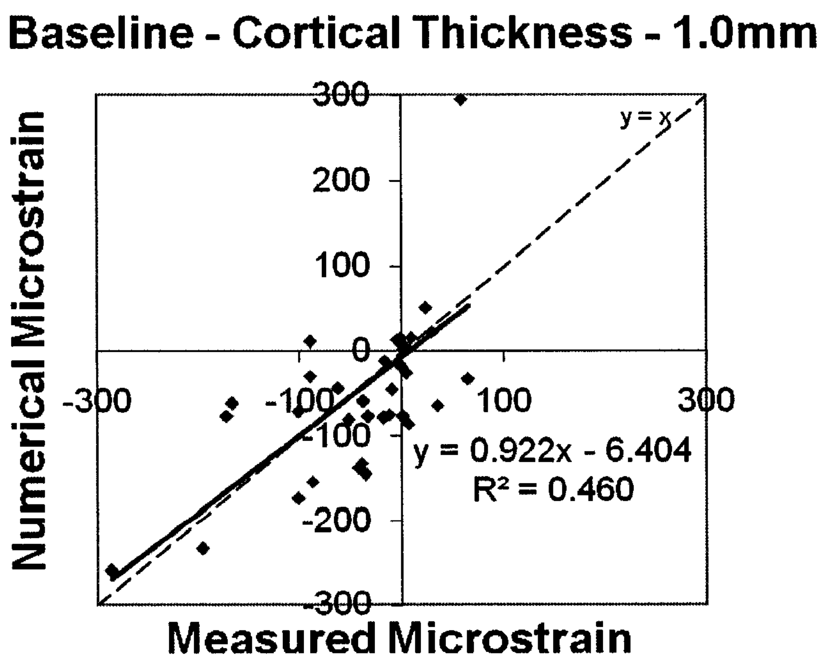

Figure 6-9 - Linear regression analysis for model with uniform cortical thickness of 1.0mm, all load cases.

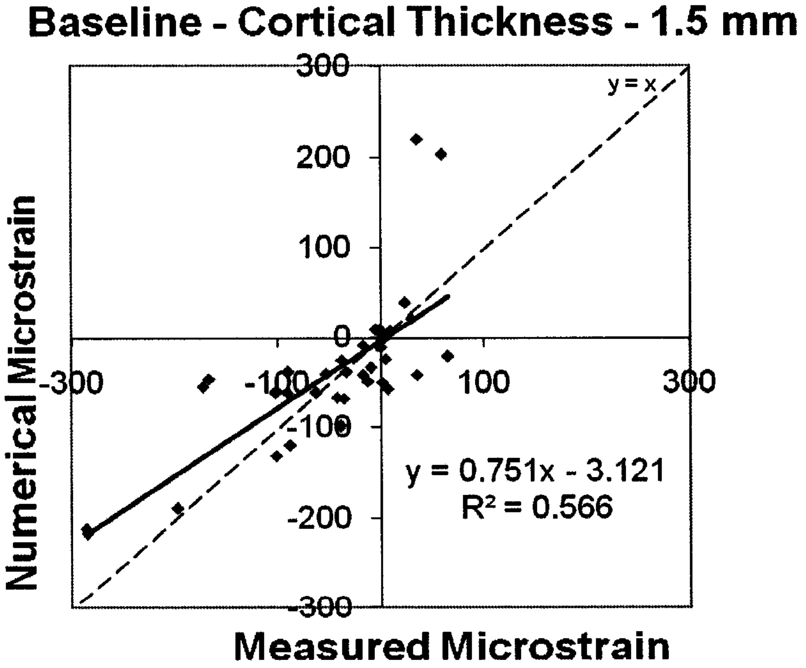

Figure 6-10 - Linear regression analysis for model with uniform cortical thickness of 1.5mm, all load cases.

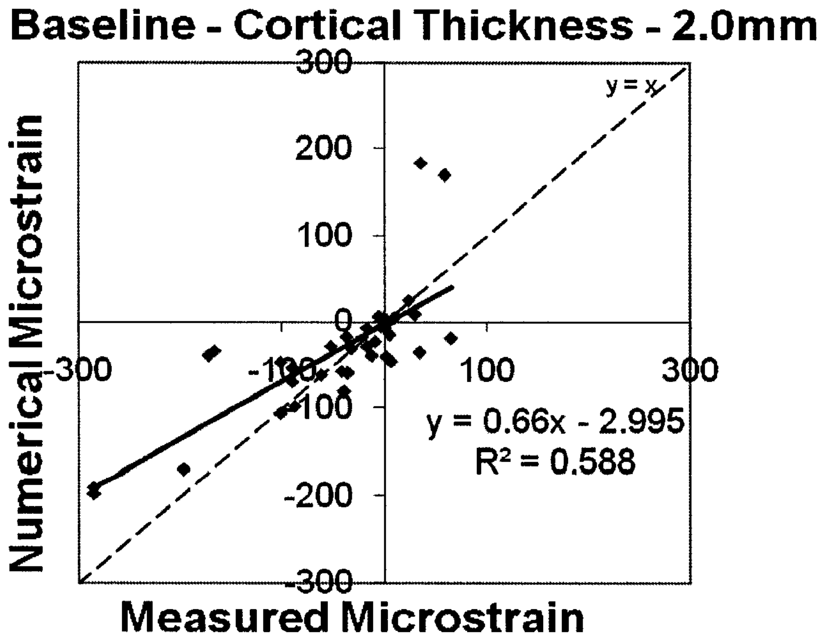

Figure 6-11 - Linear regression analysis for model with uniform cortical thickness of 2.0mm, all load cases.

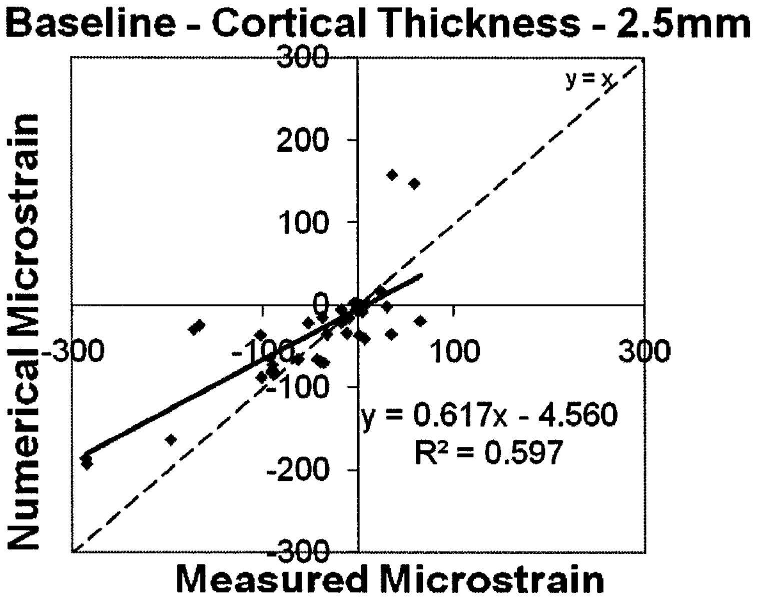

Figure 6-12 - Linear regression analysis for model with uniform cortical thickness of 2.5mm, all load cases.

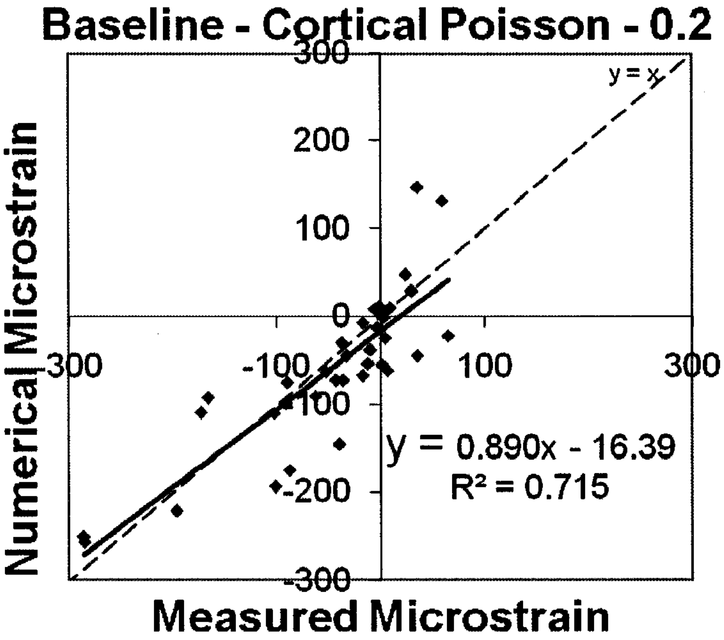

Figure 6-13 - Linear regression analysis for model with uniform cortical Poisson's ratio of 0.2, all load cases.

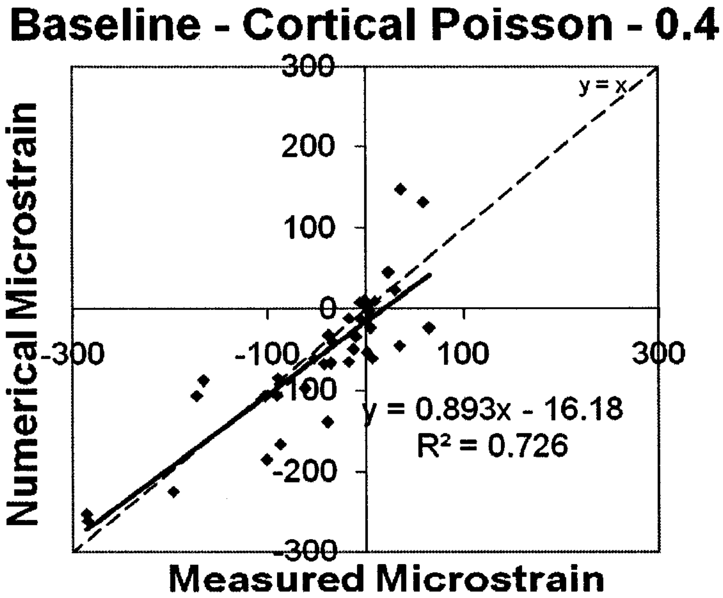

Figure 6-14 -Linear regression analysis for model with uniform cortical Poisson's ratio of 0.4, all load cases.

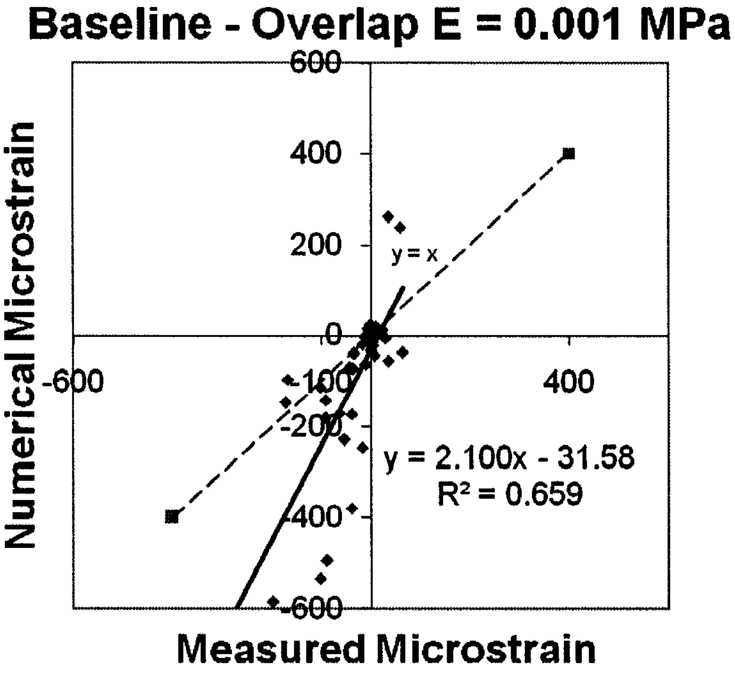

Figure 6-15 - Linear regression analysis for model with tetrahedral overlap modulus of 0.001 MPa, all load cases.

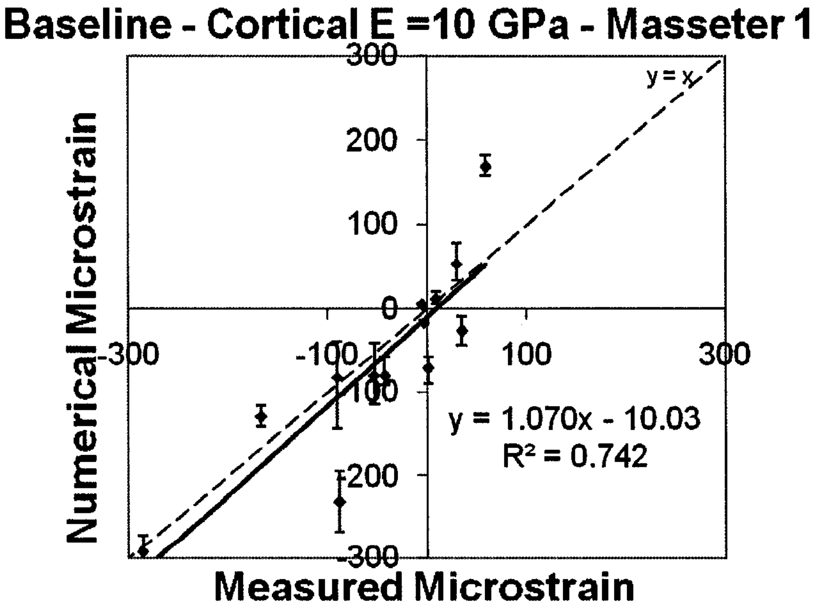

Figure 6-16 - Linear regression analysis for model with cortical elastic modulus of 10 GPa for masseter 1 load case.

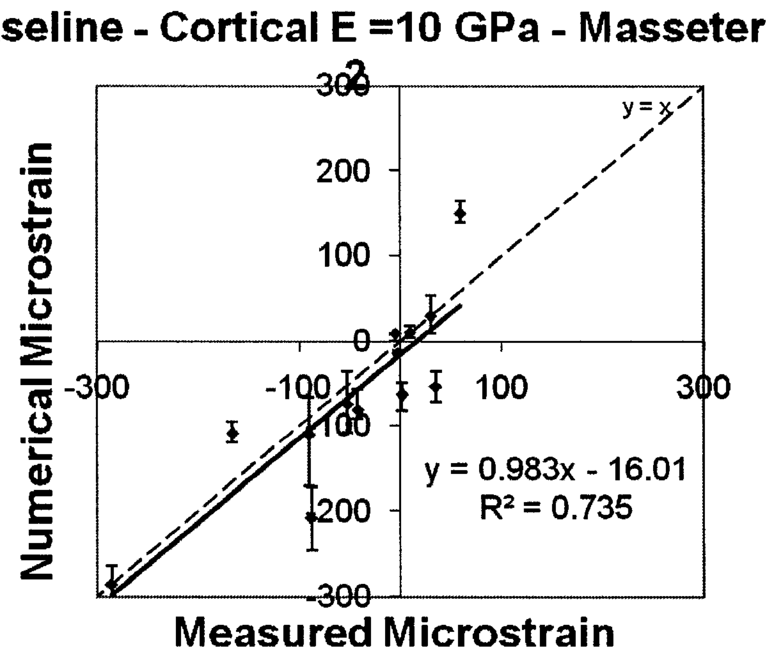

Figure 6-17 - Linear regression analysis for model with cortical elastic modulus of 10 GPa for masseter 2 load case.

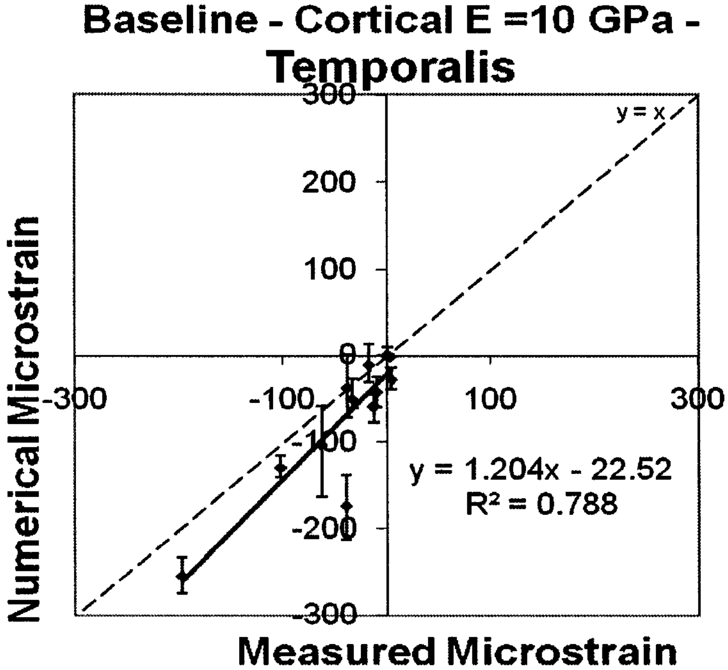

Figure 6-18 - Linear regression analysis for model with cortical elastic modulus of 10 GPa for temporalis load case.

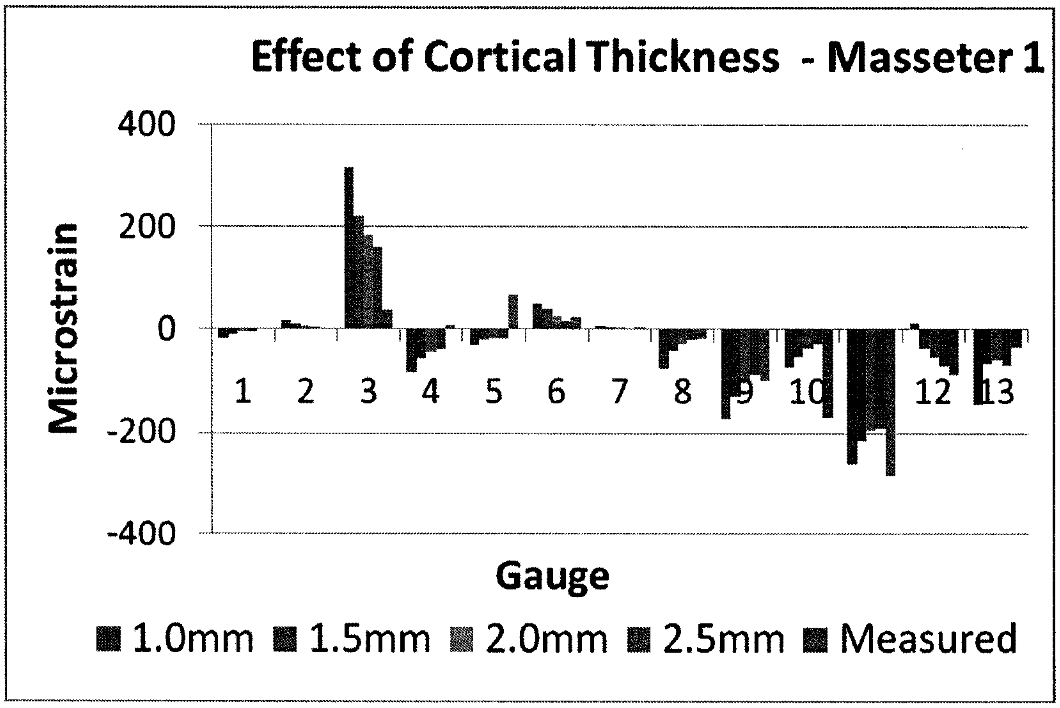

Figure 6-19 - Gauge strain variation with uniform cortical thickness estimates against measured in vitro strain for the masseter 1 load case.

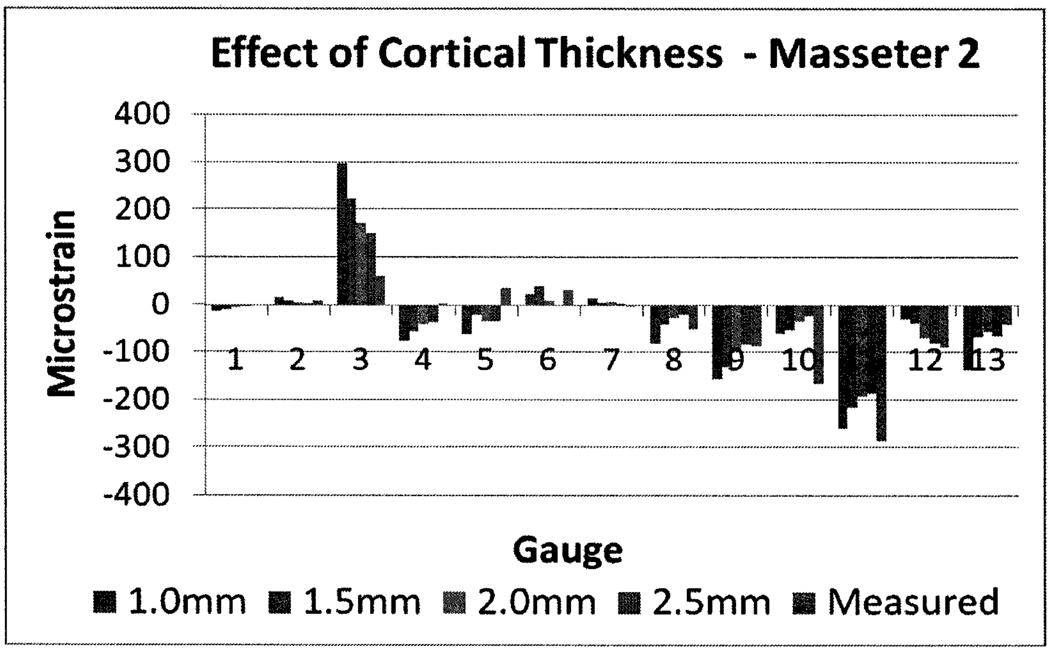

Figure 6-20 - Gauge strain variation with uniform cortical thickness estimates against measured in vitro strain for the masseter 2 load case.

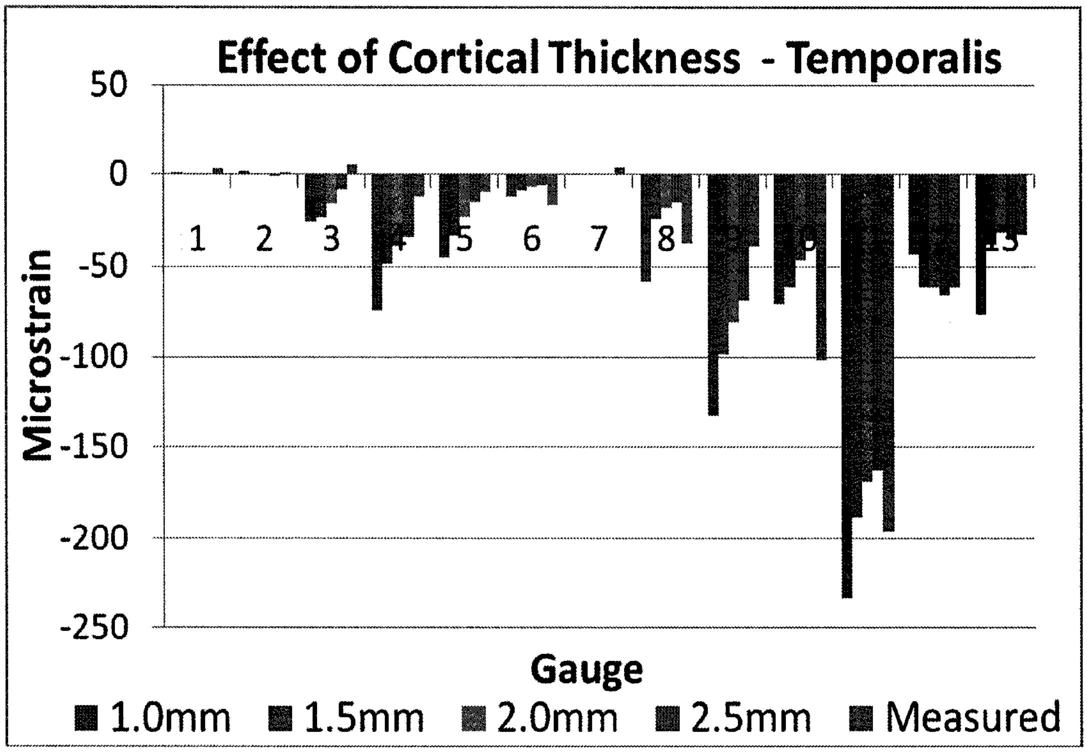

Figure 6-21 - Gauge strain variation with uniform cortical thickness estimates against measured in vitro strain for the temporalis load case.

Appendix B - Standard Operating Procedure

Surface Triangulation:

Files can be found in E:\Mesh\cfs5804\:

1. Generate surface from the segmentation. Using Amira SurfaceGen module with no smoothing.
2. Simplify the surface (+2mil triangles) to 1.5 million triangles.
3. Open the surface editor and use the smooth faces procedure 2 times, then perform intersection check and remove intersections found.
4. Simplify the surface to 1.0 million triangles. No max dist or min dist is left as the default. Preserve slice structure option

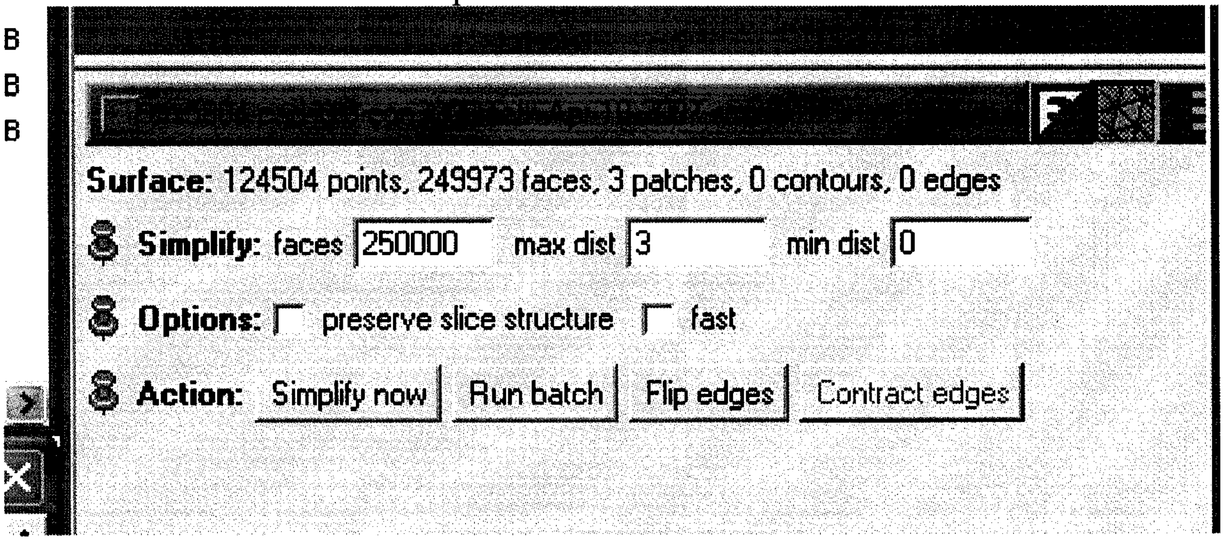

Surface: 124504 points, 249973 faces, 3 patches, 0 contours, 0 edges

Simplify: faces 250000 max dist 3 min dist 0

Options: ☐ preserve slice structure ☐ fast

5. Repeat step 3.
6. Simplify the surface to 700K triangles.
7. Repeat step 3.
8. Simplify the surface to 500K triangles.
9. Repeat step 3.
10. Simplify the surface to 400K triangles.
11. Repeat step 3.
12. Simplify the surface to 300K triangles.
13. Repeat step 3.
14. Simplify the surface to 250K triangles.
15. Repeat step 3.
16. Simplify the surface to 225K triangles.
17. Repeat step 3.
18. Simplify the surface to 200K triangles.
19. Repeat step 3.
20. Simplify the surface to 190K triangles.
21. Repeat step 3.

22. Simplify the surface to 180K triangles.
23. Open surface editor, use draw tool to select the facial region, and perform the refine faces operation. The region that was selected so that it included the facial region. This was only done to increase the facial mesh density and simplification would restore the origin 180K mesh. This then make a smaller mesh density on the cranial vault, which is not strained and therefore does not require a high mesh. This then results in a lower tetrahedral mesh density in the cranium, which would make it impossible to run on the local PC.

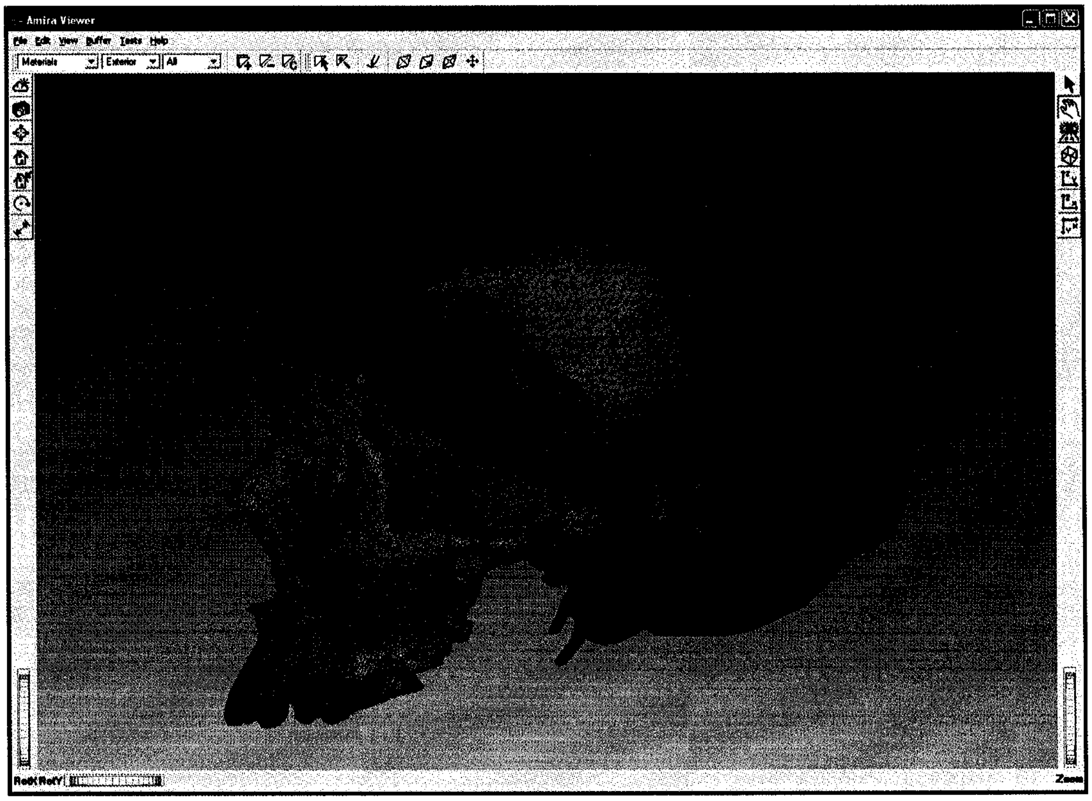

24. Simplify surface to 400K triangles.
25. Repeat step 3.
26. Simplify surface to 350K triangles.
27. Repeat step 3.
28. Simplify surface to 300K triangles.
29. Repeat step 3.
30. Simplify surface to 250K triangles.
31. Repeat step 3.

NOTE: 1) It is common to get intersections at the teeth. Simplifying to a different surface mesh density can sometimes prevent this. The iterative approach to the simplification and smoothing reduces the number of intersections that you have to deal with. To deal with the intersections that occur as below you can use the Subdivide Edges tool:

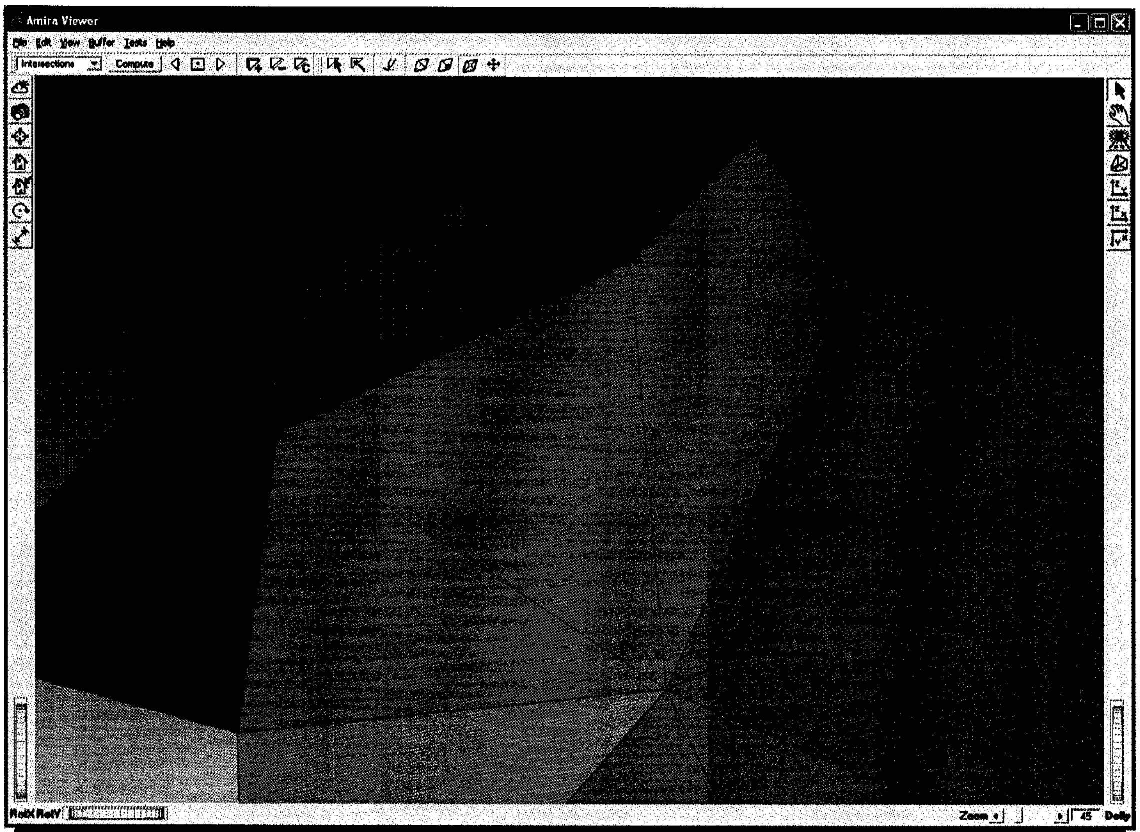
Amira Viewer
File Edit View Buffer Tools Help
Intersections
Compute
RotX RotY
Zoom
45
Dolly

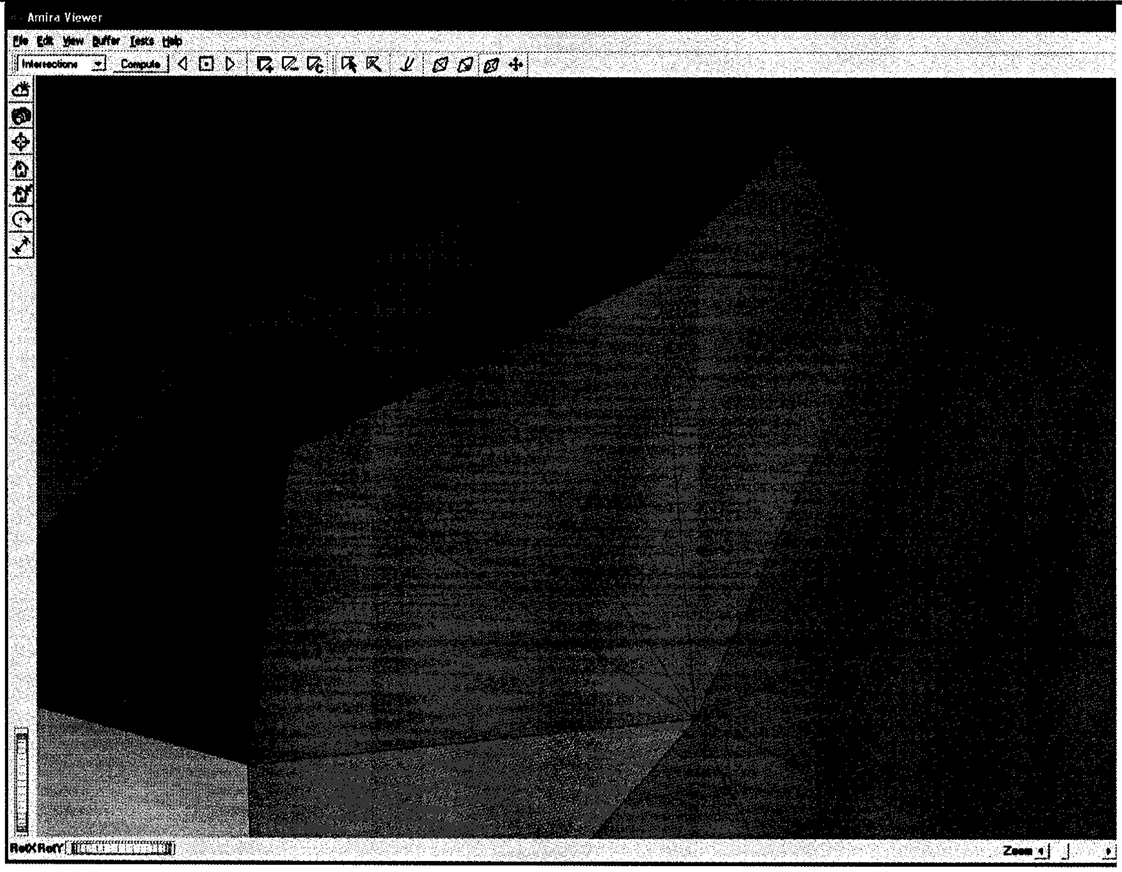
Amira Viewer
File Edit View Buffer Tools Help
Intersections
Compute
RotX RotY
Zoom

Then you can use the Translate Verticies tool (image below) to move the nodes and adjust the triangles to eliminate the intersection:

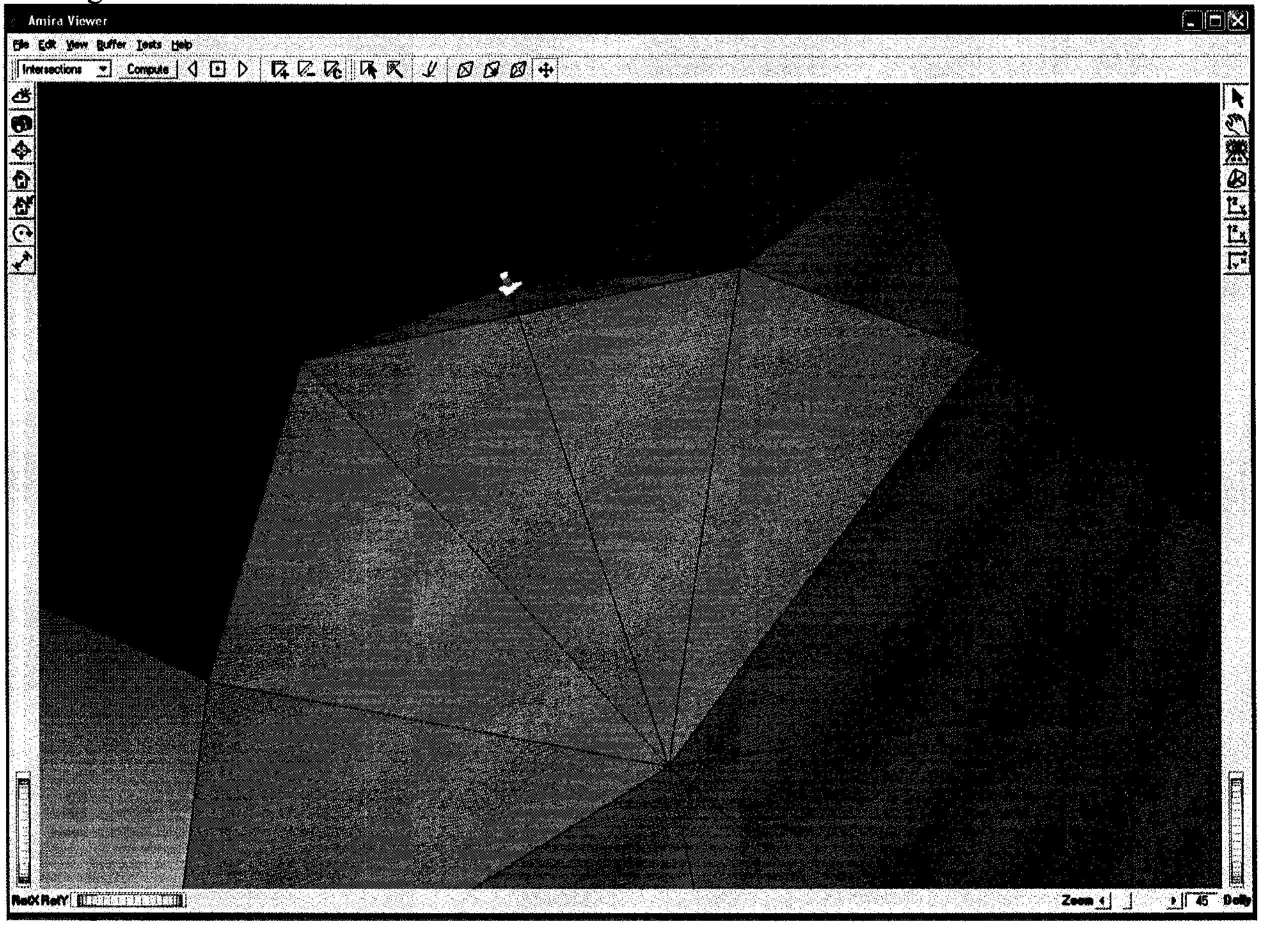

Then you can use the Contract Edges tool to remove those triangles that you have created to fix the triangulation there. This intersection is the worst that you will encounter and the same tools (Contract Edges, Subdivide Edges, Translate Tool) will be useful for dealing with all intersections.

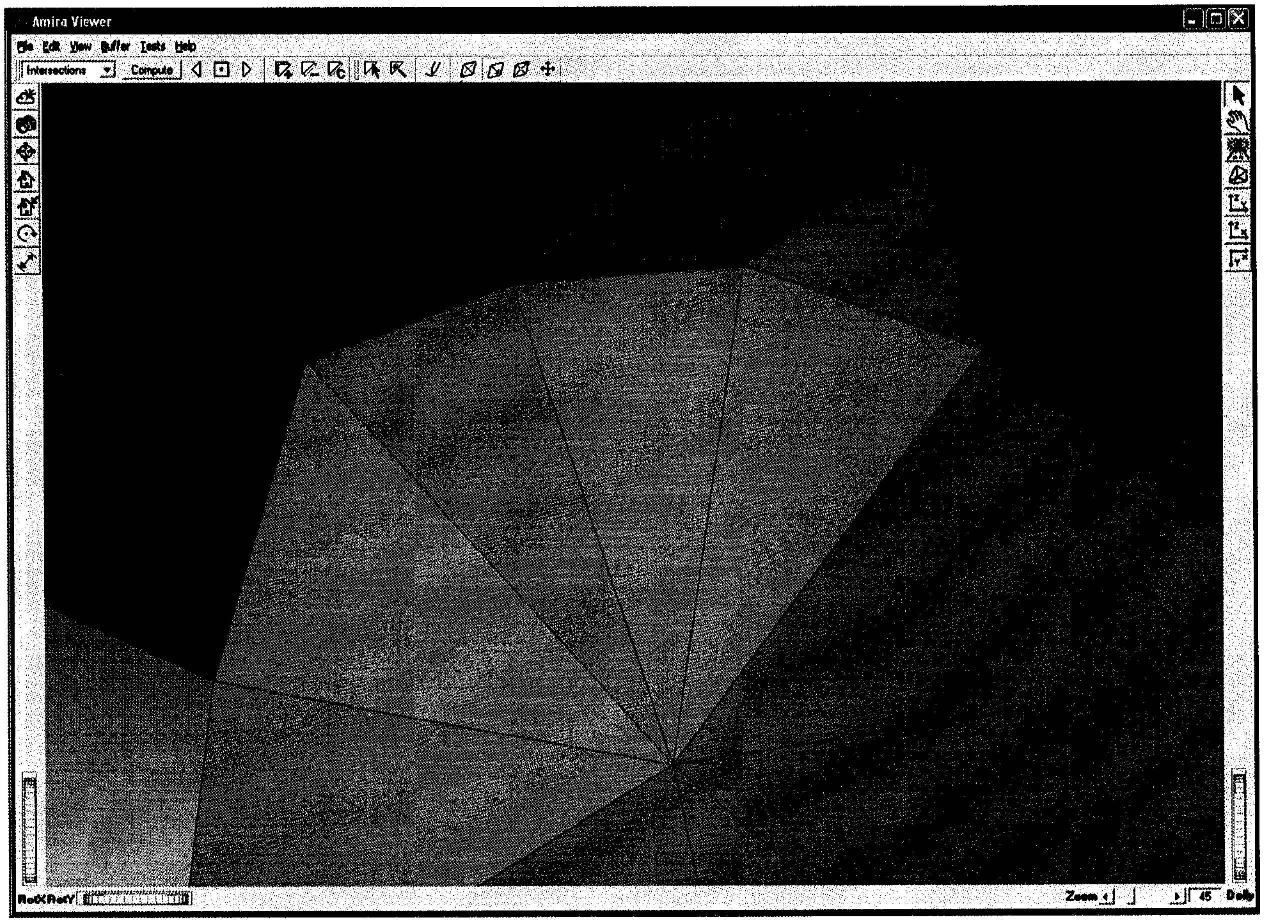

Tetrahedral Mesh Generation

Use the developed surface triangulation with the Amira TetraGen module with the improve grid option selected. This will result in a mesh of 1,819,667 tetrahedrons.

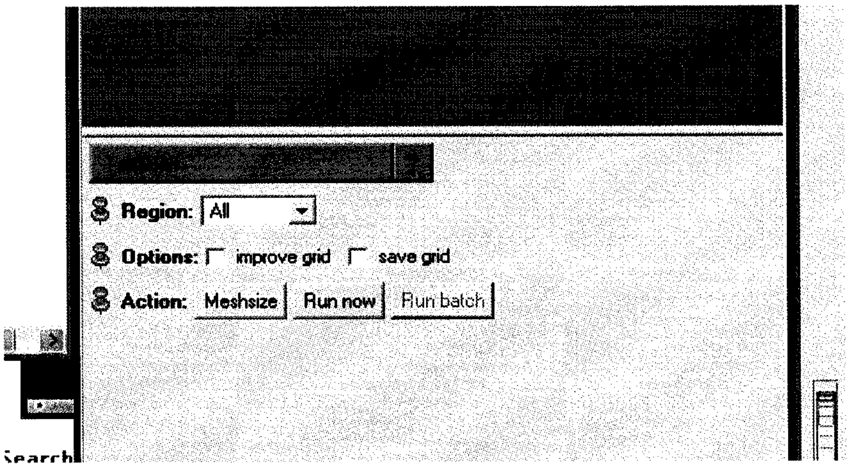

Region: All

Options: ☐ improve grid ☐ save grid

Action: Meshsize Run now Run batch

Bonemat:

Once the tetrahedral mesh is generated MatGrid (Local → MatGrid) FE mesh (Right click on MatGrid → connect FEMGrid). This uses BONEMAT V2 to assign a CT intensity to each tet which is then used to calculate stiffness.
Note: The names of the objects which correspond to the file name of the object.

- This scan is E:\Tom\Segmentation\cfs5804\scan\cfs5804-tr-iso-cr-flt.am and to use it with Matgrid it must be isotropic resolution.
- The FE mesh is cfs5804-cad-it10-con300l-teeth-Apr-10-2007-smlab-180k-ref-250k.grid
  From E:\Tom\Mesh\cfs5804\grids\cfs5804-cad-it10-con300l-teeth-Apr-10-2007-smlab-180k-ref-250k.grid

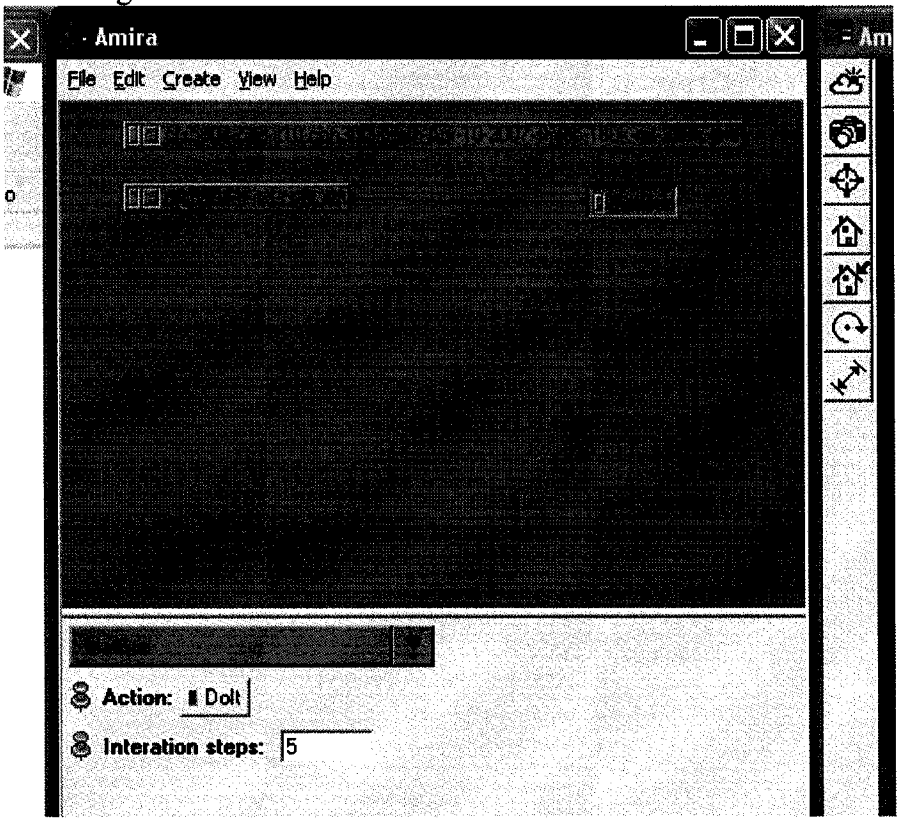

Action: DoIt

Interation steps: 5

Binning:

This creates the beginning of the Abaqus Input deck. Load the binner from the GridPackage on the combined mesh and connect the matgrid output as the colourmap. Standard options used are outlined below.

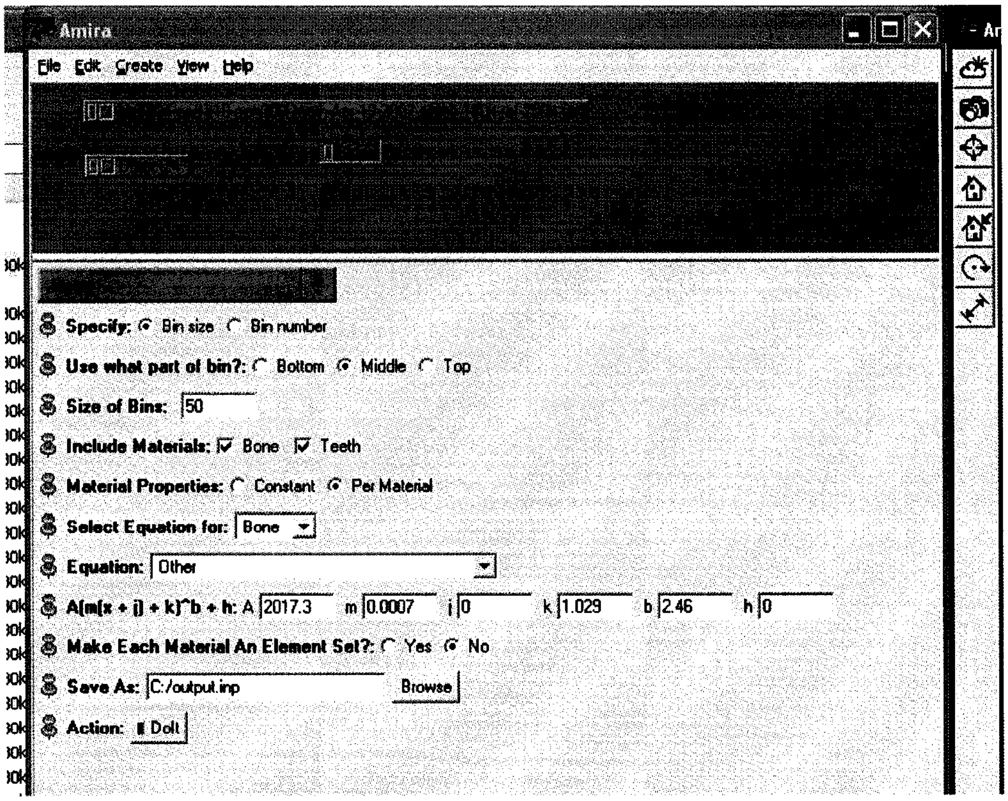

Specify: ● Bin size ○ Bin number

Use what part of bin?: ○ Bottom ● Middle ○ Top

Size of Bins: 50

Include Materials: ☑ Bone ☑ Teeth

Material Properties: ○ Constant ● Per Material

Select Equation for: Bone

Equation: Other

A(m(x + i) + k)^b + h: A 2017.3 m 0.0007 i 0 k 1.029 b 2.46 h 0

Make Each Material An Element Set?: ○ Yes ● No

Save As: C:/output.inp

1. Bin size 50 MPa.
2. Use middle of bine
3. Include all materials
4. Per Material option selected.
5. For bone use the values in above figure.
6. For teeth use value in the below figure.

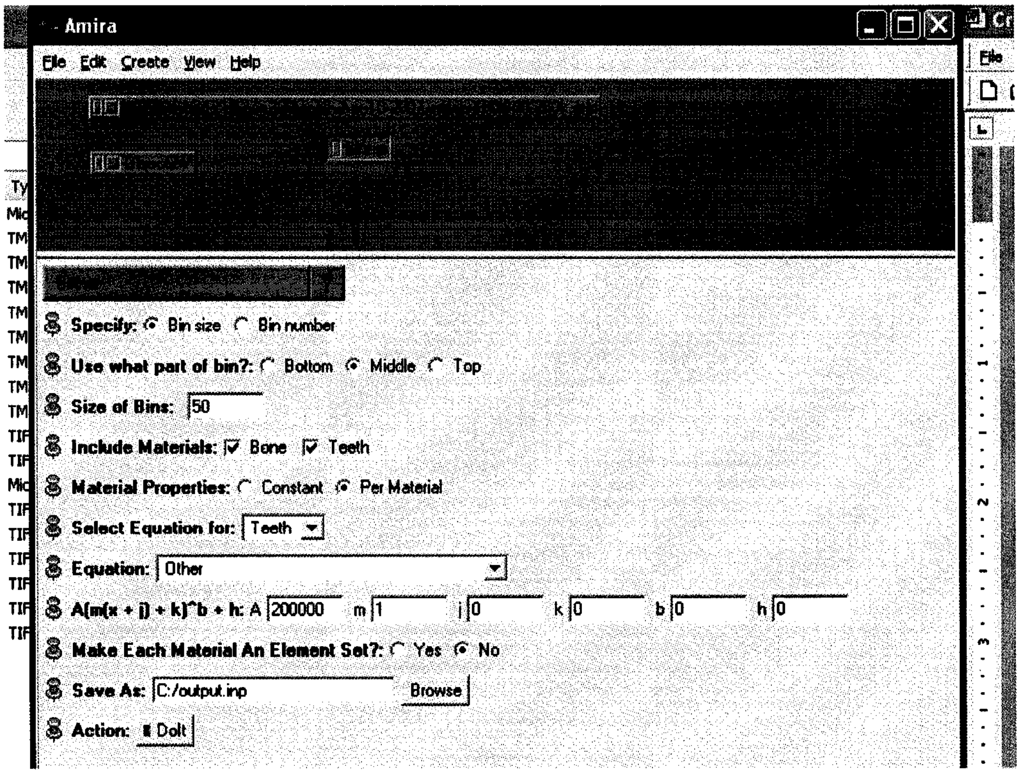

Specify: ● Bin size ○ Bin number

Use what part of bin?: ○ Bottom ● Middle ○ Top

Size of Bins: 50

Include Materials: ☑ Bone ☑ Teeth

Material Properties: ○ Constant ● Per Material

Select Equation for: Teeth

Equation: Other

A(m(x + i) + k)^b + h: A 200000 m 1 i 0 k 0 b 0 h 0

Make Each Material An Element Set?: ○ Yes ● No

Save As: C:/output.inp

Action: DoIt

Shell Element Meshing.

1. For this you need the grid.
   E:\Tom\Mesh\cfs5804\grids\cfs5804-cad-it10-con3001-teeth-Apr-10-2007-smlab-180k-ref-250k.grid
   and the cortical surface file
   E:\Tom\Mesh\cfs5804\bcsurfaces\fs5804-cad-it10-con3001-teeth-Apr-10-2007-smlab-180k-ref-250k-CORTICAL.surf
2. Use the GridPackage->SurfDist module to measure the cortical thickness. Attach to the Cortical surface and the Cortical Shell Segmentation E:\Tom\Segmentation\cfs5804\manual\cortshell.am
3. The Result should look like. This segmentation was not with the cranial vault which was included in the thesis later for visualization purposes. This does not effect the results of the models to exclude the cranial region.

Step Size: 0.001

Threshold: 0.99999

Cutoff: 1

Invert Normals: ☑

Action: DoIt

4. Use the GridPackage->Shells to write the shell element mesh to the .inp file.

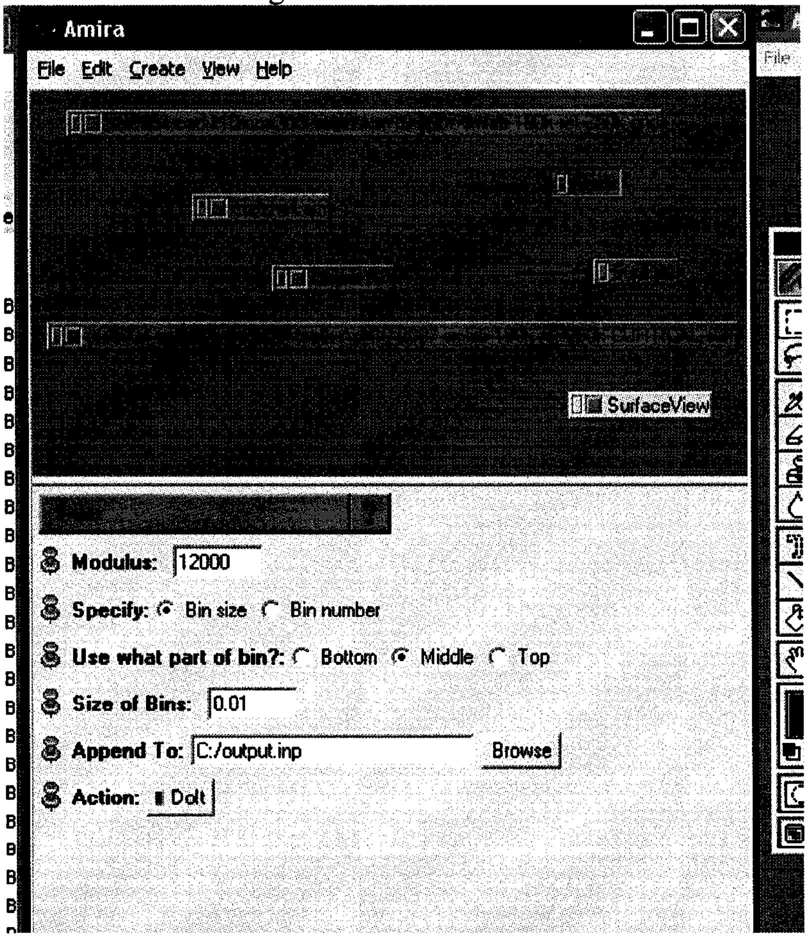

Modulus: 12000

Specify: ● Bin size ○ Bin number

Use what part of bin?: ○ Bottom ● Middle ○ Top

Size of Bins: 0.01

Append To: C:/output.inp

Action: DoIt

Nodesets:

Use the GridPackage->NodeSets as per Annies method to extract the nodesets for the Cortical shell (all surface nodes of the tetrahedral grid I called it CortNodes (change the name of the surface) and for the Occlusal boundary condition (Occlusal surface – change name of surface because that is used in the nodeset name which you must reference for the boundary condition assignment).

Boundary Conditions Surfaces:

This describes how the surfaces for the muscle insertions were created. The muscle insertions are created based upon information provided by measuring the muscle contours from the cadaver using the Microscribe and the Rhinoceros software package.

1. The Surfaces a extracted using SurfaceView draw tool to highlight and remove triangles from the Visualization buffer.
2. Once the insertion has been defined use the SurfacView-> More Options->Create Surface.
3. The surface created has all the nodes from the whole skull surface, which you have to remove by simply opening the surface editor and closing it for the newly created masseter, temporalis or occlusal surfaces.
4. The surface used can be found in :

E:\Tom\Mesh\cfs5804\bcsurfaces:

cfs5804-cad-it10-con3001-teeth-Apr-10-2007-smlab-180k-ref-250k-MASSETER.surf
cfs5804-cad-it10-con3001-teeth-Apr-10-2007-smlab-180k-ref-250k-TEMPORALIS.surf
cfs5804-cad-it10-con3001-teeth-Apr-10-2007-smlab-180k-ref-250k-OCCLUSAL2.surf
cfs5804-cad-it10-con3001-teeth-Apr-10-2007-smlab-180k-ref-250k-CORTICAL.surf

The original surface is in: E:\Tom\Mesh\cfs5804\surfaces

cfs5804-cad-it10-con3001-teeth-Apr-10-2007-smlab-180k-ref-250k.surf

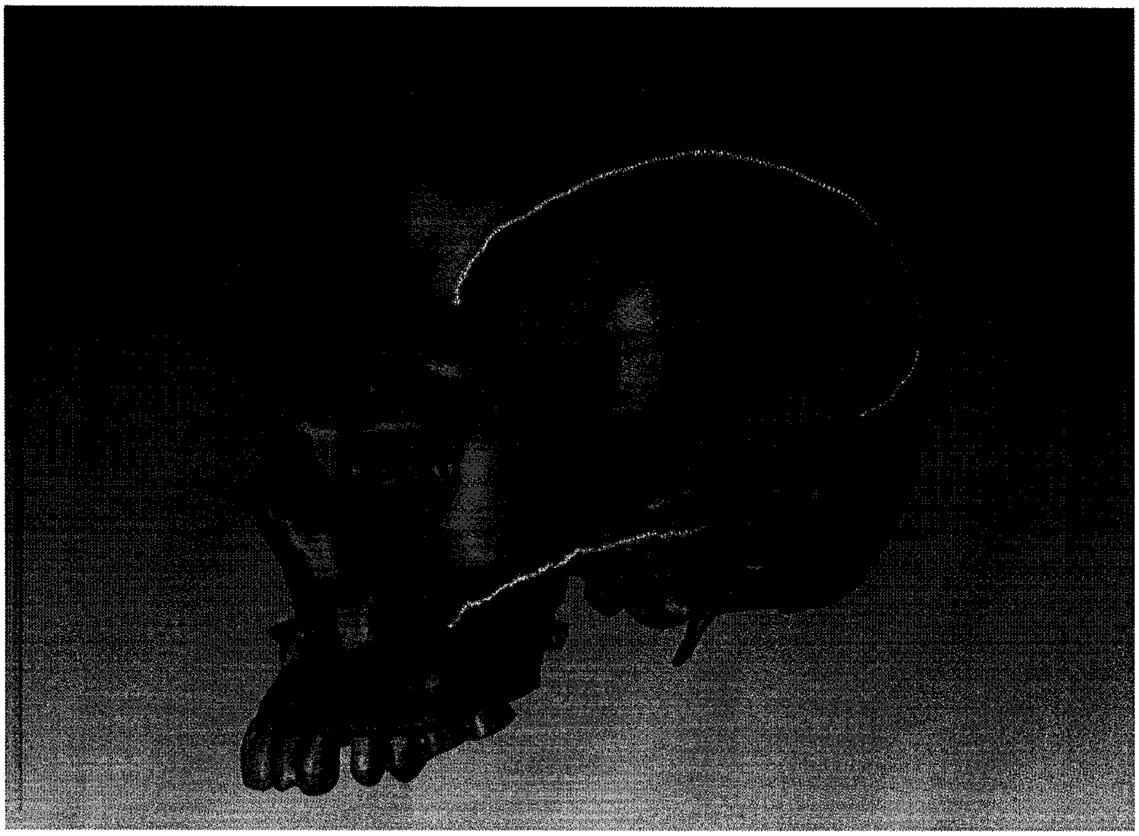

Restraints:

In the Step definition the command (2 lines) must be manual added through a text editor. Occlusal refers to the nodeset for the teeth that was created from the boundary condition surface

```
*BOUNDARY, OP=NEW
  OCCLSAL, 1, 3
```

Loads:

Loads were applied by using the Loader module in GridPackage. Loader connects to the 1) tetrahedral mesh, 2) the boundary surface and 3) the landmarks for the load point.

1. The landmarks for the temporalis (LOAD3) should be a single point found in:

E:\Tom\Experimental Data\Experiments\cfs5804 testing\Landmarks\load3\cfs5804 LOAD3 force landmarks Jan 18 2007 transformed.landmarkAscii

2. The landmarks for the masseter (LOAD1, LOAD2) should bone only 2 points forming a line segment found in:

E:\Tom\Experimental Data\Experiments\cfs5804 testing\Landmarks\load1\cfs5804 LOAD1 force landmarks Jan 18 2007 transformed.landmarkAscii

E:\Tom\Experimental Data\Experiments\cfs5804 testing\Landmarks\load2\cfs5804 LOAD2 force landmarks Jan 18 2007 transformed.landmarkAscii

The resulting inp section definition should look like this for each muscle load.

```
*STEP
*BOUNDARY,OP=NEW
OCCLUSAL,    1, 3,      0.00000E+00
**% MASSETER Load Set - Magnitude: 100.00 N
*CLOAD,  OP=NEW
7741,  1,  -0.045305
7741,  2,  0.060003
7741,  3,  -0.284345
8408,  1,  -0.050562
8408,  2,  0.060776
8408,  3,  -0.283293
8712,  1,  -0.033917
```

End of Step:

The following code completes the step definition:

```
*END STEP
```

Multiple steps with various loads and boundary conditions can be defined by repeating the above commands.

Using IDEAS, importing, running and exporting.

Importing

1. Open ideas. Don't specify a Model Filename in the start window. Click OK.
2. Set the units to Newtons-millimeters. Options (top of window)->MN-mm.
3. File->Import.
4. Choose Abaqus Input Data.
5. Type a name for the model. Click OK. New part will be created message, Click Ok.
6. Input File Name Field: browse to the .inp file generated through AMIRA.
7. Universal File Name Field: choose a file name for the IDEAS file to which the .inp file will be converted. Check the Import After Processing checkbox.
8. Once imported save the model.
9. Create group all shells. Go to Meshing-> Physical Property. Select all the Thin Shell Physical Property Table and click Create Group button (second figure bottom most

button-near cursor) and type a name for the group that will represent all the shell elements. Need for exporting data and making groups later on. NOTE: write done the STARTING number for the thin shell Family of physical properties.

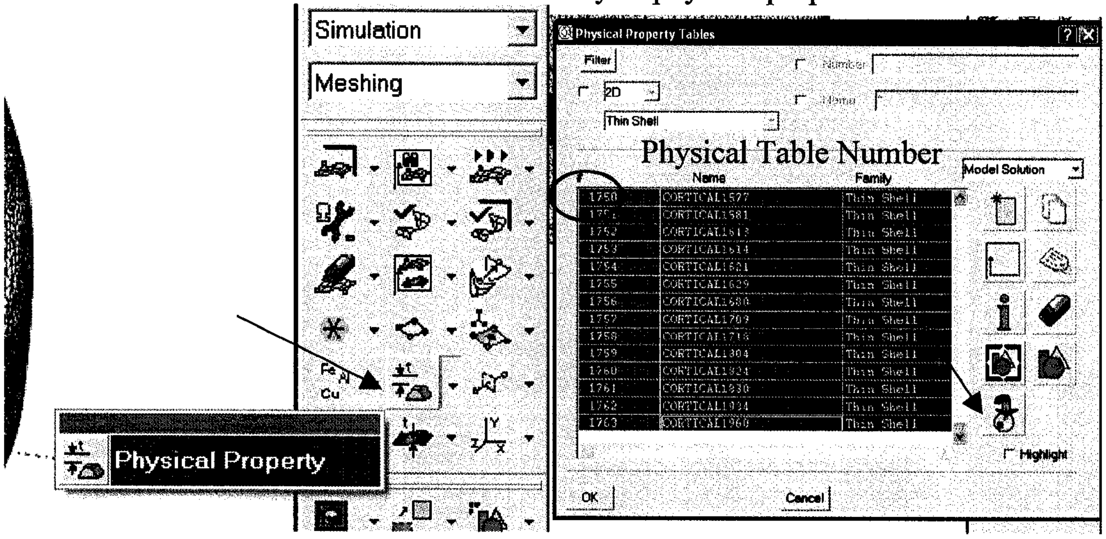

#	Name	Family
1750	CORTICAL1577	Thin Shell
1751	CORTICAL1581	Thin Shell
1752	CORTICAL1613	Thin Shell
1753	CORTICAL1614	Thin Shell
1754	CORTICAL1621	Thin Shell
1755	CORTICAL1629	Thin Shell
1756	CORTICAL1680	Thin Shell
1757	CORTICAL1709	Thin Shell
1758	CORTICAL1718	Thin Shell
1759	CORTICAL1804	Thin Shell
1760	CORTICAL1924	Thin Shell
1761	CORTICAL1930	Thin Shell
1762	CORTICAL1934	Thin Shell
1763	CORTICAL1960	Thin Shell

10. Now need to create indivdual groups for each shell element bin that is represented by a Physical Property definition. From the Left side menu: Group->Auto Create->By Physical Table. You can enter a name in the command prompt (bottom of window) but not necessary.

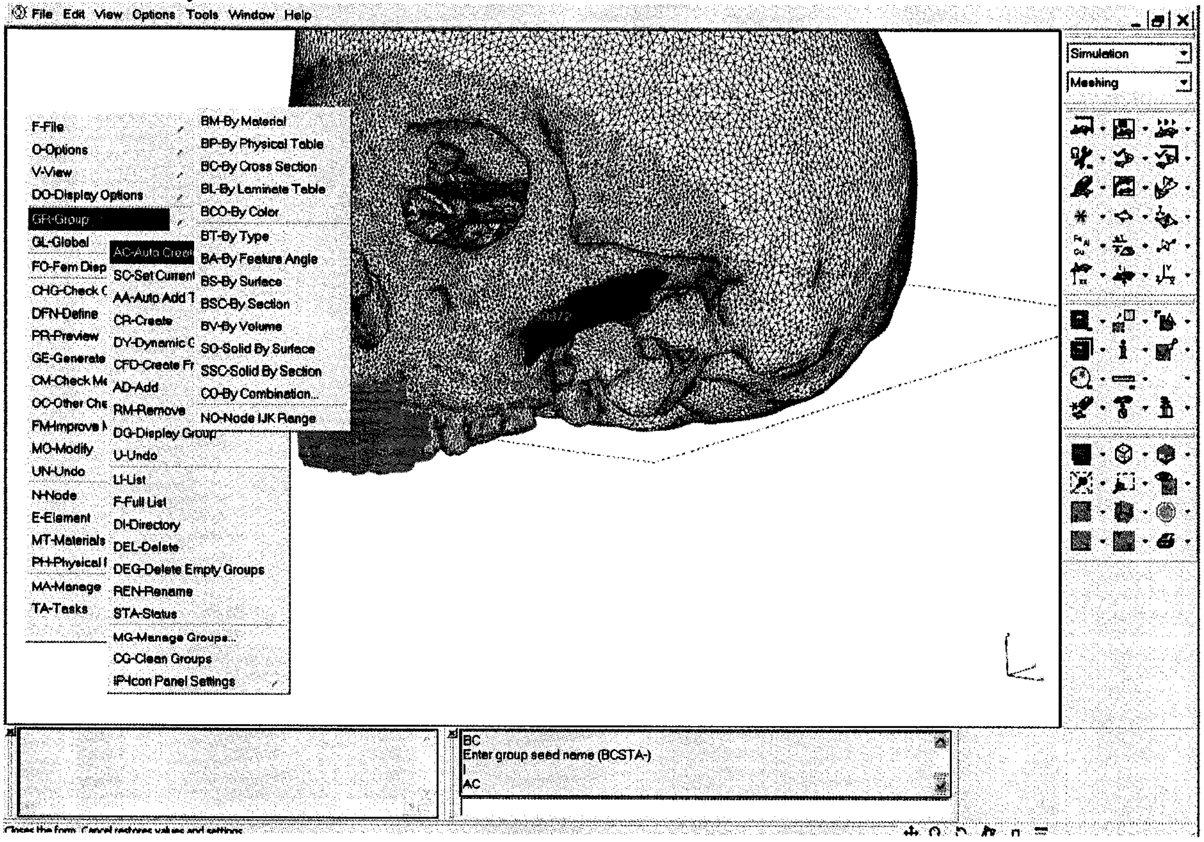

```
BC
Enter group seed name (BCSTA-)
AC
```

11. These groups created a now used for applying the shell offsets. For this you need the IDEAS script found in: E:\Tom\Models\shoffprov1.prg which is a text file of commands.

```
c : Script for IDEAS software to be used with shell element models
c : THIS IS WORKING NO PROBLEMS IN RUNNING THIS
c : ONLY THE GROUPS FROM THE PHYSICAL PROPERTY TABLES HAVE TO BE CREATED AND THE GROUP # RANGE FOR THE SHELLS IDENTIFIED
c : FOR NEGATIVE SHELL THICKNESS OFFSET (INWARD BY HALF THICKNESS IF NORMALS ARE OUTWARD POSITIVE)
k : !
C : count is the starting number of the physical tables for shells
k : #count = 447
C : stopvalue is the end number of groups
k : #stopvalue = 1038
C : number added to count is number of groups before physical tables are converted to groups
k : #groups=(count+14)
k : TA ME
k : #LOOP1:
k : !
k : ph
k : l
k : count;
k : #thickness=z_list(8)
k : #offset=(-1*(thickness/2))
k : #output offset
k : !
k : E MO UG Di
k : groups;
k : A
k : offset
k : Y
k : ;
k : !
k : #count = (count + 1)
k : #groups = (groups +1)
k : #output count
k : #output groups
k : #IF (groups LE stopvalue) THEN #GOTO loop1
c : C->comment line, K->user input, !->back up one menu level
c : Program file must always end with an empty line
```

The information that you need for this is the starting number of the Physical Table for the shell elements (Line7), the total number of groups after the auto creation (Line9) and the number of groups before the auto creation (Line11) which is added to count.

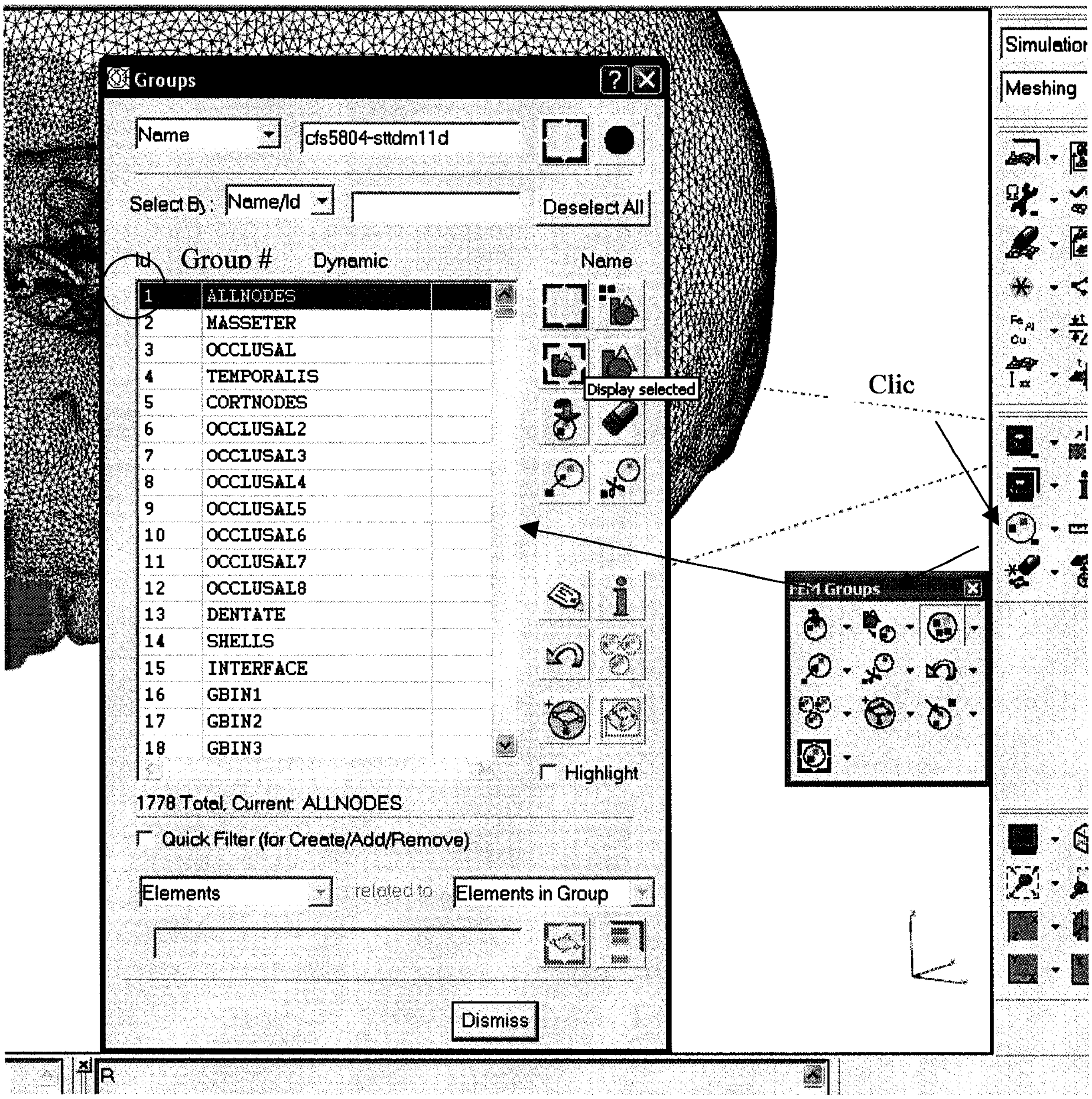

Name: cfs5804-sttdm11d

Select By: Name/Id

Id	Group #	Dynamic
1	ALLNODES	
2	MASSETER	
3	OCCLUSAL	
4	TEMPORALIS	
5	CORTNODES	
6	OCCLUSAL2	
7	OCCLUSAL3	
8	OCCLUSAL4	
9	OCCLUSAL5	
10	OCCLUSAL6	
11	OCCLUSAL7	
12	OCCLUSAL8	
13	DENTATE	
14	SHELLS	
15	INTERFACE	
16	GBIN1	
17	GBIN2	
18	GBIN3	

1778 Total. Current: ALLNODES

☐ Quick Filter (for Create/Add/Remove)

Elements related to Elements in Group

12. To run the script got he left hand menu. File->Program Files->Run-> browse to the script file. Click OK. The output at the bottom left hand side should show the thickness of each bin being read and the appropriate half thickness offset being applied. Save.
13. Now need to create the INTERFACE group of tetrahedral elements. Go to groups Menu and highlight the Cortnodes group (set of only surface nodes). Selecte Quick Filter the Elements related to Nodes in Group. Name this group Interface. This group will include the tetrahedrons and shell elements. Highlight the Interface group and use the Remove from group function. Menu disappears, then Right-Click select Use Group->Directory then select the Shells group (group of all shell elements). Do the same for the Teeth (Dentate). You can use group highlighting or the Info button (Figure) to see if changes were made.

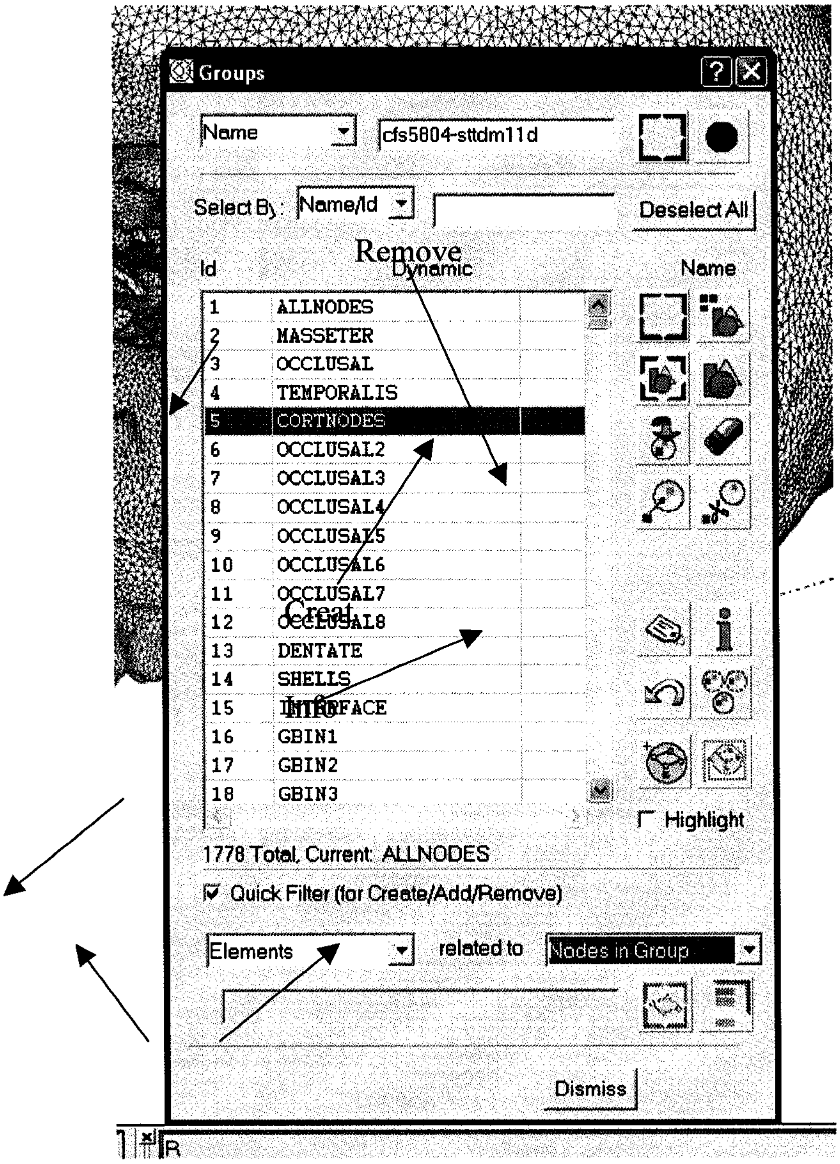

Name: cfs5604-sttdm11d

Select By: Name/Id

Id	Name
1	ALLNODES
2	MASSETER
3	OCCLUSAL
4	TEMPORALIS
5	CORTNODES
6	OCCLUSAL2
7	OCCLUSAL3
8	OCCLUSAL4
9	OCCLUSAL5
10	OCCLUSAL6
11	OCCLUSAL7
12	OCCLUSAL8
13	DENTATE
14	SHELLS
15	INTERFACE
16	GBIN1
17	GBIN2
18	GBIN3

1778 Total, Current: ALLNODES

☑ Quick Filter (for Create/Add/Remove)

Elements related to Nodes in Group

14. In the Meshing menu click on Element->Modify. Then do Right->Use Group->Directory then select the Interface group (left figure). Right-Click select Done (done selecting elements). When Menu opens select Material (right figure).

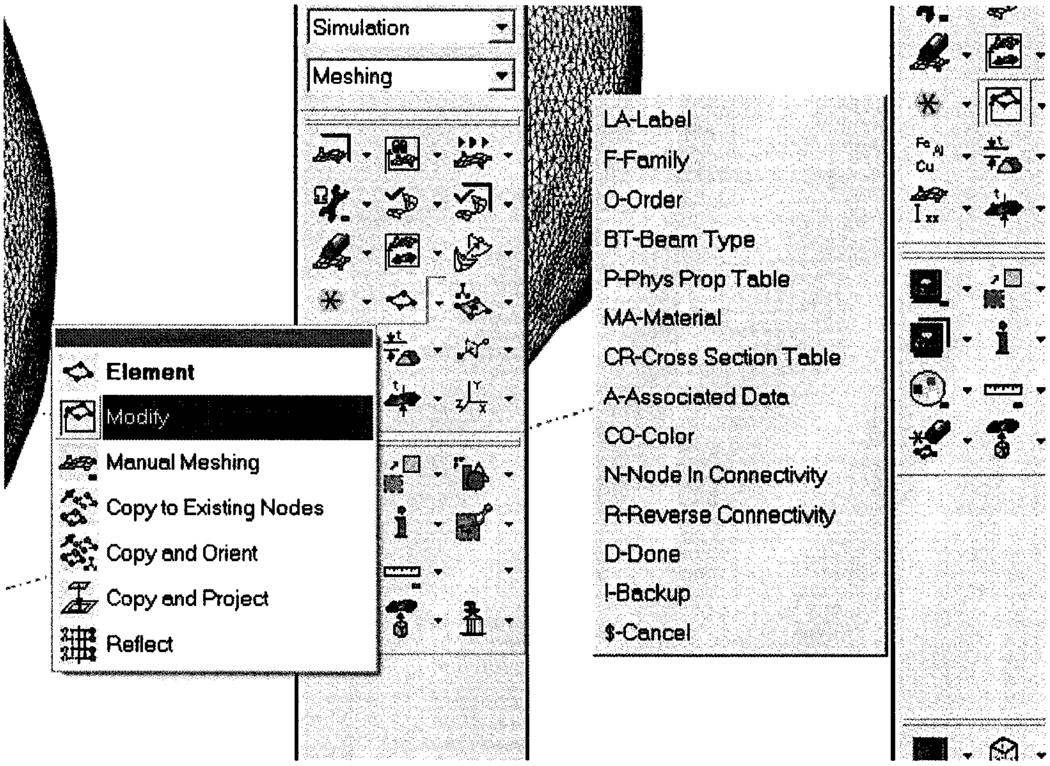

15. The Material Menu will open then select Create to make a new material definition. Then complete the creation from as show in figure. Once created select the material, this will change the tetrahedrons.

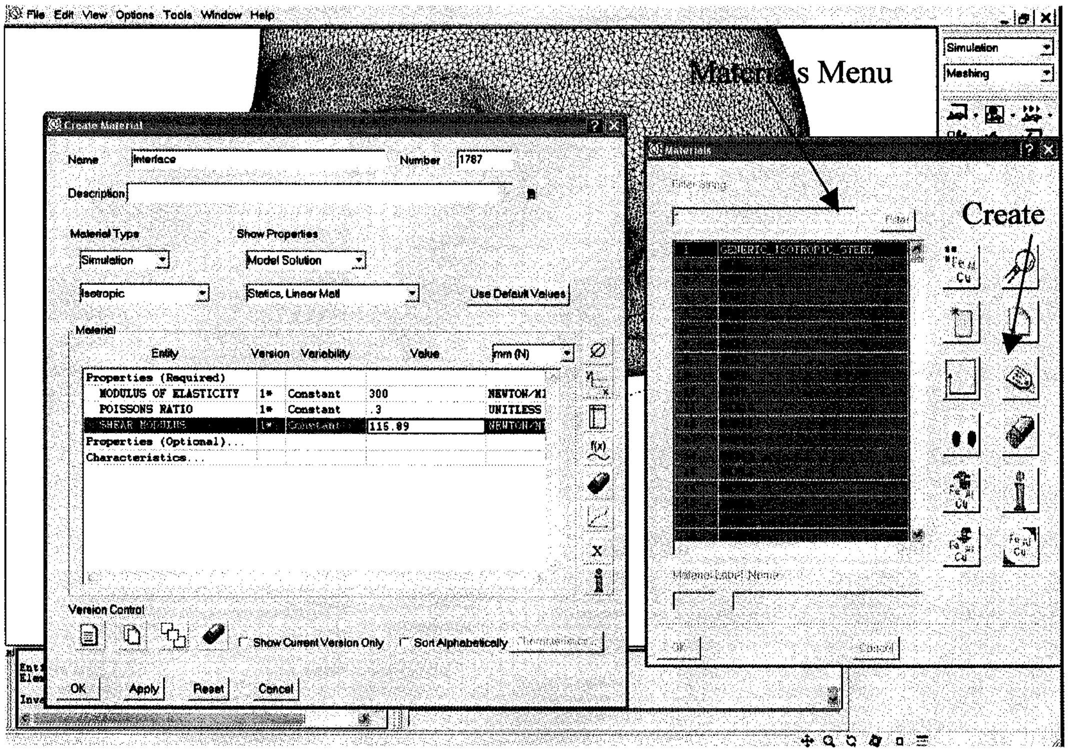

Name: Interface
Number: 1787
Description:

Material Type: Simulation, Isotropic

Show Properties: Model Solution, Statics, Linear Mat'l

Material

Entity	Version	Variability	Value	mm (N)
Properties (Required)				
MODULUS OF ELASTICITY	1*	Constant	300	NEWTON/M1
POISSONS RATIO	1*	Constant	.3	UNITLESS
SHEAR MODULUS	1*	Constant	115.89	NEWTON/M
Properties (Optional)...				
Characteristics...				

☐ Show Current Version Only ☐ Sort Alphabetically

1 GENERIC_ISOTROPIC_STEEL

16. Generate the Boundary Condition Set. In the Boundary Conditions menu select the Boundary Conditions Set Button, Then select the Create a set button and check the Restraint set (Occlusal) and highlight all three of the loads imported from the model.

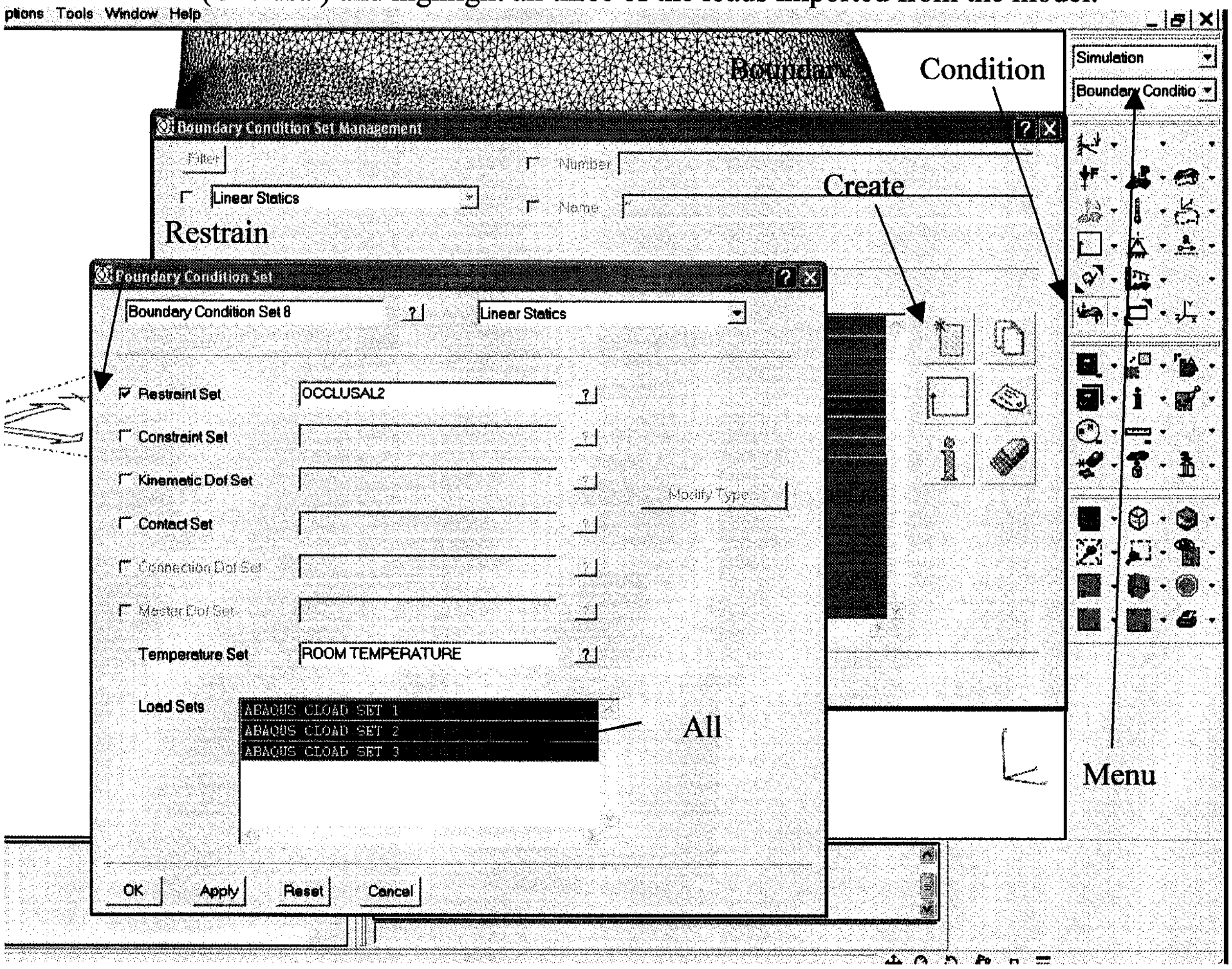
Boundary Condition Set 8 Linear Statics

☑ Restraint Set OCCLUSAL2

☐ Constraint Set

☐ Kinematic Dof Set

☐ Contact Set

☐ Connection Dof Set

☐ Master Dof Set

Temperature Set ROOM TEMPERATURE

Load Sets
ABAQUS CLOAD SET 1
ABAQUS CLOAD SET 2
ABAQUS CLOAD SET 3

17. Create the solution set. So to the Model Solution Menu. Click on Manage Solution Set button -> Create. The Boundary Condition Set should default to the one that was created. In the output selection menu you choose which output variable sot write. Normally Strain is not selected so it must be changed to include it and usually stress is not output because it is not needed. (Refer to figure)

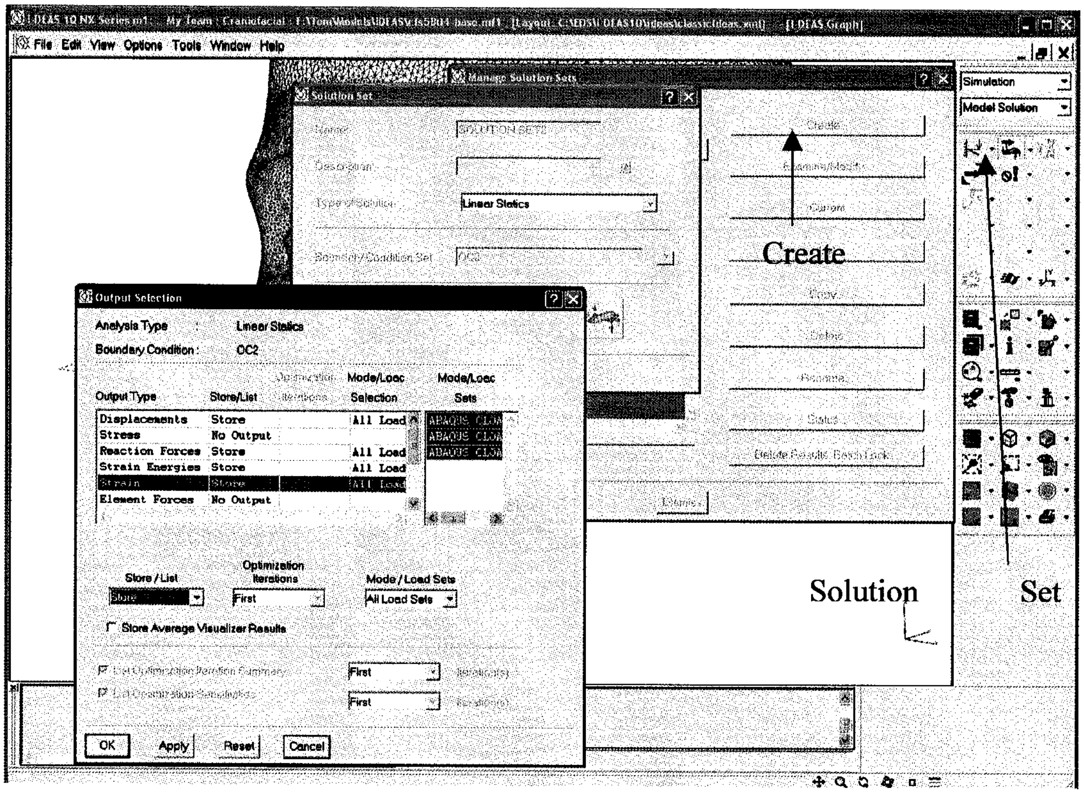

Name: SOLUTION SET2

Type of Solution: Linear Statics

Boundary Condition Set: OC2

Analysis Type : Linear Statics

Boundary Condition : OC2

Output Type	Store/List	Optimization Iterations	Mode/Load Selection
Displacements	Store		All Load
Stress	No Output		
Reaction Forces	Store		All Load
Strain Energies	Store		All Load
Strain	Store		All Load
Element Forces	No Output		

Mode/Load Sets: ABAQUS CLOA, ABAQUS CLOA, ABAQUS CLOA

Store / List: Store

Optimization Iterations: First

Mode / Load Sets: All Load Sets

☐ Store Average Visualizer Results

☑ List Optimization Iteration Summary First Iteration(s)

☑ List Optimization Sensitivities First Iteration(s)

18. The last step is to solve. See Figure.

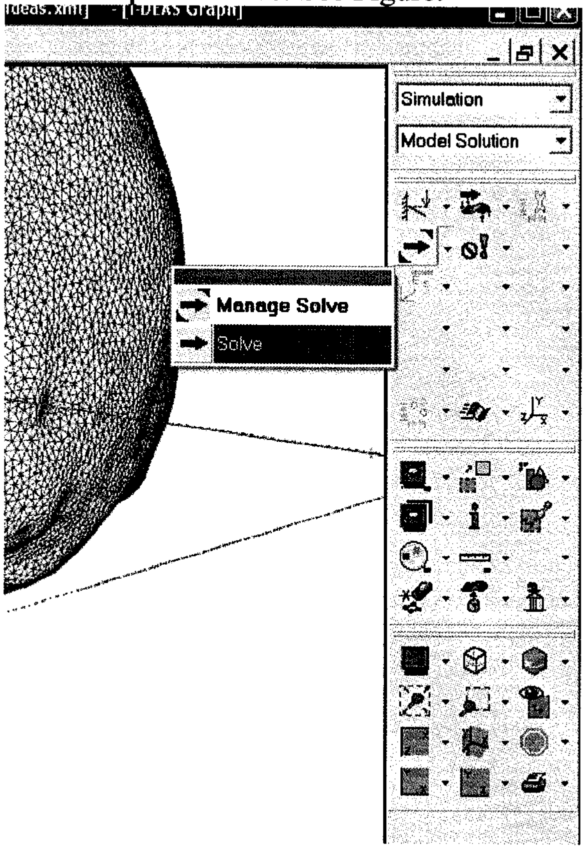

Post-Processing:

1. Exporting data from IDEAS. Open the Visualizer. See Figures. In the Write Results menu select Use Groups and select the Shell group. Must make sure that in the IDEAS Visualizer menu that element data is selected (As opposed to Node data which is the default). Choose filename and the data will be written to a text file which will look like. Which has columuns for the element number centroid coords and the tensor data. Results can be found in E:\Tom\Results\cfs5804\final.

```
 FE Model Name    :cfs5804-sttdm11d
 Result Set     : B.C. 1,STRAIN_11,MASS1
 Result Type     :STRAIN
 Units        :Dimensionless
 Data Criteria    : Maximum
 Part Coordinate System
 Top shell
 Loadset:ABAQUS CLOAD SET 1

  Element    X Coord    Y Coord    Z Coord         XX    XY Shear         YY    XZ Shear
YZ Shear       ZZ
  1819668   3.88E+01  -8.35E+01  -3.85E+01  -1.04E-04  -2.27E-04   4.06E-05   7.78E-
05  -3.31E-05   3.31E-05
  1819669   2.48E+01  -1.01E+02  -3.83E+01  -3.57E-06  -2.32E-05   7.69E-06   9.81E-
06  -1.99E-05   1.72E-06
```

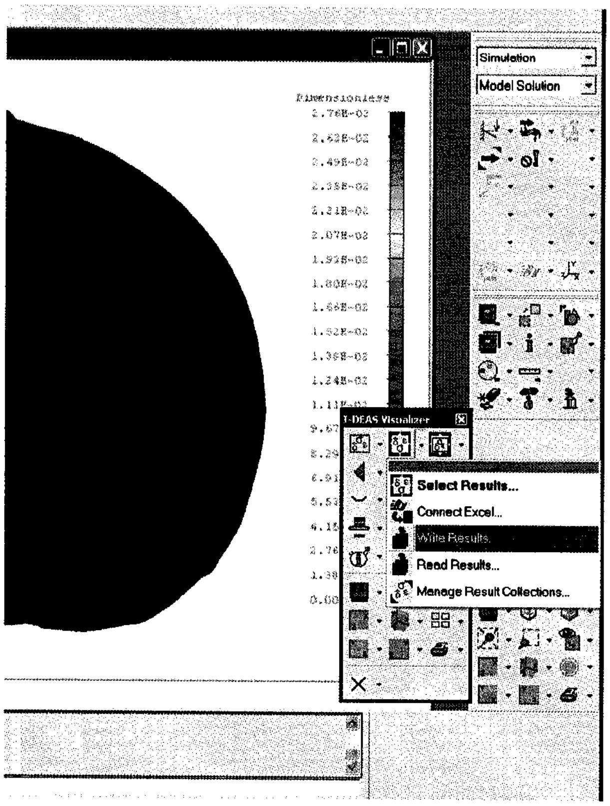

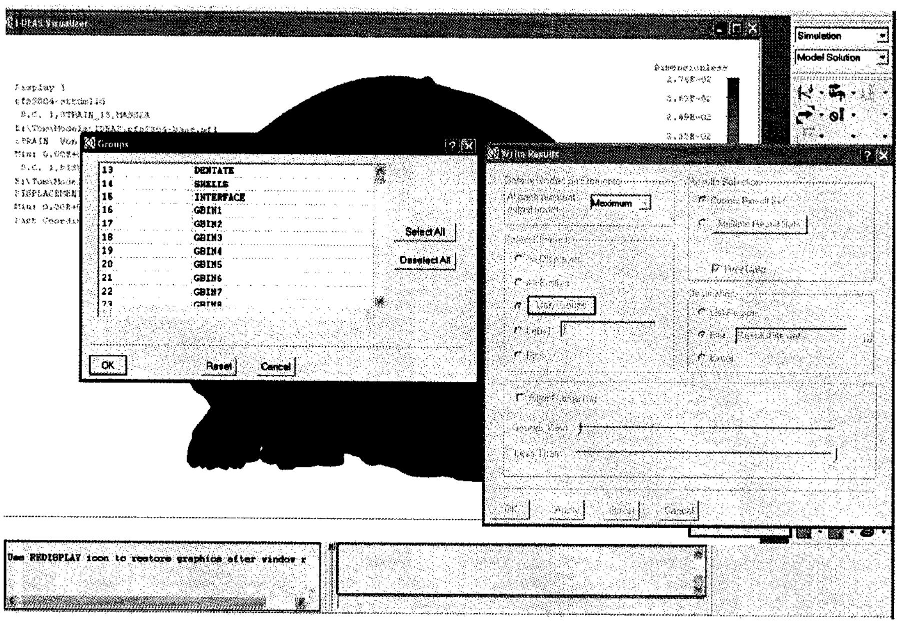

Use REDISPLAY icon to restore graphics after window r

Using the PostProcessor.scro script E:\Tom\Scripts\Post\PostProcessorv1.7.scro

The processing is just like the pelvis SOP.

1. Connect the script to the Surface and the transformed gauge positions and directions.
2. Browse to the IDEAS output file.

3. Click Import.
4. Disconnect the PostProcessorv1.7.scro object from the Surface and use the Gridpackage TriNodesAvg to same the strain data to the nodes.
5. Generate the gauge sets and remove the blank line in the gauge set file.
6. Export the strains.

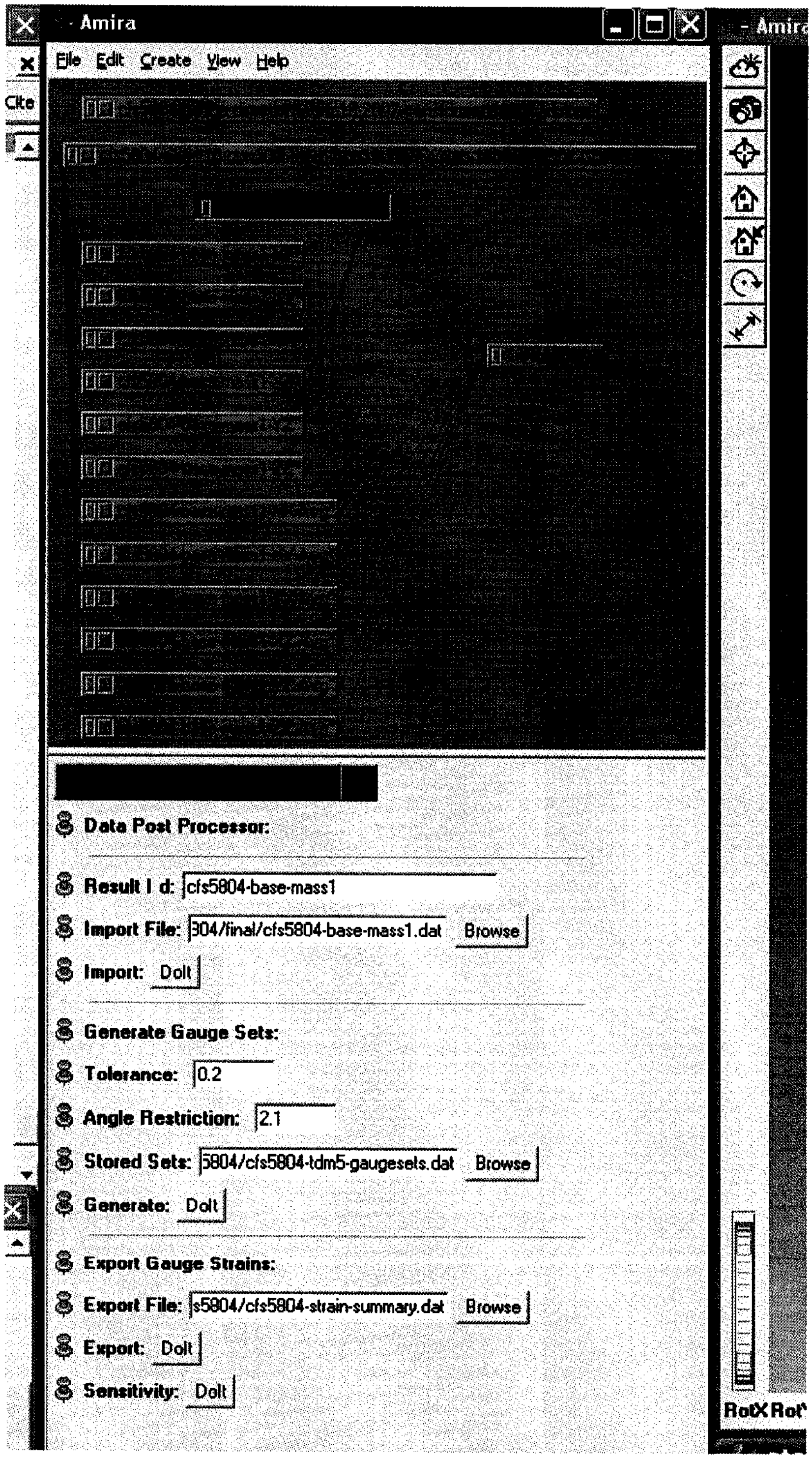

Data Post Processor:

Result I d: cfs5804-base-mass1

Import File: 304/final/cfs5804-base-mass1.dat Browse

Import: DoIt

Generate Gauge Sets:

Tolerance: 0.2

Angle Restriction: 2.1

Stored Sets: 5804/cfs5804-tdm5-gaugesets.dat Browse

Generate: DoIt

Export Gauge Strains:

Export File: s5804/cfs5804-strain-summary.dat Browse

Export: DoIt

Sensitivity: DoIt